Local Group Analogues

by

Ryan Speller

A thesis
presented to the University of Waterloo
in fulfillment of the
thesis requirement for the degree of
Master of Science
in
Physics

Waterloo, Ontario, Canada, 2012

I hereby declare that I am the sole author of this thesis. This is a true copy of the thesis, including any required final revisions, as accepted by my examiners.

I understand that my thesis may be made electronically available to the public.

Abstract

The abundance of satellite galaxies is a critical small-scale test of the standard cosmological model. From comparing the predictions of structure formation in simulations with observations of Local Group dwarf galaxies there is a clear mismatch in the abundance, leading to the so-called "missing satellites" problem. The comparison between simulation and observation have, however, suffered from a limited sample of satellite galaxies, with the only reasonably complete sample being from the most local galaxy groups. It is unknown whether the observed abundance of dwarf satellite galaxies of the nearest groups is statistically representative of the abundance of dwarf satellites in the greater universe. We construct a volume-limited sample of galaxies down to a well-defined stellar mass limit ($M_\star \geq 6 \times 10^9 M_\odot$) using the Atlas3D parent sample of spiral and ellipsoidal galaxies by Cappellari et al. 2011 [18]. In order to statistically identify bound satellites around galaxies in our primary catalogue, we apply cuts on the background based on the properties of known dwarf satellites of the Local Group using both the Sloan Digital Sky Survey Data Release 8 (SDSS DR8) (http://www.sdss3.org/dr8/) spectroscopic and photometric galaxy catalogues. We detect an over-density of faint objects at projected separations of < 500 kpc at S/N ~ 8, corresponding to an average of 4.8 ± 0.65 satellite detections per primary after stacking these systems and subtracting the background. We further find that the over-density of faint objects strongly depends on primary morphology and magnitude. While the Milky Way seems to be unusual in its number of bright satellites, our faint end satellite abundances are in agreement from the Δm luminosity function for primaries in our sample as bright as the Milky Way. Our work has extended the work of previous authors by several magnitudes further down the faint end of the luminosity function.

Acknowledgements

I owe a debt of gratitude to my supervisor, Dr. James Taylor, who took a risk in taking me on as a graduate student and whose valuable knowledge and advice have benefited me greatly in this endeavour and the experience with whom will surely leave a significant impact on me long after my graduate experience.

I would like to thank the members of my committee for taking the time to read my thesis and also for the feedback from committee meetings. I am also most grateful to my fellow graduate student Jonathan Grossauer, for many illuminating discussions.

Lastly, I would like to acknowledge the love and support of my parents, David and Corrine Speller, and my fiancé Krista Burke, whose understanding and encouragement have made this work possible.

Table of Contents

List of Tables

List of Figures

Chapter 1

Introduction

In the early 20th century there was Great Debate regarding the scale of the universe. The "Great Debate" between astronomers Harlow Shapley and Heber Curtis began in 1920 and concerned observations of spiral nebulae. Curtis thought of the universe as composed of many galaxies like the Milky Way, as suggested by observations of the spiral nebulae. Shapley opposed this view, taking the stance that the observed spiral nebulae were gas clouds within the Milky Way and that the universe consisted solely of the Milky Way galaxy. The debate was settled when Edwin Hubble first identified Cepheid variable stars in the neighbouring Andromeda galaxy in the mid 1920s. Using the Cepheid variable stars, Hubble was able to calculate the distance to Andromeda, finding that it was large enough to be considered a distinct galaxy. Since this time, the number of known galaxies has increased to the hundreds of billions, populating an intricate web of structure that is presently the focus of much research in astrophysics and cosmology.

The structure that we see in the universe today is the result of early fluctuations in the primordial plasma of baryons, photons, and dark matter that filled the early universe which have been amplified over time. Galaxy clusters are the largest virialized structures in the universe, and the satellite abundances of galaxy clusters agree well with what is predicted by simulations of structure formation from cold dark matter (CDM) models. On smaller scales, galaxy groups provide a more sensitive check on predictions from cold dark matter models of structure formation because they probe the intricacies of structure at the low mass end. Numerical simulations of structure formation using the standard cosmological model, where cold dark matter accounts for 23% of the mass energy of the universe, have led to a discrepancy with observations of structure in local galaxy groups. Large spiral galaxies like the Milky Way and neighbouring Andromeda are predicted to form inside

extended dark matter halos, which form from the accretion of smaller subhalos. We see a lack of satellite galaxies with small velocity dispersions that are predicted to populate the least massive dark matter subhalos of the Local Group in an abundance that is over an order of magnitude less than the number that is predicted by simulation. This is known as the "missing satellites" problem [70, 53]. While it is expected that dwarf galaxy star formation is suppressed by various feedback mechanisms, it is a mystery why only some of the subhalos are dark. Due to the low surface brightness of dwarf galaxies, we are currently limited in our comparison between theory and observation to the dwarf satellite galaxies that are found in the Local Group. This raises the important question of whether the dwarf satellite population we detect locally is representative of the dwarf satellites of other galaxy groups. Reconciling the predictions from of cold dark matter structure formation with present observations of the distributions and properties of small, faint dwarf galaxies thought to form inside them and addressing the question of whether the Local Group is typical form the topic of this thesis.

In the following sections we briefly introduce and discuss evidence for the ΛCDM cosmological model. We then move on to discuss the predictions for structure formation in the ΛCDM cosmological model and describe the galaxies that are thought to populate them in section 1.2. We also introduce the basic properties of galaxies including how galaxy shape, brightness, and size are quantified, and examine the properties of the Local Group of galaxies in particular. In chapter 2 we discuss neighbouring galaxy groups and compare them to our own Local Group. In chapter 3 we discuss the Atlas3D catalogue and the Sloan Digital Sky survey, and describe our methods for building an isolated sample of bright galaxies and a statistical sample of associated satellites of these galaxies. In chapter 4, we discuss the results of our search for populations of associated satellites around our sample of isolated primaries and compare to previous results in the literature. In chapter 5 we discuss the implications of these results in the context of the "missing satellite problem" and address the question of whether the Local Group is typical.

Recently, authors such as Guo et al. (2011,2012) [33, 34]; Liu et al. (2011) [59]; Lares et al. (2011) [57]; Strigari et al. (2012) [88]; and Nierenberg et al. (2011,2012) [73, 74] have performed searches for satellite galaxies around Milky Way-like hosts using methods similar to those that are described in Chapter 3. These groups have had complementary results indicating that the Milky Way seems to be unique in the number of very bright satellites that it hosts. These groups have also found that the number of associated satellites depends on central galaxy luminosity and morphology. Guo et al. [33] find that isolated MW-like galaxies host a factor of 2 fewer satellites brighter than $M_v = -14$ than the Milky Way and

Liu et al. [57] report that they find only 11.6% of such galaxies host one bright satellite analogue of the Large and Small Magellanic Cloud satellite galaxies of the Milky Way, and only 3.5% hosting two. While these authors mainly focus on detecting the brightest satellites, there is hope of reconciling the large number of satellite galaxies predicted by simulation by counting the number of faint galaxies predicted to be the most abundant and accounting for the largest discrepancy between simulation and observation. We focus on detecting faint satellites in order to compare to the number found in the Local Group to determine if the Local Group is typical and address the discrepancy with the abundance predicted by simulation.

1.1 Background Theory

1.1.1 Cosmology

The generally accepted "standard model" of cosmology is known as the ΛCDM model. Evidence indicates that the universe is 14 billion years old and began with a "Big Bang," expanding from a hot, dense state. It is currently filled with baryons, photons, a non-baryonic form of collisionless matter called *dark matter*, and a repulsive force that is responsible for the accelerating expansion of the universe that continues at the present day and accounts for the majority of the energy content of the universe, known as *dark energy*. The ΛCDM cosmological model uses Einstein's general theory of relativity and provides a description of the evolution and state of the universe.

Λ

Initially observed by Edwin Hubble in 1929, distant astronomical bodies have a measured recessional relative velocity that is proportional to their distance from Earth (known as Hubble's law) such that $v = H_0 \cdot D$, where H_0 is the proportionality parameter (Hubble parameter), v is the recessional velocity relative to Earth, and D is a proper distance to the object. Here, we use the term proper distance to indicate the distance that one would measure between two objects with a long ruler at a particular instant of cosmological time. Hubble's observation of an expanding universe led Einstein to alter his equations of general relativity to remove the "cosmological constant" Λ that he had introduced in order to produce a static universe. However, when in 1998 it was discovered that the universe was accelerating the cosmological constant came back into use as the effect of

adding the constant produces a universe which is static but unstable. The most direct evidence for accelerated expansion of the universe comes from high-redshift supernovae and the discovery that distant supernovae appear dimmer than they would have been in a decelerating universe. This result has been found by two independent groups, the Supernova Cosmology Project [78] and the High-z SN Search [82]. The results of Perlmutter et al. [78] and Riess et al. [82] indicated that the expansion of the universe had been accelerating for the past 5 Gyr and provided evidence for a negative pressure component of the universe driving accelerated expansion, deemed dark energy, at greater than 99% confidence. Current estimates of the Hubble parameter put it in the range:

$$H_0 = 71.0 \pm 2.5(\text{km/s})/\text{Mpc}\ [46].$$

Other evidence for accelerated Hubble expansion comes from measurements of galaxies' large scale spatial correlation and angular anisotropies in the Cosmic Microwave Background (CMB). In the standard (ΛCDM) cosmological model, accelerated expansion is understood as being a consequence of repulsive dark energy, which has come to define a smooth component of the universe with repulsive gravity and large negative pressure and accounting for 73% of the mass-energy of the universe.

Cold Dark Matter (CDM)

As an exotic form of matter, dark matter interacts differently from ordinary baryonic matter, and the way that dark matter clumps together, forming a dark matter halo, determines the structure of the universe. While studying the Coma cluster in 1933, Swiss astronomer Fritz Zwicky calculated a gravitational mass of the cluster much greater than could be accounted for by visible matter alone. This discrepancy led Zwicky to coin the term "dark matter" to describe the additional unseen matter that he posited to account for the discrepancy in his mass calculations. Zwicky thought the additional matter might be gas or some other material much less luminous than stars. Subsequently, starting with observations of galactic rotation curves in the mid 1970s, further evidence has mounted to confirm Zwicky's suspicion of the existence of an unseen form of *dark* matter. Today dark matter is a part of our standard model of cosmology as a collisionless, non-baryonic form of matter that does not interact electromagnetically and whose presence can only be inferred gravitationally, constituting 23% of the mass-energy of the universe.

Evidence

- **Rotation Curves**. A galactic rotation curve is a plot of the orbital speed of a galactic satellite against its distance from the center of the galaxy. From the balance of a gravitational attractive force and centrifugal force on a satellite orbiting a central mass distribution

$$\frac{mv^2}{r} = \frac{GMm}{r^2},$$

we would expect the velocity to fall off as $v \propto r^{-1/2}$. Observations of the rotation curves of galaxies has shown this not to be the case, however; rotation speeds are not found not to fall off at large distances from the galactic core but rather flatten out. By the mid to late 1970s, improvements in observation allowed researcher Vera Rubin to obtain rotation curve data at larger radii than ever before, revealing for the first time that the rotation curves of galaxies appeared to be flat further out than one could trace luminous stars and gas. The accepted explanation is the presence of an additional (dark) matter component of the galaxy that adds mass in the extended regions of the galaxy and accounts for over 85% of the total mass of the galaxy.

- **Gravitational Lensing**. Gravitational lensing is a phenomena in which light is bent by the gravitational potential of an astronomical body, acting as a lens, before reaching a distant observer. The extent to which the light is bent, and therefore the degree of magnification (or distortion) of an object located behind the lens, can be used as a measure of the gravitational mass of the lens. An important example of the application of gravitational lensing of great importance, the Bullet cluster (1E 0657-558), is a collision of two galaxy clusters. The Bullet Cluster shows that the baryonic mass inferred from x-ray observations of hot gas in the cluster is offset from the mass inferred through gravitational lensing. This spatial offset from the center of mass provides strong evidence for a ("collisionless": as having a very small interaction cross section) mass component that has been unaffected by the collision and accounts for a large fraction of the total mass of the cluster. The Bullet Cluster not only provides some of the strongest evidence for of dark matter to date, but also favours dark matter as the leading candidate for explanations of flat galaxy rotation curves rather than theories that involve a modified form of gravity, since theories of modified gravity (MOND) are usually unable to explain the apparent spatial offset of the center of mass from the baryonic center of mass.

- **Peaks in the angular correlation function of CMB fluctuations**. The Cosmic Microwave Background (CMB) is radiation left over from the Big Bang and was initially discovered as a 3.5 K excess antenna temperature on a Dicke radiometer by Penzias and Wilson in 1964. The CMB has a black-body spectrum at a temperature of 2.73 K with a maximum in the microwave range at a frequency of 160.2 GHz. As the universe became transparent around 300,000 years after the Big Bang, the rate of Compton scattering decreased as the universe expanded. As the mean free path for photons increased they were able to propagate without being scattered. After being redshifted into the microwave range of the electromagnetic spectrum at a few degrees Kelvin, these photons are detected today as the CMB. Dark matter leaves its signature on the CMB in the form of anisotropies. Before the time of last scattering, when photons are still coupled to baryons, the universe is filled with a plasma of electrons, protons, and neutrons, where photons are trapped by Thompson scattering with the plasma. Dark matter does not feel the outward pressure from the photon-baryon plasma and only interacts gravitationally. Acoustic oscillations are created in the plasma as gravity acts as a restoring force against the outward pressure when overdensities form. At the time of last scattering photons free-stream from the overdense regions, leaving behind the baryons and dark matter particles at the sound horizon of the original overdensity. This effect can be seen in the power spectrum of CMB anisotropies, and has since been confirmed as peaks in the spectrum first measured by COBE and later by WMAP.

Dark Matter Halos

N-body simulations reveal that dark matter "halos" form as a conglomeration of collisionless dark matter particles. Galaxies are thought to form inside these dark matter halos, as they provide a gravitational potential in which baryonic matter can collect. The dark halo dominates the mass of the galaxy and extends far past its visible extent. The density of a dark matter halo is most often described by a Navarro-Frenk-White (NFW) profile [72]:

$$\rho(r) = \frac{\rho_0}{(r/r_s)(1 + r/r_s)^2} \tag{1.1}$$

Where r is the distance from the center, and ρ_0 and r_s are the halo scale density and scale radius, respectively. The NFW profile is a fit resulting from numerical n-body simulations of collisionless dark matter particles. The "virial radius" ($r_{\rm vir}$) is used to describe the radius of a sphere of matter, such that the density of matter contained is two hundred times the

critical density of the universe. The critical density is defined as the density required in order to obtain the flat, expanding universe that we observe today using the ΛCDM model. While the edges of galaxy halos are not well defined, a standard convention for the size of a halo is to use the radius at which the halo density is 200 times the background density p_m, which is a very good approximation to $r_{\rm vir}$. The total mass of the halo is then

$$M_h = \Delta_h p_m (4\pi/3) r_{\rm vir}^3 \tag{1.2}$$

In a ΛCDM universe, dark matter halos are assembled by accretion of smaller subhalos, leading to structure formation that is hierarchical, with structure forming from small density perturbations that have been present since early times. Halo mergers and hierarchical structure formation are discussed in greater detail in the following section.

1.1.2 Structure Formation

The seeds for the large scale structure that we see today in an expanding universe with cold dark matter were planted in an era where the energy of the universe was dominated by its matter content, called the era of matter-domination [83]. Anisotropies observed in the Cosmic Microwave Background allow us to infer the statistical properties of the primordial density fluctuations in the matter. It is useful to decompose the density field into its Fourier components $\delta_{\vec{k}}$, where the power spectrum $P(k)$ is then defined as the mean square amplitude of these Fourier components $P(k) = \langle |\delta_k|^2 \rangle$. When the phases of different Fourier components are uncorrelated, the density field is one such that randomly chosen points produce a Gaussian probability distribution with a peak at nearly the critical mean density - called a Gaussian Random Field. Further, if we impose the conditions of homogeneity and isotropy then all statistical properties are summed up in the power spectrum $P(k)$. The expected power spectrum for inflationary fluctuations has a scale-invariant, power-law form $P(k) \propto k^n$ [83]. For this initial scale-invariant, power-law form of the power spectrum, the smallest mass scales produce the largest amplitudes of fluctuation. This scenario and indeed structure formation in our ΛCDM universe is described as *hierarchical*, as the smallest objects are the first to form, with larger structures being assembled from mergers of these pre-collapsed regions. The high densities of the pre-collapsed dark matter halos that jointly form the larger structure allow them to survive the strong tidal forces, and, while gravitational interactions have the effect of stripping mass from the merged subhalos, most of these will survive as bound substructures [70, 53]. In summary, structure formation in a ΛCDM universe is hierarchical, from the bottom up, where the

lowest mass scale fluctuations are the first to freeze out from expansion, collapsing at high redshift when the universe is very dense. More massive objects are then later formed from the merging of the denser, pre-collapsed regions.

In early attempts to simulate cosmological structure formation on galaxy cluster scales it was found that there there was a lack of dark matter halo formation within about half of a galaxy cluster virial radius. This inability to resolve sub-structure in dense environments became known as the overmerging problem, which would eventually be overcome with increased numerical resolution [71]. Later high-resolution N-body simulations run by authors like Moore et al. [70] and Klypin et al. [53] in 1999 successfully reproduced the observed mass function in clusters, but then reversed the previous problem of finding a lack of halos by predicting a large number of cold dark matter subhalos also surviving inside galactic halos, with the result that galaxy halos appear as scaled versions of galaxy clusters. These simulations, which had resolutions of over a million particles per halo, predicted that Milky Way sized halos should contain around 500 satellite galaxies - an order of magnitude greater than the number observed. As a proxy for mass, Moore et al.[70] used circular velocities of bound dark matter particles from simulation in order to facilitate comparison with observations of satellite galaxies of the Milky Way. By assuming isotropic velocity dispersions and calculating circular velocities from velocity dispersions for the satellite galaxies of the Milky Way where necessary, Moore et al. were able to directly compare substructure abundances in terms of cumulative subhalo counts as a function of circular velocity. This was done by making the necessary approximation that the velocity dispersion of the stellar content of a dwarf galaxy is the same as the host subhalo. The overabundance of dark matter subhalos with small velocity dispersions $\sigma_r \approx 10 - 15$ km/s predicted by simulation compared to the number of satellites known to exist in the Local Group is known as the "Missing Satellites Problem" [70, 53]. The mismatch in abundance indicates that either our picture of hierarchical structure formation is incorrect, or that there are too few baryons inside dark matter subhalos for them to be observed [70]. While it is expected that dwarfs are darkened by mechanisms that suppress star formation such as ionizing feedback from star formation or re-ionization, it is not understood why only some dwarf galaxies are observed.

1.2 Galaxies

Galaxies are massive, gravitationally bound systems that range widely in size, shape, and mass, and consist of: gas, dust, stars, and dark matter. Galaxies typically host on the

order of 10^{11} stars and typically have luminous masses on the order of $\sim 10^{11} M_{\odot}$ [76].

Figure 1.1: The Hubble Sequence morphological classification of galaxies.

Galaxies are often classified by their morphology, most commonly using Edwin Hubble's systematized classification scheme (the Hubble sequence), which classifies galaxies into 3 broad types: elliptical, spiral, and lenticular (Figure 1.1). Elliptical (E) galaxy morphologies progress from nearly spherical ($E0$) to highly elongated ($E7$). Lenticular ($S0$) galaxy morphologies lie between elliptical and spiral. Spiral galaxy morphologies are then broken down as barred (SB) or unbarred (S), followed by a letter indicating the size of the central bulge and tightness of the spiral arms, with a indicating a galaxy that has a large central bulge with tightly wound but diffuse spiral arms. A fourth class of galaxy morphology which is not shown in the tuning fork is irregular; these do not show regular shapes and can be further subdivided into *Irr I*: galaxies that show some identifiable spiral or elliptical features but cannot be identified as such, and *Irr II*: those that show no semblance to any Hubble sequence shapes. A third subdivision of irregular galaxy morphology is used to classify irregular dwarf (*dIrrs*) galaxies not having an elliptical or spherical structure, which are classified as *dE* or *dSph*. De Vaucouleurs [20] created an expanded morphological classification system in 1959, adding to Hubble's scheme extra classification criteria of bars, rings, and spiral arms. De Vaucouleurs also assigned a number scale to the Hubble sequence (Table 1.1).

Elliptical and lenticular galaxies are commonly referred to together as "early-type" galaxies, while spirals and irregular galaxies are referred to as "late types". The description of early/late type is meant to indicate the position on the Hubble "tuning fork"

Hubble stage T	-6	-5	-4	-3	-2	-1	0	1	2	3	4	5	6	7	8	9	10	11
de Vaucouleurs class	cE	E	E^+	$S0^-$	$S0^0$	$S0^+$	S0/a	Sa	Sab	Sb	Sbc	Sc	Scd	Sd	Sdm	Sm	Im	
Hubble Class	E			S0			S0/a	Sa	Sa-b	Sb	Sb-c	Sc			Sc-Irr	Irr I		

Table 1.1: Hubble T morphological scale

diagram (Figure 1.1). The disks of spiral galaxies are observed to be home to many young (blue) stars and regions of active star formation, while the typically much larger elliptical galaxies are composed of predominantly old (red) stellar populations.

A galaxy's brightness is described in magnitudes. The apparent magnitude (m) of a celestial object is a logarithmic measure of the flux received as measured from Earth. The absolute magnitude (M) is a logarithmic measure of the intrinsic brightness of a celestial object, the total energy radiated per unit time, and is the apparent magnitude standardized to a distance of 10 parsecs. The difference between the apparent and absolute magnitudes of a celestial object can then be used as a measure of distance, known as the distance modulus:

$$m - M = 5 \cdot \log(d) - 25 = D \tag{1.3}$$

where d is the distance to the galaxy measured in Mpc.

Modern observational schemes attempt to determine galaxies' quantitative parameters using calibrated images. To determine galaxies' sizes, galaxy images are fitted with light profiles. The Sersic profile is a well known light profile describing how the surface brightness of a galaxy varies as a function of distance from the center (R), having a functional form:

$$I(R) \propto \mathrm{e}^{-kR^{1/n}} \tag{1.4}$$

The parameter n, called the "Sersic index," controls the degree of curvature of the profile. Small values of n produce less centrally concentrated profiles with shallower logarithmic slopes at small radii, while Sersic profiles with larger n are centrally concentrated and have steeper logarithmic slopes at large radii. Two very common Sersic profiles used to describe galaxy light profiles are the de Vaucouleurs profile (n = 4) and the exponential profile (n = 1). The de Vaucouleurs profile describes how the surface brightness of an elliptical galaxy varies as a function of distance from the center:

$$I(r) = I_0 \mathrm{e}^{-7.67\left[\left(\frac{r}{re}\right)^{1/4}-1\right]} \tag{1.5}$$

and the exponential profile, which differs only in the power-law index, better fits spiral and dwarf elliptical galaxies:

$$I(r) = I_0 \mathrm{e}^{-1.68\left(\frac{r}{re}\right)} \tag{1.6}$$

where I_0 and I(r) are the intensities at radii 0 and r, and r_e is the half-light radius, the radius of the isophote (a contour line of constant surface brightness) containing half the luminosity of the galaxy.

1.2.1 Dwarf galaxies

Dwarf galaxies are small galaxies with low luminosity and up to several billion stars. These types of galaxies can be subdivided further morphologically as: dwarf irregular, dwarf ellipsoidal, or dwarf spheroidal. Dwarf galaxies range in luminosity, being broadly described as either classical: having an absolute magnitude $M \lesssim -8$, or ultra-faint: having a magnitude $-8 \lesssim M$, making them difficult to detect observationally. Fits to luminosity functions obtained from galaxy redshift surveys indicate that dwarf galaxies are the most commonly found type of galaxy in the universe[64], and that they were even more numerous in the earlier stages of the universe [24]. Due to dwarf galaxies' characteristically low luminosities, the only statistically significant population of dwarf galaxies that we are able to study are those closest to us in the Milky Way and neighbouring Andromeda galaxies, together comprising the Local Group.

Chapter 2

The Local Group and Neighbouring Galaxy Groups

The Local Group (LG) is the group of galaxies which contains the Milky Way and its nearest neighbour Andromeda and their respective satellite systems. Of all of the galaxies in the universe, the Local Group dwarfs are some of the most well-studied. We often extrapolate our knowledge of the LG galaxies to those in the broader universe. Although the only significant observational opportunity to test the abundance of dwarf galaxies predicted by theories of structure formation in a ΛCDM universe is for our own Local Group, it is currently unknown whether the Local Group is statistically representative of other galaxy groups, and the Local Group dwarfs representative of all dwarf galaxies [94]. Within 5 Mpc of the Local Group, there exist a number of other galaxy groups: M81, M83, Cen A, IC342, Maffei, Canes Ven I, and the Sculptor Filament. Karachentsev et al. [48, 50] have compiled a useful summary of the properties of these neighbouring galaxy groups and their known satellites, which we can use for a limited comparison with the brightest members of the LG. While not as well sampled as the Local Group, these groups offer a chance to address the question of Local Group is typical of other galaxy groups in a limited context. Authors such as Weisz et al. have suggested that the properties of LG dwarf galaxies are typical for dwarfs in the local universe [94]. In this chapter we introduce the nearest neighbouring galaxy groups and compare the properties of the known Local Group dwarf satellites to those of neighbouring galaxy groups.

2.1 The Local Group of Galaxies

The galaxies of the Local Group are found within a 10 million light-year (or $\sim$ 3 Mpc) diameter with an estimated total mass of $1.29 \pm 0.14 \times 10^{12} M_{\odot}$ [65]. The group itself is part of a larger supercluster of galaxies known as the Virgo Supercluster. Of the Local Group member galaxies, the Milky Way and M31 are by far the most massive, and therefore dominant members, and each of these galaxies has a system of satellite galaxies. The Milky Way system contains many known (nearby) dwarf galaxies, including: Sag DEG, LMC, SMC, Canis Major Dwarf, and the classical dwarf galaxies: Ursa Minor, Draco, Carina, Sextans (dwarf), Sculptor, Fornax, Leo I, Leo II, the Phoenix Dwarf, Leo A, and ultrafaint dwarf spheroidal galaxies: SgrDSph, Ursa Major I, Ursa Major II, Bootes I, Bootes II, Bootes III, Segue I, Segue II, Coma Berenices, Leo IV, Leo V, Pisces II, Canes Ven I, Canes Ven II, Hercules, and Willman I. The Andromeda galaxy system is grouped around its main galaxy M31 in Andromeda, and contains bright nearby M32 and M110 as well as fainter and more distant classical dwarfs NGC 147, NGC 185, And I, And II, And III, And IV, And V, And VI (Pegasus dwarf), And VII (Cassiopeia dwarf), And VIII, And IX, And X, And XIV, AndXV, AndXVI, AndXVII, AndXVIII, AndXIX, AndXXI, AndXXIII, AndXXV, as well as the newly discovered ultra-faint dwarf spheroidals And XI, And XII, And XIII, AndXX, AndXXII, AndXXIV, AndXXVI, AndXXVII. Around irregular galaxy NGC 3109 exists a subgroup whose membership to the Local Group is uncertain due to their large distances, which contains Sextans A, Sextans B, the Antlia dwarf and Leo A.

2.1.1 Local Group Dwarf Satellites

The population of known dwarf satellites of the Local Group has more than doubled in the last 10 years, with the most recent detections of Local Group dwarf satellites found as overdensities of resolved stellar objects in the Sloan Digital Sky Survey (SDSS). Considering that the search for dwarf galaxies orbiting our own Milky Way is partially obscured when looking into the plane of the Milky Way (the so-called zone of avoidance) (Figure 2.1), there is sure to be a population of undiscovered dwarfs lying there [65]. In Figure 2.1, we see that the cumulative dwarf count as a function of the absolute value of Galactic declination $|b|$ flattens in the zone of avoidance ($|b| < 10^{\circ}$ and $|b| > 80^{\circ}$), indicating there are dwarfs that have not yet been detected there.

It is typically difficult to obtain reliable photometry for the Local Group dwarf satellites due to their close proximity and low surface brightness. Because they are nearby, these

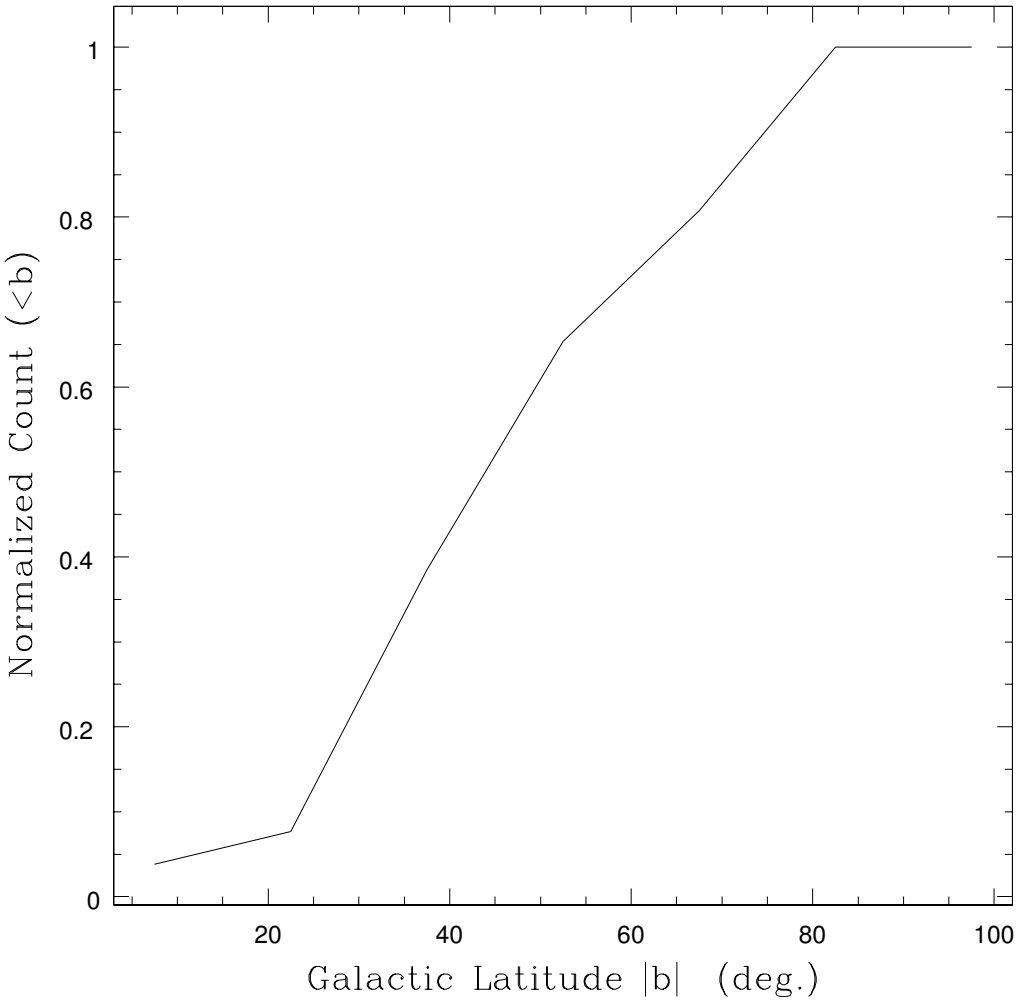

Figure 2.1: A cumulative plot of normalized Milky Way dwarf counts as a function of Galactic declination b, showing a dwarf galaxy count that flattens at low galactic declination indicating there are dwarfs that have not yet been detected that lie in the zone of avoidance.

small galaxies have an extended spatial distribution, ranging from 10 arcmin to over 40° [65]. The first dwarf spheroidal satellites: Draco, Ursa Minor, Fornax, Carina, Sculptor, Leo I, and Leo II were discovered by visual inspection of photographic plates. Recently,

more Local Group dwarf satellites have been found using a variety of methods [43, 41], the most fruitful of which has been from searching for resolved stellar populations in photometric surveys such as the Sloan Digital Sky Survey (SDSS). Willman et al. were the first to discover a new dwarf galaxy, Ursa Major [99] as well as Willman 1 [97] in 2005, using SDSS to perform a systematic search for these objects in 2002 [98]. The discovery of Canes Venatici, Bootes I and Ursa Major II by Belokurov et al. in 2006 [42, 5, 105, 104] quickly followed. In 2007 a host of new dwarfs were found, including: Coma Berenices, Canes Venatici II, Segue 1, Hercules, and Leo IV by Belokurov et al [4] and Bootes II by Walsh et al. [93]. In 2009, Grillmair et al. discovered probable dwarf galaxy Bootes III as a stellar debris stream [30], and Belokurov et al. discovered Segue 2 [3], one of the faintest dwarf satellites known ($M_v = -2.5$).

Distances, morphologies, half-light radii, velocities, V and B-band magnitudes, and derived SDSS r-band magnitudes of known dwarf satellites of the Local Group have been compiled from various sources, including Mateo [65], Willman et al. [99], Belokurov et al. [4] and Irwin [42] are presented in Table(s) 2.1 and 2.2. Here, we focus on dwarf spheroidal galaxies and exclude satellites like M33 from our analysis as we are interested in probing the morphologies and photometry of known Local Group dwarf galaxies with the intent of studying analogues of this satellite population in more distant galaxy groups. For the Local Group dwarf spheroidals we have derived SDSS r-band magnitudes following the colour conversions between photometric magnitude systems presented in Fukugita et al. (1995) [27]. Fukugita performed a synthetic study of galaxy colours in various photometric band systems, and from these obtained colour transformation laws among various photometric band systems. Following Mateo [65], the integrated absolute r-band magnitudes in Tables 2.1 and 2.2 are used to plot the luminosity function for the Local Group dwarfs (Figure 2.2). The Schechter function is often used as a fit for the luminosity distributions of galaxies, giving the number of galaxies per magnitude bin:

$$\Phi(L)dL = n^* \left(\frac{L}{L^*}\right)^{\alpha} \exp\left(\frac{L}{L^*}\right) d\left(\frac{L}{L^*}\right) \tag{2.1}$$

L^*: characteristic galaxy luminosity where the power-law form of the function cuts off
n^*: normalization at L^*

The Schechter function, which was originally used by Paul Schechter to fit the luminosity distribution of galaxies in Abell clusters, results in an excellent fit. It is interesting to note that the Schechter function fit to the luminosity function of the Local Group (Figure

2.2) extrapolated to lower magnitudes suggests that the Local Group may contain many (undiscovered) galaxies less luminous than $M_B = -12$ [65].

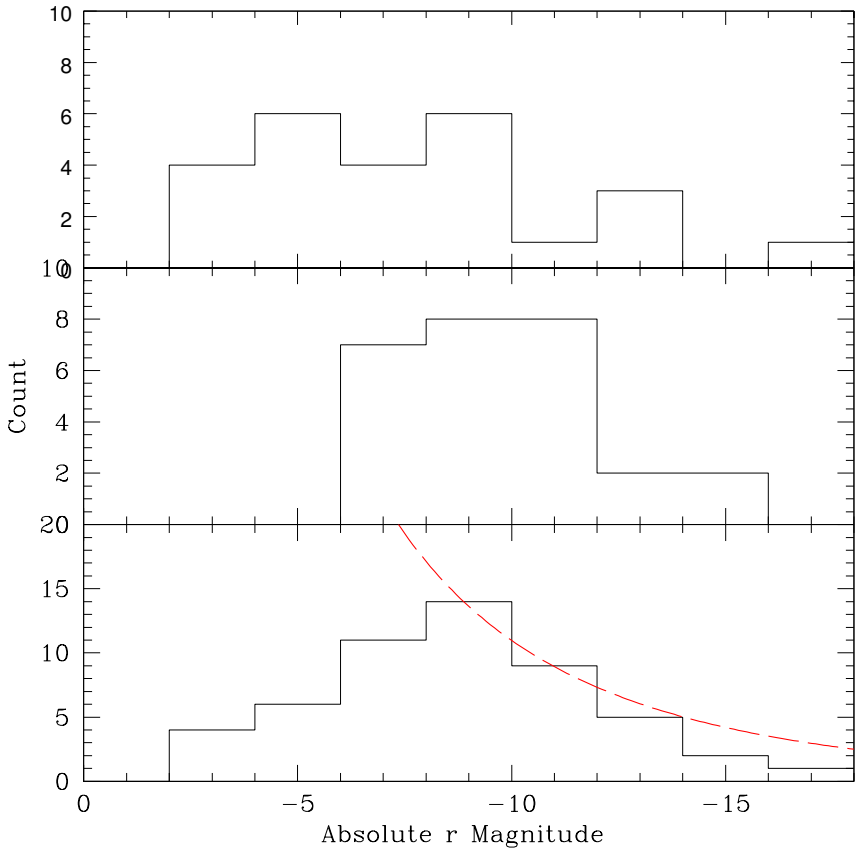

Figure 2.2: The luminosity function for the Milky Way (top), Andromeda (middle), and the combined Local Group (bottom). The Schechter function is shown as a red dashed line. Here, the Schechter function indicates that there are likely many undiscovered galaxies less luminous than $M_B = -12$ [65].

Half-light radii and integrated absolute r-band magnitudes are used to plot the magnitude-size relation for Local Group dwarfs (Figure 2.3). This relation will become important later when we describe our methodology for searching for dwarf satellite galaxies based on the

properties of the Local Group dwarfs.

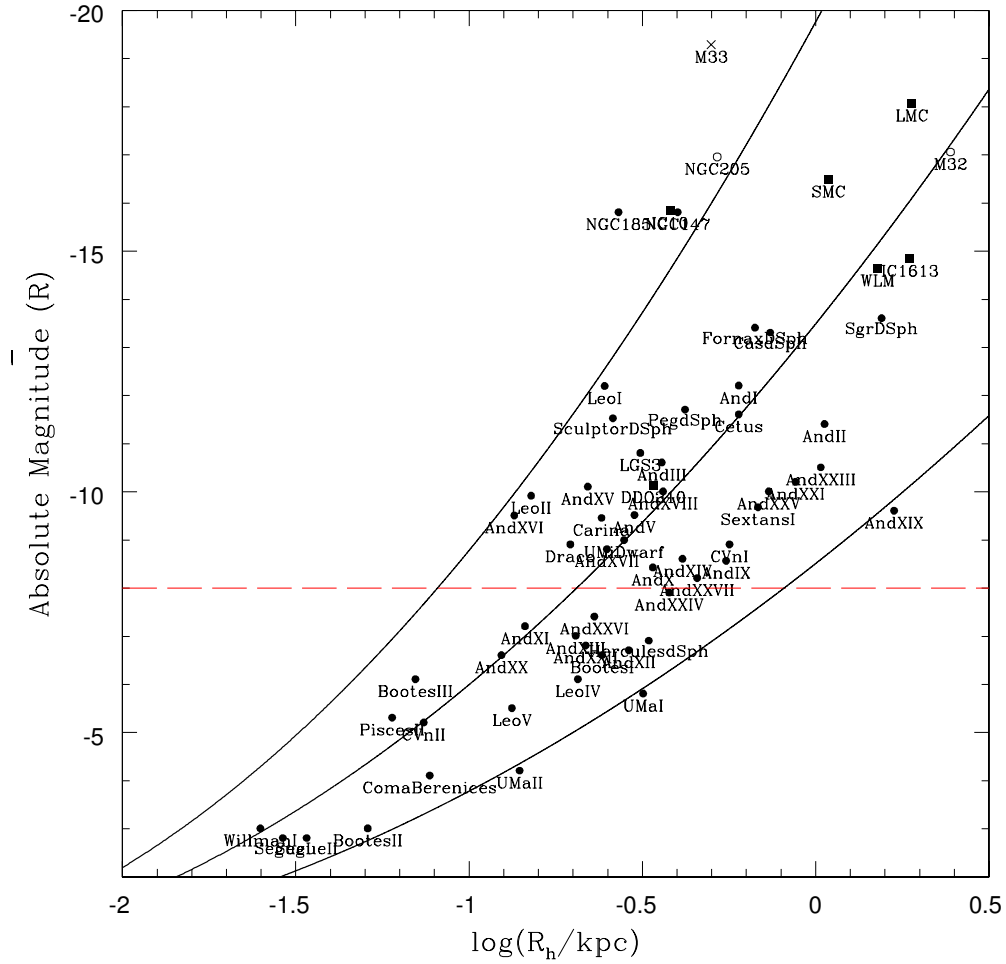

Figure 2.3: Here we show the location on the plane of absolute magnitude vs. half-light radius of the Local Group dwarf galaxies. Lines of constant surface brightness are shown in black. A (red dashed) line corresponding to absolute magnitude -8, delineating the ultra-faint from the classical dwarfs, is also plotted. We plot dwarf spheroidal galaxies as solid circles, dwarf elliptical galaxies as open circles, irregular galaxies as solid squares and spiral galaxies (M33) as crosses.

The color-magnitude diagram of the Local Group is presented in Figure 2.4, based on the integrated V-band absolute magnitudes [65] where available, and M_{V0} and $(B-V)_0$ colours. We show the colour-magnitude plot for Local Group dwarf satellites here as these properties will become important when we describe our methodology for searching for dwarf satellites in the next chapter.

Galaxy	**T-Type**	**RA** (J2000)	**DEC** (J2000)	$\mathbf{V}_{\mathrm{MW}}$ (km/s)	$\mathbf{M}_V$ (mag)	$\mathbf{M}_B$ (mag)	$\mathbf{M}_R^*$ (mag)	$\mathbf{R}_{\mathrm{eff}}$ (kpc)	**D** (mpc)
Ursa Minor	-3	227.285	70.3375	-85	-7.13	-8.69	-9	0.063	0.280
Carina	-3	100.403	-35.5083	7	-8.97	-9.15	-9.46	0.10	0.241
Sculptor	-3	15.0388	-22.3625	77	-9.77	-11.22	-11.53	0.088	0.260
Draco	-3	260.052	70.7292	-98	-8.74	-8.6	-8.91	0.079	0.196
Sextans I	-3	153.262	8.22083	74	-7.98	-9.37	-9.68	0.086	0.682
Fornax	-3	39.9971	-27.2625	-36	-11.50	-13.1	-13.41	0.14	0.668
Leo II	-3	168.37	24.275	22	-9.23	-9.61	-9.92	0.21	0.151
Leo I	-3	152.117	16.5958	177	-10.97	-11.89	-12.2	0.25	0.246
Sagittarius	-3	292.498	-6.7875	171	-12.67	-13.3	-13.61	0.024	1.550
Ursa Major I	-3	158.72	64.8	1149	-	-5.5	-5.81	0.101	0.318
Ursa Major II	-3	132.875	64.95	-17	-	-3.9	-4.21	0.035	0.140
Bootes I	-3	210.025	21.5	107	-	-6.3	-6.61	0.061	0.242
Bootes II	-3	209.5	24.75	-116	-	-2.7	-3.01	0.052	0.051
Bootes III	-3	209.3	38	-	-	-5.8	-6.11	0.049	0.070
Segue I	-3	151.767	17.2292	111	-	-2.5	-2.81	0.023	0.029
Segue II	-3	34.8167	22.6292	43	-	-2.5	-2.81	0.035	0.034
Coma Berenices	-3	186.746	36.5625	82	-	-3.8	-4.11	0.044	0.077
Leo IV	-3	173.237	8	10	-	-5.8	-6.11	0.158	0.206
Leo V	-3	172.79	5.3	59	-	-5.2	-5.51	0.178	0.133
Pisces II	-3	89.2875	19.2875	-	-	-5.0	-5.31	0.180	0.060
CVn I	-3	202.015	41.3375	78	-	-8.6	-8.91	0.215	0.564
CVn II	-3	194.292	38.8125	-96	-	-4.9	-5.21	0.151	0.074
Hercules	-3	247.758	23.875	145	-	-6.6	-6.91	0.135	0.330
Willman I	-3	162.338	51.75	35	-	-2.7	-3.01	0.042	0.025
LMC	9	13.1867	-59.5708	84	-18.2	-17.93	-18.07	2.6	0.050
SMC	9	80.8937	-57.6583	17	-16.7	-16.35	-16.49	1.0	0.063

Table 2.1: Properties of the known dwarf spheroidal satellites and the Magellanic Clouds, compiled from Mateo [65], Willman et al. [99], Belokurov et al. [4, 3, 2], Lokas et al. [60], McConnachie and Cole [66], and the NASA/IPAC Extragalactic Database (NED) (http://ned.ipac.caltech.edu).

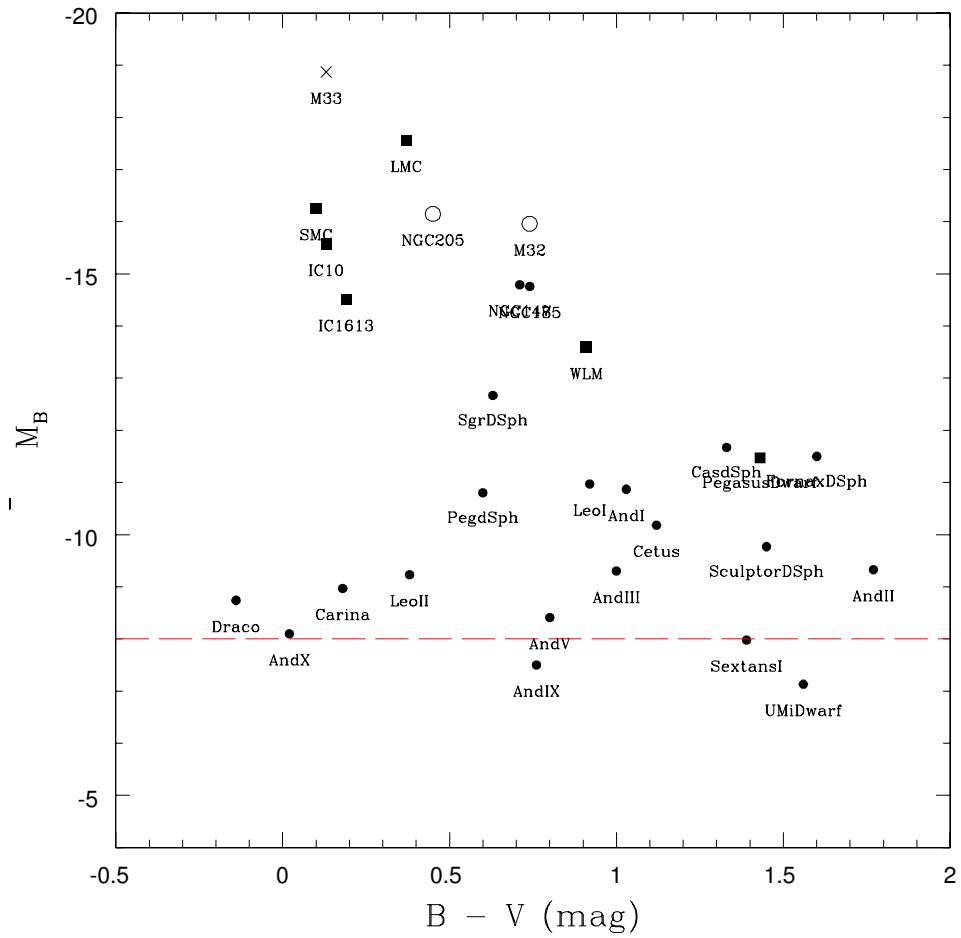

Figure 2.4: A plot of Local Group dwarf B-V colour vs. absolute (B-band) magnitude for satellites that have published B and V magnitudes. Here again, we distinguish the classical dwarfs from the ultrafaint with a red, dashed line corresponding to absolute magnitude -8. We plot dwarf spheroidal galaxies as solid circles, dwarf elliptical galaxies as open circles, irregular galaxies as solid squares and spiral galaxies (M33) as crosses.

Galaxy	**T-Type**	**RA** (J2000)	**DEC** (J2000)	$\mathbf{M}_V$ (mag)	$\mathbf{M}_B$ (mag)	$\mathbf{M}_R^*$ (mag)	$\mathbf{R}_{\text{eff}}$ (kpc)	**D** (mpc)
AndI	-3	11.4158	38.6167	-10.87	-11.9	-12.21	0.81	0.60
AndII	-3	19.1242	39.2875	-9.33	-11.1	-11.41	0.68	1.06
AndIII	-3	8.89083	43.4667	-9.30	-10.3	-10.61	0.76	0.36
AndV	-3	17.5712	56.4208	-8.41	-9.21	-9.52	0.81	0.30
AndIX	-3	13.2208	45.9375	-7.5	-8.26	-8.57	0.79	0.552
AndX	-3	16.6404	56.0667	-8.1	-8.12	-8.43	0.70	0.339
AndXI	-3	11.5833	45.0208	-	-6.9	-7.21	0.87	0.145
AndXII	-3	11.8625	39.6208	-	-6.4	-6.71	0.85	0.289
AndXIII	-3	12.9625	33.0667	-	-6.7	-7.01	0.87	0.203
AndXIV	-3	12.8958	39.4542	-	-8.3	-8.61	0.74	0.413
AndXV	-3	18.5779	39.7625	-	-9.8	-10.11	0.770	0.220
AndXVI	-3	14.8742	37.65	-	-9.2	-9.51	0.525	0.135
AndXVII	-3	9.27917	48.8333	-	-8.5	-8.81	0.79	0.250
AndXVIII	-3	0.560417	46.3333	-	-9.7	-10.01	1.36	0.363
AndXIX	-3	4.88375	35.6542	-	-9.3	-9.61	0.93	1.683
AndXXI	-3	358.699	49.0625	-	-9.9	-10.21	0.86	0.875
AndXXIII	-3	22.3408	48.7833	-	-10.2	-10.51	0.77	1.035
AndXXV	-3	7.53708	58.7792	-	-9.7	-10.01	0.812	0.732
NGC185	-3	9.74167	53.0625	-14.76	-15.5	-15.81	0.62	0.27
NGC147	-3	8.30042	55.6292	-14.79	-15.5	-15.81	0.76	0.40
CasdSph	-3	351.632	60.1375	-11.67	-13.0	-13.31	0.79	0.74
PegdSph	-3	357.943	32.7375	-10.80	-11.4	-11.71	0.82	0.42
AndXX	-	1.87792	36.9833	-	-6.3	-6.61	0.80	0.124
AndXXII	-	21.9167	29.3542	-	-6.5	-6.81	1.00	0.217
AndXXIV	-	19.625	51.4917	-	-7.6	-7.91	0.60	0.378
AndXXVI	-	5.94	60.7417	-	-7.1	-7.41	0.762	0.230
AndXXVII	-	9.36292	50.8042	-	-7.9	-8.21	0.757	0.455

Table 2.2: Properties of the known dwarf spheroidal satellites of Andromeda, and those whose morphology is undetermined, compiled from Mateo [65], McConnachie and Irwin [68], McConnachie et al. [67], Richardson et al. [81], Martin et al. [63], Irwin et al. [44], Majewski et al. [62], Zucker et al. [106], and the NASA/IPAC Extragalactic Database (NED) (http://ned.ipac.caltech.edu).

The number of known dwarf satellites of the Local Group has more than doubled in the last 10 years. Is it possible that there are enough undiscovered dwarf galaxies to resolve the missing dwarf problem? Authors like Mateo have speculated that there could be as many as 15-20 Local Group galaxies remaining to be found at low altitudes, up to half of which being satellites of the Milky Way [65]. The prospects of finding hidden galaxies at low altitudes using HI observations is summarized by Henning [37]. Although observa-

tions at 21 cm offer the ability of illuminating the zone of exclusion, these observations are faced with the challenge of distinguishing between clouds of neutral hydrogen in the Milky Way that are moving with respect to the galactic rotation, known as low-velocity galactic emission, and the Milky Way satellites. Also, as Mateo points out [65], early-type dwarfs known to be gas-poor would not be detected.

Whether the Local Group is statistically representative of other galaxy groups, and the Local Group dwarfs representative of all dwarf galaxies, is still an open question [94]. In the next section we introduce the neighbouring galaxy groups and, after discussing suitability for comparison, examine whether the Local Group is typical in the limited context of the local universe to 5 Mpc.

2.2 The Karachentsev Catalogue

Within 10 Mpc of the Local Group, there exist several galaxy groups. These galaxies groups have been studied extensively by Karachentsev et al. [48],[50],[49],[51],[52]. The Karachentsev Catalogue is an all-sky catalogue of the 451 nearest galaxies published in 2004 by Karachentsev et al. [50], with each galaxy having a distance estimate $\leq$ 10 Mpc or a radial velocity $V_{LG} < 550$ km/s. The catalogue is a compilation of the basic optical and HI properties of neighbouring galaxy groups, in particular: diameters, absolute magnitudes, morphological types, circumnuclear region types, optical and HI surface brightnesses, rotational velocities, mass-to-luminosity and HI mass-to-luminosity ratios, and a quantification of the galaxy environment known as the tidal index. While many more dwarf galaxies have been detected since the publication of this catalogue in the Local Group alone, it is still a useful resource for the properties of more distant galaxy groups within 10 Mpc. In this section, following Karachentsev et al. 2007 [48], we introduce the nearest galaxy groups and briefly discuss their properties and suitability for comparison to the Local Group, before making a comparison between these groups to the Local Group.

2.2.1 The M81 Group

The M81 group is a galaxy group at 3.6 Mpc from the Local Group [23], centred on the giant spiral galaxy M81 in the constellation Ursa Major. Karachentsev et al. [48] provide both

orbital and virial mass estimates for this group, where the virial mass is calculated from the measured radial velocity dispersion with respect to the group centroid and applying the virial theorem to obtain a mass estimate assuming spherical symmetry and isotropic velocity dispersions. A robust estimator of the mass - the "orbital" mass of the galaxy group is the mass inferred from Kepler's second law using the ensemble average of the product of the spatial separation (R_p) and the velocity offset (ΔV_r) of each companion

$$M_{\rm orb} \propto \langle R_p \Delta V_r^2 \rangle,$$

assumed to be moving on Keplerian orbits with average eccentricity $e = 0.7$ [48]. The orbital mass of this group has been estimated at $1.17 \times 10^{12} M_\odot$, and virial mass $1.97 \times 10^{12} M_\odot$ [48]. The M81 group has slightly more detected satellites than the Milky Way and M31, as the count currently stands at 29. The velocity dispersion in this group is $\sigma_V = 91$ km/s [48]. The most prominent galaxies of the group: Messier 81, Messier 82, and NGC 3077 have been shown to be strongly interacting with each other based on observations of the HI content of the group (Yun et al. 1994 [101]). Strong starburst activity at the centres of Messier 82 and NGC 3077 has resulted from gas that has been stripped as a result of the interaction and fallen into the centres of these galaxies, creating filamentary gas structures ("tidal bridges") within the group.

2.2.2 The Centaurus A/M83 Group

Located at distances of 3.8 Mpc [36] and 3.66 Mpc respectively, galaxy subgroups centred around radio-loud elliptical galaxy Centaurus A and face-on spiral galaxy M83 galaxy together form the CenA/M83 complex, a Local Group analogue of two galaxy subgroups that are separated by 1.43 ± 0.11 Mpc [52]. Together these subgroups host a total of 42 known dwarf satellites. Velocity dispersions of Centaurus A group is $\sigma_V = 105$ km/s and $\sigma_V = 71$ km/s for M83 [48], indicating that the Centaurus A group is much more massive than the M83 subgroup. The masses of either subgroup have been estimated by Karachentsev, with the Centaurus A subgroup having a $4.89 \times 10^{12} M_\odot$ virial mass and $2.88 \times 10^{12} M_\odot$ orbital mass, and the M83 subgroup having a $1.09 \times 10^{12} M_\odot$ virial mass and $1.00 \times 10^{12} M_\odot$ orbital mass [52]. The total mass of the Centaurus A/M83 Complex is therefore estimated to be $\sim 6 \times 10^{12} M_\odot$. The Hubble flow around the Centaurus A/M83 complex has been studied by Karachentsev et al. 2007 [101], and it was found that the centroids of both groups have a very small peculiar velocity of $v_P < 25$ km/s [48]. Centaurus A is believed to have interacted recently and this is discussed in more detail in the last section in this chapter.

2.2.3 The IC342/Maffei Group

The IC342/Maffei Group is a binary galaxy group known to host 16 satellites galaxies in total, with the IC342 and Maffei subgroups hosting 8 each. The IC342 subgroup is centred on the giant face-on spiral galaxy IC342 at a distance of 3.3 ± 0.3 Mpc and has a velocity dispersion of $\sigma_V = 54$ km/s, virial mass estimated by Karachentsev et al. as $0.57 \times 10^{12} M_\odot$ and orbital mass $0.95 \times 10^{12} M_\odot$ [48]. The Maffei subgroup is centred on the brightest members of the Maffei subgroup, giant elliptical galaxy Maffei 1 and intermediate spiral galaxy Maffei 2 and has a velocity dispersion of $\sigma_V = 59$ km/s, virial mass $0.65 \times 10^{12} M_\odot$, and orbital mass $1.35 \times 10^{12} M_\odot$ [48]. The IC342/Maffei complex lies close to the plane of the Milky Way and is therefore obscured by galactic dust and stars, so the satellite list for this group is very likely to be incomplete.

In the following section we compare the Local Group to neighbouring galaxy groups and subgroups: M81, M83, Maffei, CenA, and IC342. We study satellite spatial distribution, clustering, and velocity offset as our basis for comparison. We exclude from our comparison the Canes Ven I Cloud and the Sculptor Filament because these systems are not virialized [48]. In unvirialized systems, individual satellite galaxy dynamics do not map to the gravitational potential of the group [8] and therefore are unsuitable for comparison with virialized systems. The virial radii $r_{\rm vir}$ used were calculated from estimates of the virial masses from Karachentsev et al. [48], where r_{200} is used as a good approximation of the virial radius (Equation 1.2).

2.2.4 Spatial Distribution of Satellite Galaxies

The satellite distributions for 3 projections of the Milky Way, Andromeda, and neighbouring galaxy groups scaled to the virial radius of the group are presented in Figure 2.6, with 1/2, 1, and 2 virial radii indicated by dotted, dashed and solid circles, respectively. Padilla measured the clustering of galaxy groups in the 2dFGRS Percolation-Inferred Galaxy Group (2PIGG) catalogue, finding that the degree of clustering of groups increases with increasing group luminosity [75]. While the Centaurus A group represents the median in the absolute magnitudes of neighbouring galaxy groups reported by Karachentsev [48], it is the least strongly clustered. While it is also the case that within groups, early-type galaxies tend to be more centrally concentrated [29], we see from Figure 2.7 that the satellites of Centaurus A are only marginally more clustered or closer to the center than late types. While most of these appear spatially clustered within the first virial radius of the

central galaxy, as are the satellite galaxies of the Milky Way and Andromeda, the Centaurus A group is an interesting exception. Figure 2.5 shows the cumulative number count as a function of distance from the central galaxy normalized to the virial radius of the galaxy. While most groups show a cumulative count that flattens near the virial radius of the group, we see that the Centaurus A group defies the trend, having a much lower count for smaller radii and turning off much further past the virial radius than the other groups. We have used a Kolmogorov-Smirnov test [80], the maximum value of the absolute difference between the cumulative distribution function of galaxy counts of Centaurus A and the mean of the other neighbouring galaxy groups in the sample, and from this we quantify the difference between the mean distribution S_0 and Centaurus A distribution S, finding a KS statistic of

$$D = \max_{-\infty<x<\infty} |S_0(x) - S(x)| = 0.41$$

This gives a probability of less than 1% that the spatial distribution of satellite galaxies of Centaurus A is drawn from the same statistical distribution as that of the other groups; this is a disproof of the null hypothesis that the distributions are the same.

2.2.5 Velocity Offset

Satellite galaxies that are gravitationally bound to a group have fallen into the group and therefore do not appear to be moving with the local Hubble flow, as one would expect from Hubble's Law. Rather, they move with the central galaxy to a peculiar velocity v_p, the radial component of the orbital velocity of the satellite about the central galaxy, and have a total radial velocity $v_r = v_c + v_p$, where v_c is the radial velocity of the central galaxy assuming that the galaxy has fallen into a fixed potential. By computing the velocity dispersion of the group, radial velocities of satellite galaxies provide an estimate the mass of these neighbouring galaxy groups via the virial theorem [48]. Virial masses of galaxy groups that far exceed mass estimates from luminous matter alone also provide an indication of (the amount of) dark matter present in these groups. Figure 2.8 shows the velocity offset Δv from the central member of the known satellites of the neighbouring galaxy groups presented in Karachentsev [48], as well as the stacked version and the Local Group, for comparison.

We expect from the virial theorem that the kinetic energy of associated satellites is $K = -U/2$, and therefore with the simplifying assumption of a satellite of mass m in

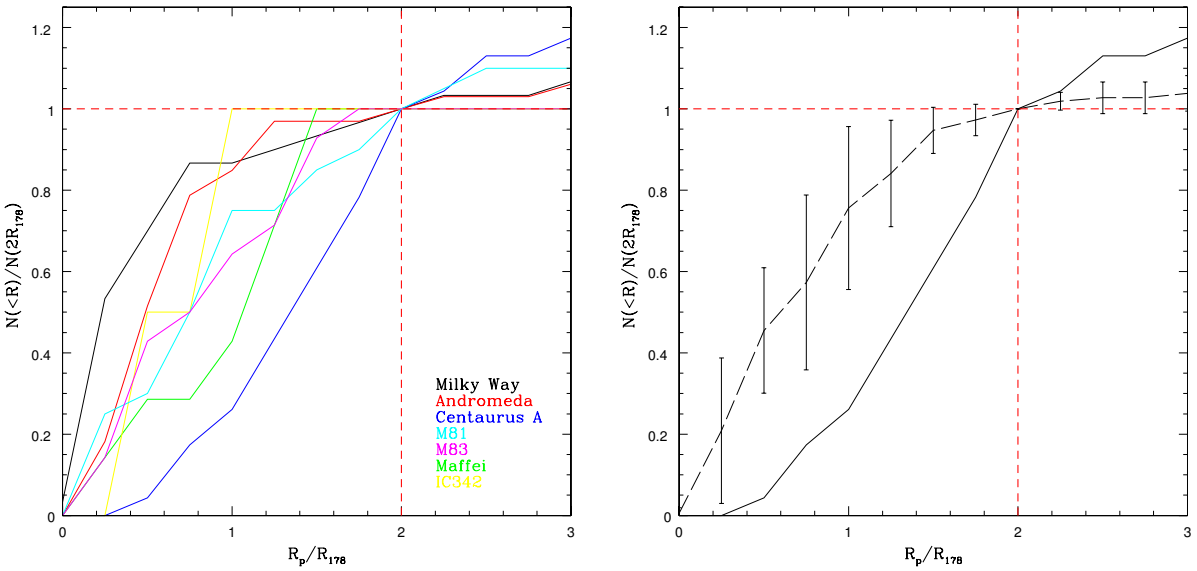

Figure 2.5: The cumulative satellite number counts of Milky Way, M31, M81, M83, Maffei, IC342, and CenA galaxy groups normalized to the virial radius of the central galaxy (left). On the right we compare Centaurus A (solid line) to the mean distribution of the other galaxy groups (dashed), showing standard deviation plotted as error bars.

circular orbit about a central galaxy with mass $M >> m$ we have a circular velocity of

$$v_c^2 = \frac{GM}{2r}.$$

Since we are able to measure velocities only along the line of sight, we expect that the maximum (radial) velocity of these satellites will occur at the turnaround radius of the group, when $v_r = v_p$. With the masses of these groups inferred from the orbits of their satellites on the order of $10^{12} M_\odot$ [48], we expect the maximum radial velocity of the satellite galaxies to go as

$$v_{\max} \sim \pm\sqrt{\frac{10^{12}\mathrm{M}_\odot \times G}{2r}}\ \mathrm{km/s}.$$

In Figure 2.8 we indicate this maximum radial velocity as a dashed line. Most satellite galaxies are contained within this envelope, confirming their association, and indeed Karachentsev has shown σ_V for each of these groups ranges from 54 km/s for IC342 to

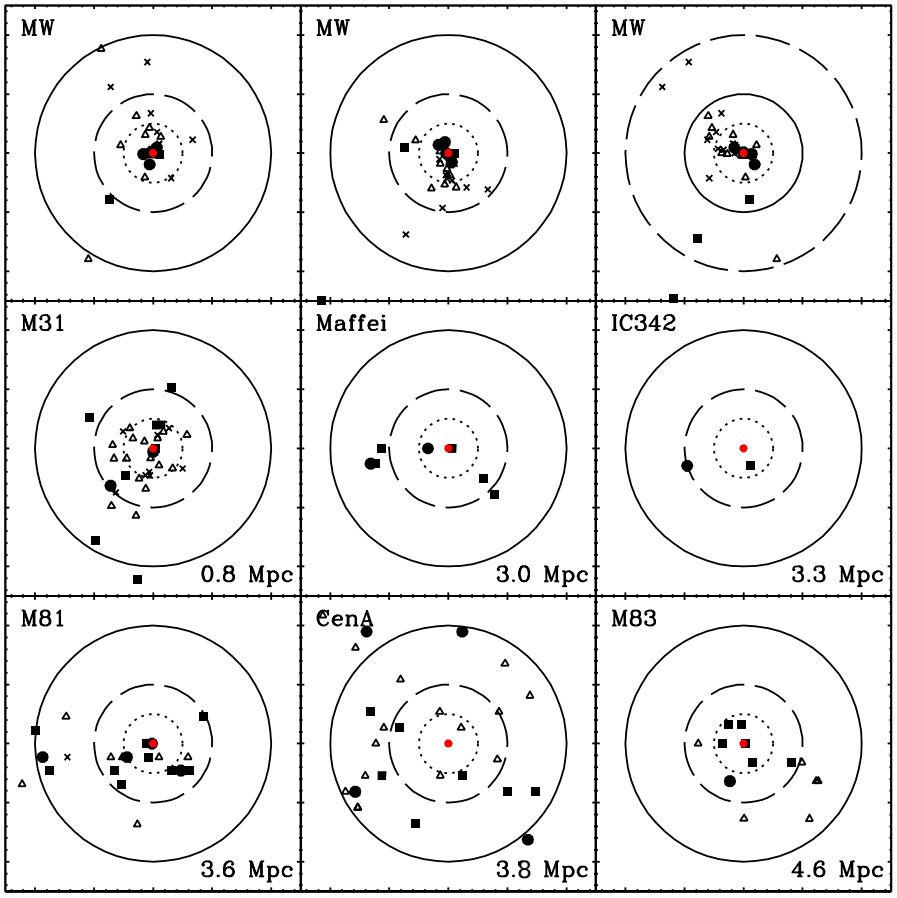

Figure 2.6: Projected satellite positions scaled to the virial radius of the host galaxy, for the Milky Way (3 projections), M31, M81, M83, Maffei, IC342, and CenA galaxy groups. Here we indicate satellite absolute magnitude by symbol, with the faintest satellites (with $M > -8$) indicated by a cross, satellites with $-12 \leq M < -8$ by open triangles, brighter satellites with $-16 \leq M < -12$ by filled squares, and the brightest satellites ($M < -16$) by closed circles. Here, we show the 0.5, 1, and 2 virial radii by dotted, dashed, and solid lines, respectively.

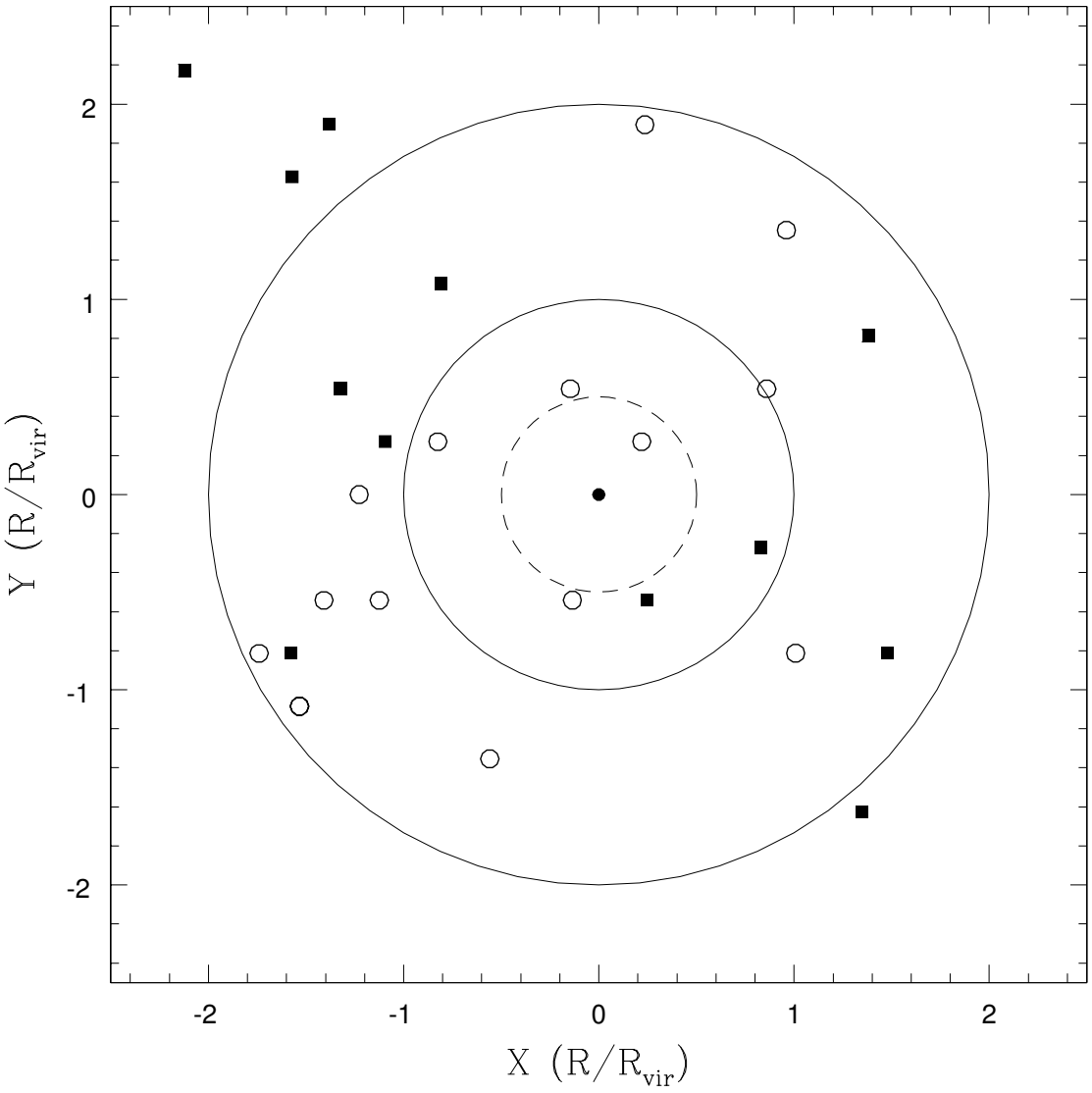

Figure 2.7: Projected positions of satellite galaxies of the Centaurus A subgroup scaled to the virial radius. Satellites are broken down by morphology, to early (open circle) and late-type (filled square).

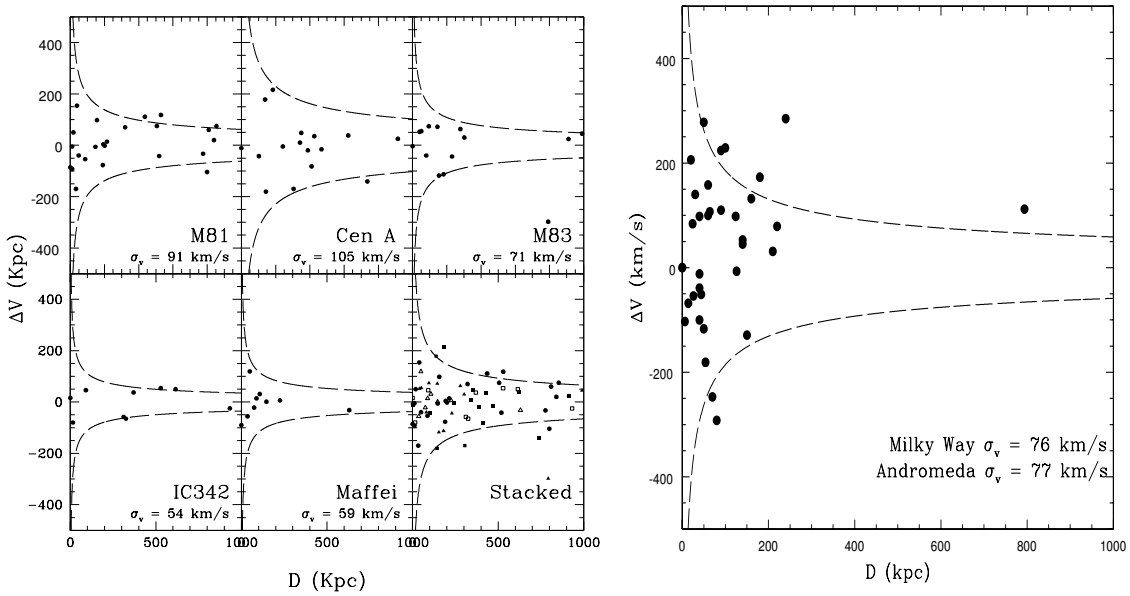

(a) Neighbouring groups

(b) Local Group

Figure 2.8: Plot of velocity offset vs. distance for the satellites of neighbouring galaxy groups. Maximum radial velocities indicated based on the virial radius of each group (dashed line). The same plot is shown for the Local Group on the right.

91 km/s for M81, with Centaurus A having the largest $\sigma_V = 105$ km/s. It is important to note that some of these satellites are believed to have just begun infall and that these groups have not finished collapsing; the Local Group, for instance, is expected to merge with Andromeda in ≈ 4 Gyr [92]. In the context of velocity offset from the central galaxy, these neighbouring galaxy groups appear roughly analogous to the Local Group, with the satellite galaxies of Centaurus A having the largest velocity dispersion of $\sigma_V = 105$ km/s [48].

2.2.6 The Curious Case of Centaurus A

The Centaurus A group, which is dominated by the active radio galaxy Centaurus A (NGC 5128) appears to be an exception to the trends found in the dwarf galaxy populations of

the neighbouring galaxy groups. Although most of the properties of Centaurus A are not unlike that of other luminous early-type galaxies, the galaxy itself shows unusual features that are generally regarded as overwhelming evidence of of past merger activity.

While there has been considerable debate in the literature as to the morphology of Centaurus A, with opinions split between elliptical and lenticular morphologies, here we adopt the convention of Harris [35] and consider Centaurus A a giant elliptical galaxy. Centaurus A hosts a radio source with giant outer lobes extending to 250 kpc and a complex structure [45]. Prominent features in the jets include bright knots in the optical, the roughly S-shaped structure of the radio lobes and filamentary structures in the inner lobes [45]. The origin of the radio source has been suggested as evidence of past merger activity, with the accumulation of matter onto the center via the transfer of angular momentum from viscous damping as a consequence of merger activity [45]. Also consistent with a merger event is the warped morphology of the radio lobes and disk, with the lobes appearing to be in the same direction as the central dust lane. The dust lane itself provides more hints of past merger history, as it is a site of active star formation, as starburst activity is a consequence of gaseous inflows of a merger.

Interestingly, Centaurus A in the only giant elliptical central galaxy in our sample of neighbouring galaxy groups. As such, we are interested to know if the properties of the dwarf satellites in this group are different from those of neighbouring galaxy groups, and hence if group properties are dependent on central galaxy morphology in general. In the preceding sections we have seen that the Centaurus A satellite galaxies are unusual in several respects. It is clear that the dwarfs of the Centaurus A group are not heavily clustered within the virial radius of the host galaxy, as appears to be the trend with other neighbouring galaxy groups (Figures 2.6,2.5). They have the largest velocity dispersion of the sample, $\sigma_v = 105$ km/s. The group itself is unusual in that several of the most prominent members of the Centaurus A group: NGC 4945, NGC 5236, and NGC 5253 also show unusually high rates of star formation [45], suggesting these galaxies were involved in past merger-activity. Centaurus A also has an anomalously large number of early-type dwarfs, with about 60% of the total being early-type [65], having more luminous early-types than in our own Local Group [48]. This observation is consistent with expectations of a more evolved group.

As we investigate the dependence of the statistical population of satellites on central galaxy mass and morphology, we will have an opportunity to see if our results are in concordance with the trends found in satellite galaxies of the Centaurus A group, and whether

the properties of group satellites are dependent on central galaxy morphology.

2.2.7 Sample Completeness

In Figure 2.9 we show the absolute magnitudes of known galaxies to 42 Mpc from the Karachentsev and Tully V8k catalogues. Beyond 1 Mpc, few galaxies fainter than $M_V \sim -10$ are known, and beyond 10 Mpc this limit increases to $M_V \sim -15$. Compared to a median absolute magnitude of satellite galaxies of the Local Group of ~ -9, the median absolute magnitude of the satellite galaxies of nearby galaxy groups increases to -14.5 magnitudes at 8 Mpc, showing a lack of known faint galaxies at the edge of the Local Volume. If we assume our sample of satellite galaxies within the Local Group is nearly complete, this indicates that there may be hundreds of faint, undiscovered galaxies within our own extragalactic backyard, within 10-40 Mpc of the Local Group. In the next chapter we present a method for detecting faint satellite galaxies around a complete sample of bright, isolated spiral and elliptical primaries that extends to 42 Mpc.

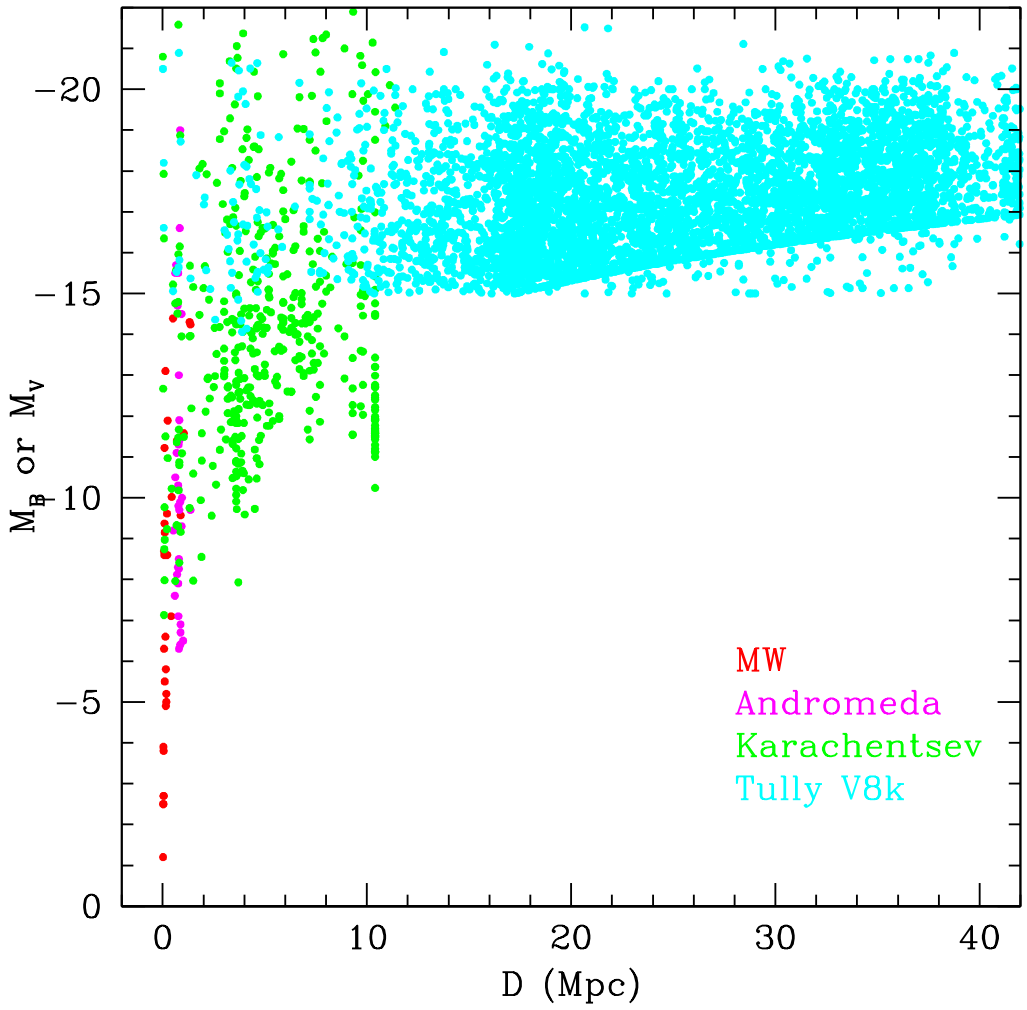

Figure 2.9: The absolute magnitudes of known galaxies as a function of distance, including those of the Milky Way (red) and Andromeda (magenta). Also included are the Karachentsev (green) and Tully V8k (blue) catalogues, which include galaxies with radial velocities $v < 550$ km/s and $v < 8,000$ km/s, respectively.

Chapter 3

Searching for Faint Satellites in SDSS

Simulations predict that large spiral galaxies such as the Milky Way or M31 form inside extended dark matter halos. These dark matter halos form as a conglomeration of smaller dark matter subhalos. These subhalos are predicted to survive the accretion and merging process to host satellite galaxies. Observationally, we find a lack of dwarf galaxies believed to populate these subhalos in the nearest observable group - the Local Group. The Local Group offers the most complete sample of dwarf galaxies with which we can compare to simulations of CDM structure formation due to magnitude limits of imaging surveys. So far it has been challenging to reconcile theory with observation, leading to the so-called "missing dwarf problem". Our conclusions on the success or failure of structure formation in the ΛCDM model have been based on comparison with the Local Group alone, and whether the Local Group is statistically representative of other galaxy groups is unknown. Within the nearest 5 Mpc there exist several other galaxy groups that appear roughly analogous to the Local Group with an interesting exception in Centaurus A. Centaurus A is the only elliptical central galaxy of the nearby groups, which has had an active merger history but otherwise suggests that dwarf galaxy populations may be dependent on central galaxy morphology. In order to make firm conclusions, we require samples of satellites around a larger number of bright central galaxies.

In this section we describe our methodology for obtaining a statistical sample of satellite galaxies around a complete sample of bright central galaxies to a distance of 42 Mpc. We provide a description of how we construct an isolated sample of bright primaries, providing the foreground around which we search for satellite galaxies in the photometric and spectroscopic catalogues of the Sloan Digital Sky Survey. We then describe how we obtain the background around each of our primaries and make cuts on the data in order to statis-

tically discern associated structure from background galaxies when the samples are stacked together. This section addresses the problem of uncertain satellite real-space position and non-uniform background. We then perform a preliminary estimate of the signal and signal to noise that we might expect to find after making a few simple assumptions. In the final section of this chapter we contrast our approach with the methods of recent authors: Guo et al. (2011,2012) [33, 34]; Liu et al. (2011) [59]; Lares et al. (2011) [57]; Strigari et al. (2012) [88]; and Nierenberg et al. (2011,2012) [73, 74].

3.1 Foreground

To look for evidence of the abundance of dark matter subhalos predicted by ΛCDM we want to uncover evidence for the existence of dwarf galaxy satellites to betray the presence of such substructure. Since galaxy-sized dark matter halos are expected to form through the accretion of smaller subhalos, we require a sample of bright (primary) galaxies to search for dwarf galaxy satellites around. We construct a volume-limited sample of galaxies down to a well-defined stellar mass limit ($M_\star \geq 6 \times 10^9 M_\odot$) using the Atlas3D (http://www-astro.physics.ox.ac.uk/atlas3d/) parent sample of spiral, lenticular and elliptical galaxies, which provides a complete sample of galaxies brighter than $M_K < -21.5$ mag within the local (42 Mpc) volume.

3.1.1 Atlas3D

The primary sample of galaxies is drawn from the Atlas3D parent catalogue by Cappellari et al. 2011 [18], a carefully selected, volume-limited 1.16×10^5 Mpc^3 sample of elliptical, lenticular, and spiral galaxies brighter than $M_K = -21.5$ mag (stellar mass $M_\star \geq 6 \times 10^9 M_\odot$) to a distance of 42 Mpc. Using K-band magnitudes as the best proxy for determining stellar mass, the Atlas3D catalogue uses K-magnitudes from the Two Micron All Sky Survey (2MASS) by Skrutskie et al. 2006 [86] and is complete. It is complete in that it contains all galaxies in the nearby volume above $M_\star \geq 6 \times 10^9 M_\odot$ and is statistically representative of the nearby galaxy population [18]. Distances to the primaries were assigned by the Atlas3D team based on (in order of priority): the surface brightness fluctuation (SBF) method for the ACS Virgo Cluster Survey, SBF distance from ground-based observation, and distances from the NED-D compilation.

3.1.2 Isolation Criteria

In order to obtain a sample of potential satellites of bright primary galaxies that is free from contamination by neighbouring galaxies and galaxy clusters, an isolation criterion is applied to each galaxy in the Atlas3D parent sample. The clean subsample of primaries is selected to have no neighbours with $M_K < -21.5$ within a projected 0.5 Mpc. Any pair of Atlas3D primaries closer than a projected 0.5 Mpc is eliminated from the final sample in order to avoid overlapping samples of galaxy satellites. Also removed are any primaries projected to appear within 3° of the positions of neighbouring galaxy clusters (Virgo, Eridanus, Fornax, Antlia) on the sky. So as to avoid possible contamination with background groups and clusters, we select primaries such that there are no more than 2 galaxies found in the background within 0.25 Mpc that are within 2 magnitudes of the host. From an initial 871 galaxy Atlas3D parent sample this leaves an isolated 249 galaxy final sample consisting of the (K-band) brightest, isolated spiral and elliptical galaxies extending to 42 Mpc from the Atlas3D parent catalogue. Around this final sample, we obtain backgrounds to a projected 1 Mpc (subtending an angle of 2.86° at a distance of 20 Mpc, and 1.43° at 40 Mpc) of the host (Figure 3.1).

3.2 Background

Around each of the 249 isolated primaries, we wish to search for associated systems of satellite galaxies analogous to the dwarf galaxies of the Local Group. We search around the bright primaries using the Sloan Digital Sky survey to obtain a background to a projected 1 Mpc from the central host using the Sloan Digital Sky Survey. This poses the challenge of uncertain satellite real-space positions and non-uniform backgrounds (Figure 3.1). In order to overcome these difficulties, we stack our background distributions after cuts are made on the data, in order to reduce the noise.

3.2.1 SDSS

The Sloan Digital Sky Survey (SDSS) (http://www.sdss3.org/dr8/) is a multi-band imaging survey using a dedicated 2.5-meter telescope at Apache Point Observatory in New Mexico. The telescope is equipped with a 54-CCD imaging and astrometric camera [31] and two dual fibre-fed spectrographs. SDSS photometric data covers 14,555 square degrees on the sky with a pixel scale of 0.396 arc seconds and an average exposure time per

band of 53.9 seconds. The SDSS photometric catalogue contains an estimated 208,478,448 galaxies and has photometric magnitude limits of 22.0, 22.2, 22.2, 21.3, and 20.5 in the u, g, r, i, and z bands, respectively. SDSS spectroscopic data covers 9,274 square degrees on the sky with a wavelength coverage of 3800 - 9200 angstroms. The spectroscopic limiting (Petrosian) magnitude for main sequence galaxies of is 17.7 in the r-band. The SDSS spectroscopic catalogue contains spectra for the brightest galaxies in the main sample that were selected for spectroscopic follow-up; an estimated 952,740 galaxies. The magnitude scale used in SDSS is placed on the AB system, which is calibrated using standard stars [27].

SDSS provides several measures of galaxies' apparent magnitudes. Of these, we have chosen to use composite model (*cmodel*) magnitudes. These are calculated from the best fit of the exponential and de Vaucouleurs fits in each photometric band, using the linear combination of the two that best fits the image. Strauss et al. [87] report that cmodel magnitudes account for the effects of local seeing, are less dependent on local seeing variations than other measures, are overall a reliable estimate of the galaxy flux, and an adequate proxy to use as a universal magnitude for all types of objects. We use exponential scale radii provided by SDSS to quantify galaxy size. SDSS DR8 catalogue data is retrieved using the Catalogue Archive Server (CAS) from an SQL database and a Science Archive Server for retrieval of calibrated spectra and images. An SQL query is used to obtain the background of each galaxy in the final Atlas3D sample. The query retrieves all objects within a projected 1 Mpc from the primary to a photometric redshift of 0.15. SDSS-obtained photometric redshifts for satellites of our primary catalogue are expected to be unreliable due to the closeness of the sample (D $<$ 42 Mpc). The photometric redshift cut was chosen after obtaining SDSS photometric redshifts for known satellites with redshift-independent distance measurements. We found that distances from SDSS photometric redshifts were in excess of the redshift-independent distances by up to a factor of 15. For this reason, for primaries that extend to a distance of 42 Mpc (a redshift of 0.01), we choose an upper limit on the SDSS DR8 photometric redshift of 0.15 (Figure 3.1). The SQL returns: the SDSS object id, right ascension, declination, photometric redshift, photometry flags, object type, exponential scale radius in all imaging bands, apparent magnitude in all imaging bands, galactic extinction, and the errors in all of these quantities where available:

```
SELECT
p1.objid, p1.z, p1.zErr,
p2.objid, p2.ra, p2.dec, p2.clean, p2.flags, p2.type,
p2.expRad_u, p2.expRad_g, p2.expRad_r, p2.expRad_i, p2.expRad_z,
p2.expRadErr_u, p2.expRadErr_g, p2.expRadErr_r, p2.expRadErr_i, p2.expRadErr_z,
```

p2.cmodelMag_u, p2.cmodelMag_g, p2.cmodelMag_r, p2.cmodelMag_i, p2.cmodelMag_z,
p2.cmodelMagErr_u, p2.cmodelMagErr_g, p2.cmodelMagErr_r, p2.cmodelMagErr_i, p2.cmodelMagErr_z,
p2.extinction_u, p2.extinction_g, p2.extinction_r, p2.extinction_i, p2.extinction_z,
FROM DR8.PhotoObj **AS** p2
JOIN DR8.Photoz **AS** p1 **ON** p1.objid = p2.objid
JOIN dbo.fGetNearbyObjEq(RA,DE,DA) **AS** p0 **ON** p2.objid = p0.objid **WHERE** p1.z < .15
AND p1.z > 0

The following analysis uses the extinction-corrected photometry, where both the extinction coefficients and un-corrected photometry have been retrieved.

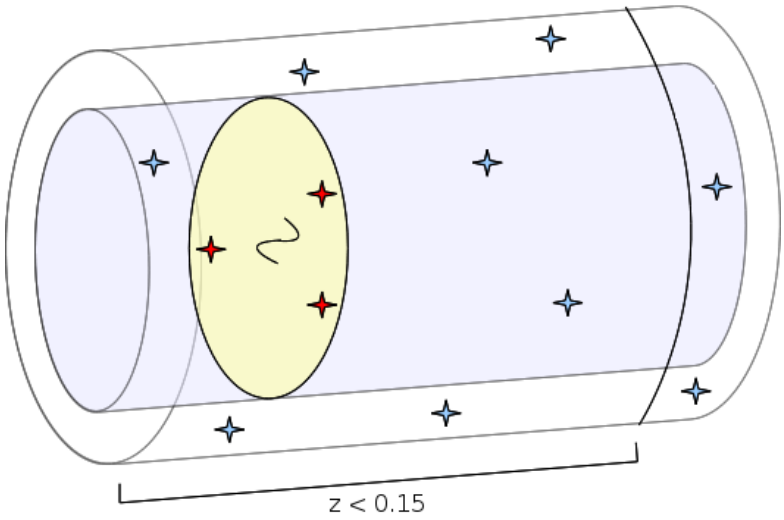

Figure 3.1: Here we show a schematic diagram of our sample selection. The cosmological volume included in the area of our search is pictured as concentric cylinders indicating the inner and outer search regions, respectively. Associated satellites are indicated in red and unassociated detections surviving the cuts shown in blue. We indicate the inner search radius as a blue cylindrical region and show the redshift restriction, which limits the inclusion of the most distant background galaxies in the sample.

3.2.2 Masking

SDSS DR8 data contains imaging "masks," which define those areas of the survey that have been excluded from analysis due to bad seeing or containing undesirable objects, such as satellite trails or bright stars that have caused bleeding in the CCD pixel data. Masked areas are identified as rectangular regions on the sky which show a deficit of data, which can be easily identified when returned detections are plotted according to their celestial coordinates. Tabular imaging mask data was not released as a part of DR8, and in order to obtain reliable background statistics such as galaxy counts in circular annuli, it is necessary to detect these masks and determine the area masked area. We correct for the effect of the masking by renormalizing the area of the mask which has been cut out of the data.

To detect masks algorithmically, a square grid is implemented as a 2D histogram with cells sized such that each cell should contain 4 uniformly distributed points, on average. Masks are detected as adjacent cells which have no points inside. Once a masked region is found (Figure 3.2) the adjacent, empty cells are added to find the area of the masked region. To test the accuracy of this procedure simulations were performed where galaxies were placed uniformly on the sky before rectangular masked regions of random size and shape are cut out of the data. It was found that the true masked area was systematically underestimated proportional to the size of the mask. A correction factor was therefore required as it was found that mask boundary cells were underestimated by approximately half. This simulation-calibrated correction factor of $1 + \alpha$, where alpha is the ratio of $1/2$ of the mask perimeter to the total masked area, was then applied and found to correct the computed mask area to reliably determine the area of masked regions in the simulation (Figure 3.3).

Masked areas are computed and plotted against the known total masked areas in simulated galaxy distributions in Figure 3.3, showing excellent agreement. Further, when the total masked area in all retrieved SDSS data is calculated as above and the total masked area is plotted as a fraction of the total area, we see that the masked area accounts for only a very small fraction of the total (Figure 3.4).

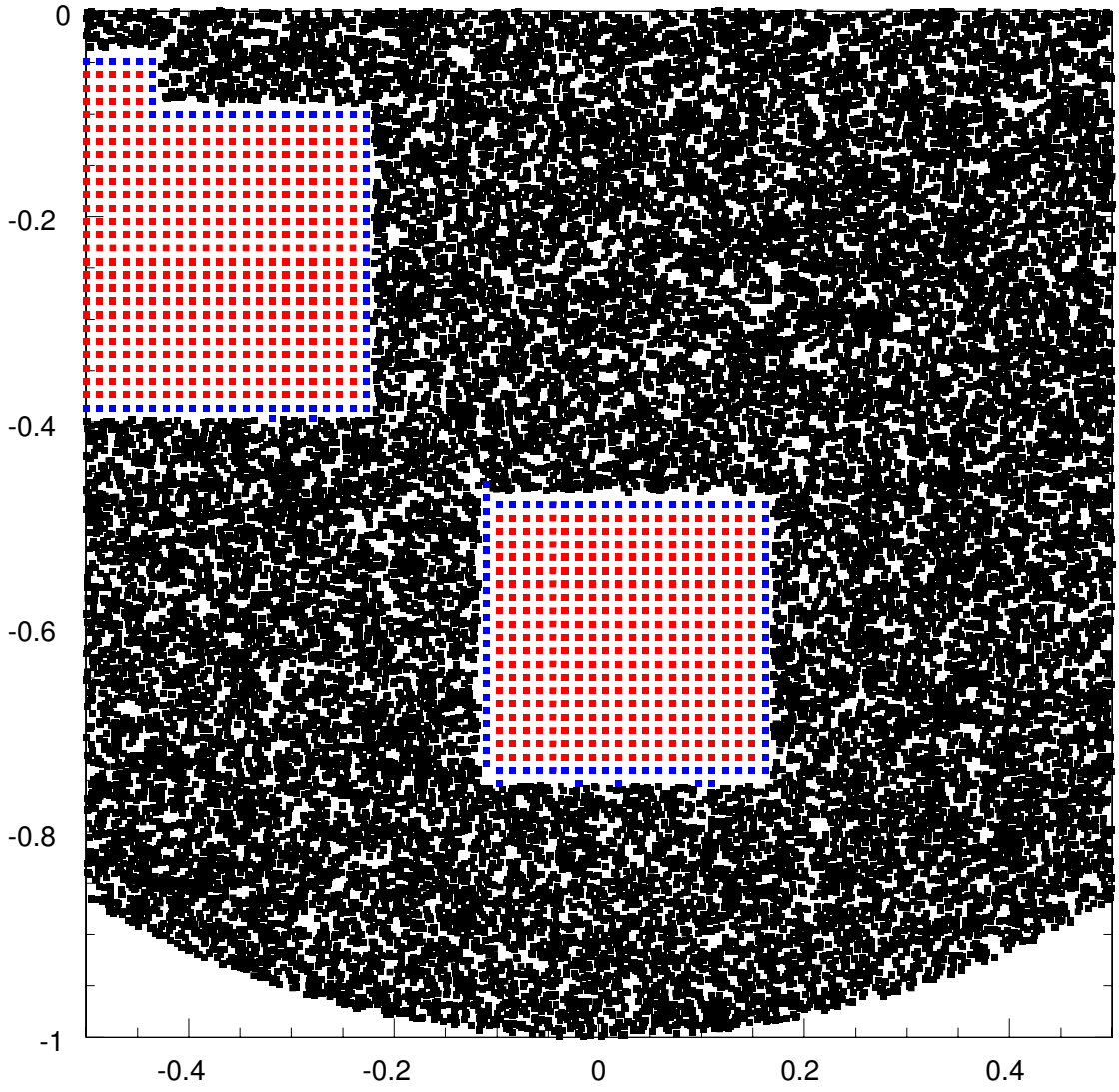

Figure 3.2: Simulated galaxy distribution with galaxies in black. Cells detected as being part of a mask are red. Blue cells indicate mask perimeter.

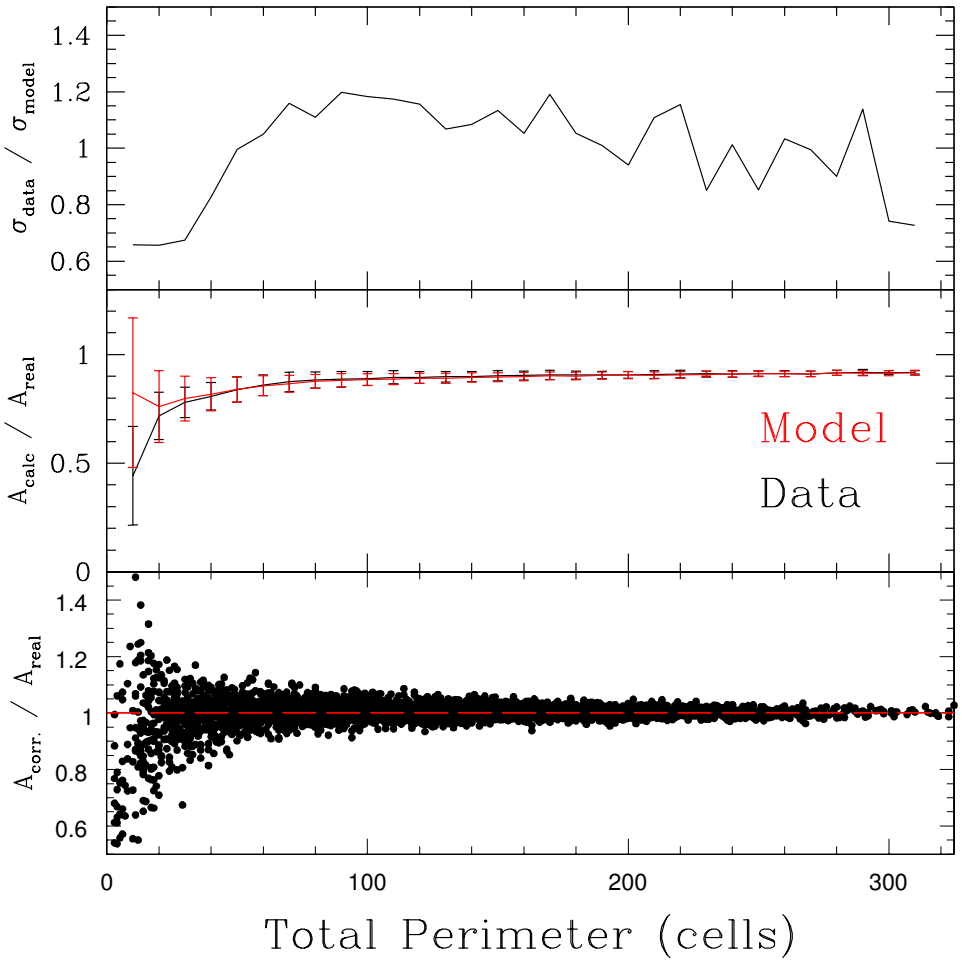

Figure 3.3: The top panel shows the ratio of the error bars in the middle panel - the standard deviation of masked fraction model to standard deviation of computed masked fraction in bins of perimeter cell count. The middle plot shows the uncorrected masked area as a fraction of the real masked area (black), showing the underestimation and our model for this (underestimated) masked fraction (red), which serves as the correction factor corresponding to 1/2 of the mask perimeter. The ratio of the (corrected) mask area to true mask area is shown in the bottom panel.

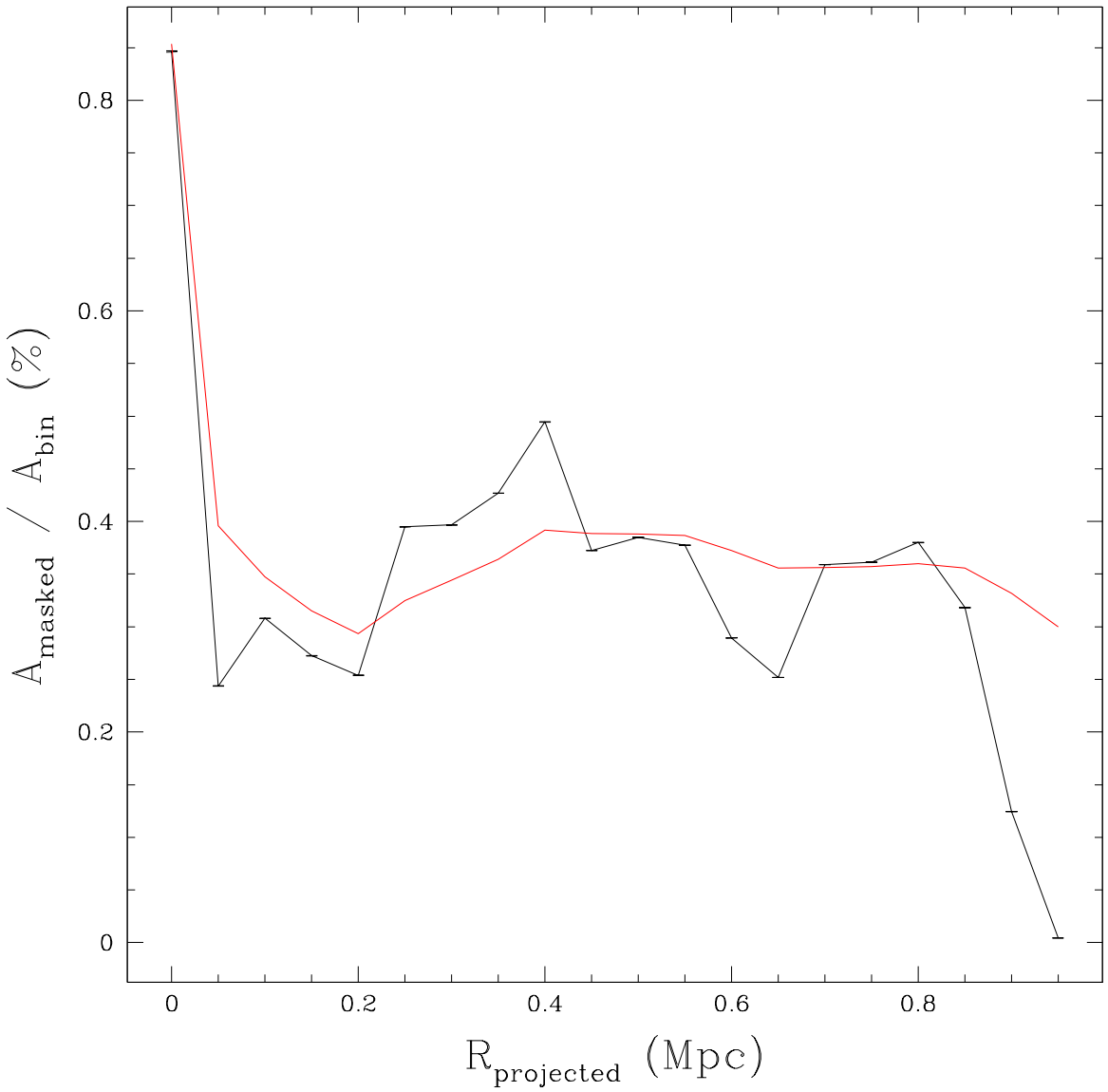

Figure 3.4: Total fraction of masked area is plotted in each radial bin. The total masked area for radial bins $< R_{\rm projected}$ is shown in red.

3.2.3 Cuts

In order to discern the background from possible associated satellites of the primary galaxies, cuts are performed on the SDSS data. Local Group dwarfs are used as representative of populations of satellites that could possibly exist around Atlas3D galaxies, and cuts are made on the data based on Local Group dwarf size, magnitude, surface brightness, and colour. In general, our strategy is to maximize $N_{\text{sat}}/N_{\text{background}}$, the number of associated satellites to the number of unassociated background galaxies. To do this, we compute m_r and r_{exp} for Local Group dwarfs observed from a distance of 25 Mpc (Figure 3.5), choosing cuts on these observables to maximize $N_{\text{sat}}/N_{\text{background}}$. As can be seen from Figure 3.5, a significant population of Local Group dwarfs (observed at 25 Mpc) are excluded by the survey magnitude limits and our cuts on the data. Future comparisons between our results and the Local Group are based on properties of the satellites of the Local Group placed at 25 Mpc which would not have been excluded based on our cuts or survey magnitude limits.

Detections with exponential scale radii less than 0.65 arc seconds are cut in order to eliminate potential stars and point-sources, and only detections with a g-r colour between -1 and 0.85 are included. Since the limiting r-band photometric magnitude in SDSS is 22.2, galaxies that appear to be dimmer than this, or brighter than an apparent magnitude of 10, are eliminated as well. Together, these cuts reduce the background by 45%. The biggest cut on the data is done in terms of a size-dependent magnitude cut. Dwarfs are difficult to detect, with nearby dwarfs appearing quite extended, and having low surface brightness. Thankfully, dwarf satellites tend to lie along broad sequences of near-constant surface brightness [6], as can be seen in Figure 2.3. For this reason, we use a size-dependent magnitude cut, based on the Local Group dwarfs, so that only galaxies with magnitudes such that

$$24 - \frac{r_{\text{exp}}}{1 \text{ arc second}} < m_r < 30 - \frac{r_{\text{exp}}}{1 \text{ arc second}},$$

where r_{exp} is the exponential scale radius (in arc seconds) and m_r is the cmodel magnitude, are included. Together, these cuts eliminate a total of $\sim 98\%$ of the background (Figure 3.5). The final, average density is approximately 105 detections per Mpc^2.

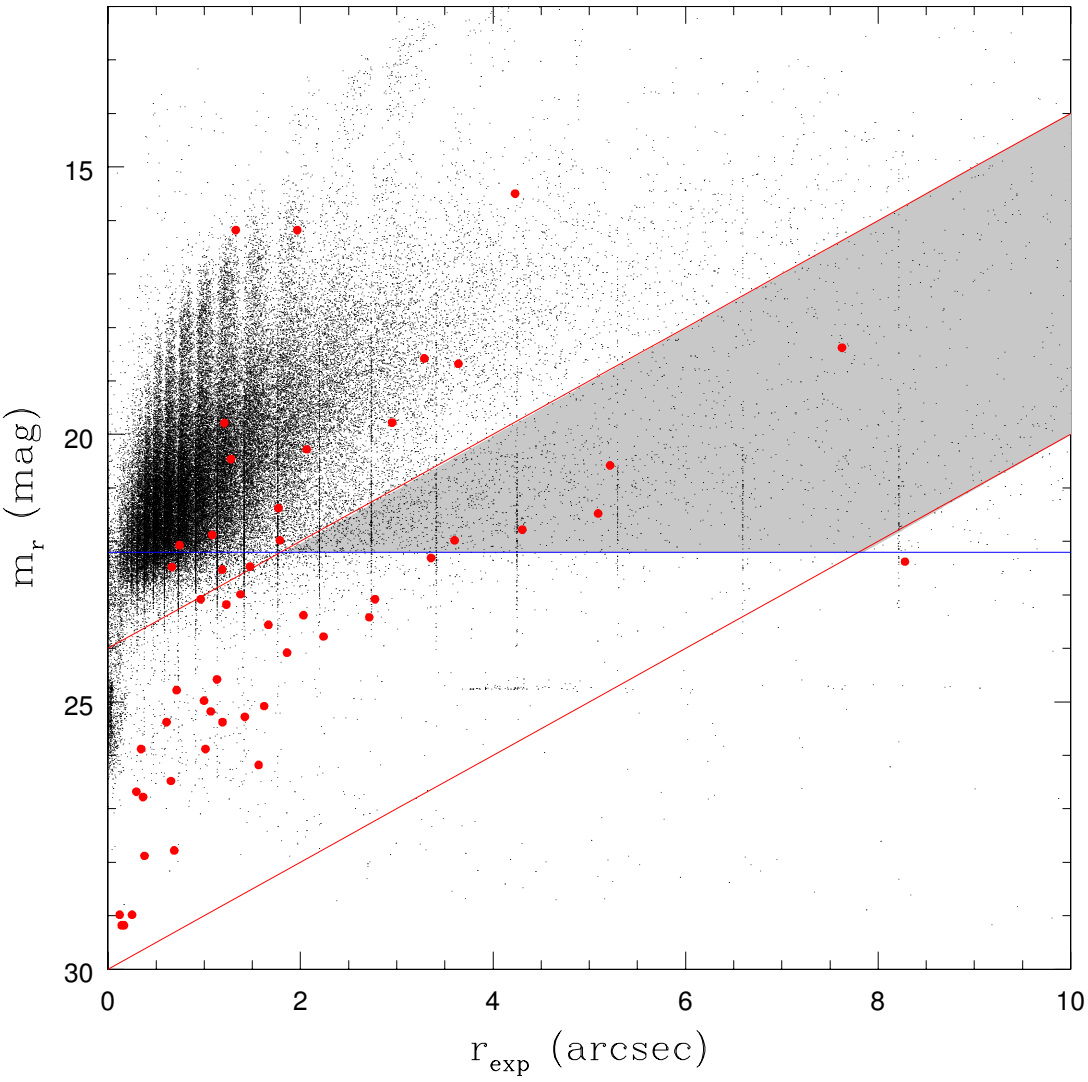

Figure 3.5: A size-magnitude diagram of SDSS data (black points) with the Local Group dwarf galaxies (placed at a distance of 25 Mpc) indicated as red points. The size-dependent magnitude cut of (Eqn 3.2) is indicated as red lines, with the magnitude limit indicated in blue. The shaded region indicates the data not excluded by the cut.

3.3 Preliminary Estimate

From the surface density of galaxy detections in the Sloan Digital Sky Survey Data Release 8 (DR8), we expect roughly 100,000 background detections over a surface area on the sky of 4 Mpc^2 [25]. This leaves 25,000 detections over a 1 Mpc^2 search area. Traditionally, it has been difficult to discern associated structure as the statistical sample is drowned out by unassociated background galaxies. This also poses the problem of uncertain real-space satellite positions and non-uniform backgrounds. If we assume that there exist 5 detectable, associated satellites within 300 kpc of a bright primary we are left with a statistical signal from associated structure of:

$$\frac{5 \text{ satellites}}{\pi \left(\frac{300 \text{ kpc}}{1000 \text{ kpc}}\right)^2 25,000 \text{ detections}} = 0.07\%$$

A sample of 5 detectable satellites is understandably drowned out amidst the sea of background detections, leaving a negligible (0.07%) signal from a single sample. However, if cuts are imposed on the background data, we have found that it is possible to reduce the background by $\sim$ 98%, leaving $\sim$ 141 background detections. Further, if we stack our searches around individual primaries, the signal to noise adds in quadrature and therefore signal-to-noise is increased as the square of the number of stacked samples. Here, we use the Poisson noise on the background count. We define signal to noise as the ratio of the number of associated primaries to the Poisson noise on the background. As before, we assume that there are 6 detectable, associated galaxies (on average) around each primary. Then, cutting out 98% of the background and stacking our 249 samples we expect the signal-to-noise to be:

$$\frac{\text{Signal}}{\text{Noise}} = \frac{5}{\sqrt{141}} \times \sqrt{249} = \sim 7$$

3.4 Comparison With Other Groups

We now compare the methods of other groups to detect associated satellites around bright, isolated primaries, to our own. We will examine the how the primary catalogue is built, the scope of the search, the isolation criterion that is applied to the primary subsample,

and the cuts performed on the data. We contrast the methods of other authors (Guo et al. (2011,2012) [33, 34]; Liu et al. (2011) [59]; Lares et al. (2011) [57]; Strigari et al. (2012) [88]; and Nierenberg et al.(2011/2012) [73, 74]) with the one described in this chapter, and point out how our results are likely to be different. In the next chapter, after the results are discussed we will return to our comparison by discussing our complementary results.

3.4.1 Guo et al. 2011

Guo et al. 2011 [33] study the luminosity function of satellites of isolated primaries in SDSS DR7. They restrict the photometric sample to galaxies brighter than $m_r = 20.5$ and build a primary catalogue from the SDSS DR7 spectroscopic subsample, including all objects with robust redshift estimates (zconf > 0.7 and specClass $= 2$) and a Petrosian magnitude $m_r \leq 17.77$. These authors bin potential primaries in the SDSS spectroscopic catalogue by absolute magnitude, from M_V from -19 to -23 with bin widths of 1 mag, in order to study the effect of primary brightness on satellite luminosity function. Guo et al. build an isolated, clean sample by excluding primaries with neighbours within 600 kpc and 0.5 mag of the host, unless they have a substantially different spectroscopic redshift of $\Delta z_s \geq 0.002$. If the bright neighbour has only a photometric redshift, the required redshift separation is 2.5× the photometric redshift error of the primary. For primaries with $M_c = -21.0 \pm 0.5$ mag, Guo et al. find a $\sim 90\%$ reduction in primary candidates, with: 88, 2661, 21346, 51733, 26982 isolated primaries in the final sample in absolute magnitude bins of -19,-20,-21,-22, and -23, respectively.

While this group has a larger sample of primary galaxies in all but one absolute magnitude bin (and a very similar isolation criteria), they extend over a much larger total spectroscopic redshift range of $0.016 < z_s < 0.522$ (66 - 2300 Mpc). In contrast, our primary catalogue contains galaxies from 11 to 42 Mpc ($0.003 \leq z \leq 0.01$), and therefore with a limiting photometric r-band magnitude of 21.3 we expect to detect satellites down to absolute magnitudes of ~ -9 at 11 Mpc, to ~ -12 at 42 Mpc. By comparison, Guo et al. are only sensitive to galaxies with $M_R \leq -12.8$ at 66 Mpc, to $M_R \leq -20.5$ at 2300 Mpc.

3.4.2 Lares et al. 2011

Similar to Guo et al. [33], Lares et al. (2011) [57] use SDSS DR7 photometric data to study the satellite luminosity function and projected density profile of associated satellites with $M_R \leq -14.5$ for primaries brighter than $M_R = -20.5$ in the redshift range $0.03 < z < 0.1$. They also examine the dependence of the luminosity function and projected density profile on primary galaxy luminosity and colour. Lares et al. use the New York Value Added Catalogue (NYU-VAGC) [9] to obtain photometry for satellite galaxies around primaries from the spectroscopic sample. Guo et al. restrict primaries in their final sample to have no neighbours brighter than $M_{\rm host} + 2$ within projected distance 700 kpc and relative radial velocity difference 700 km/s, which equates to $z_{\rm host} \pm 0.0023$. The final primary sample totals 51,710 galaxies between $0.03 < z < 0.1$ with $M_r < -20.5$. The methodology of Lares et al. allows this group to study the bright end of the luminosity function with primaries at redshifts $10\times$ greater than in our sample, and this allows us to be sensitive to satellites down to ~ 5 magnitudes fainter. The isolation criteria applied by these authors are the most stringent compared to that of the other groups considered, and our own. With M31 at ~ 700 kpc distant, it is not assured that under this criterion the Milky Way subgroup would be considered isolated.

3.4.3 Liu et al. 2011

Liu et al. (2011) [59] study the occurrence of Magellanic Cloud analogues around Milky Way-like primaries by using a sample of bright primaries drawn from the SDSS DR7 spectroscopic sample in the Northern Galactic Cap. Like Lares et al. [57], Liu et al. use the NYU value added catalogue for spectra and k-corrected luminosities. Around primaries drawn from the spectroscopic catalogue, Liu et al. search for bright satellites analogous to the Large and Small Magellanic Clouds by searching for satellite galaxies within 150 kpc of the host that are 2-4 magnitudes fainter than their host galaxy. The search for Milky Way-like primaries is limited to galaxies with $m_r < 17$ and those having an r-band magnitude $M_r = -21.2 \pm 0.2$. This was chosen by converting the best available estimate of the absolute magnitude (in the v-band) of the Milky Way in the Vega photometric system ($M_V = -20.9$; van den Bergh (2000) [91]), to the SDSS photometric system r-band. To obtain a sample of isolated MW-like primaries, Liu et al. eliminate potential primary galaxies if, within an isolation radius of 0.5 Mpc, a brighter galaxy (in absolute magnitude) is found within ± 1000 km/s of the host redshift, or if a galaxy brighter in apparent magnitude is found with no redshift information. From these criteria, Liu et al. obtain

an isolated sample of 22,581 primaries, which extend to a redshift of $z = 0.12$. As the aim of this group is to search for bright satellite galaxies like the Magellanic Clouds of the Milky Way, their search criterion is designed to look for satellites that are 2-4 magnitudes fainter than their hosts. Our search, on the other hand, is optimized to statistically detect the faintest satellites to the limiting SDSS photometric magnitudes. Therefore the main difference between methods is our extended search range around each primary (500 kpc compared to 150 kpc) and sensitivity to satellite galaxies that are as faint as ~ 10 magnitudes fainter than the host. It is also important to note that this groups restricts the absolute magnitudes of their primaries to $M_r = -21.2 \pm 0.2$, while our primary sample has a k-band absolute magnitude range which is much more extended, from $M_k = -21.52$ to the brightest $M_k = -25.58$.

3.4.4 Strigari et al. 2012

Similarly to Liu et al. 2011 [59], Strigari et al. 2012 [88] build a primary catalogue using one set of primaries in the magnitude range $M_r = -20.4 \pm 0.25$ for comparison with the Milky Way subgroup, and a second set having a magnitude range of $M_r = -20.7 \pm 0.25$, for comparison with M31 subgroup. Strigari et al. select primaries from the SDSS DR8 spectroscopic survey, which is combined with the more complete spectroscopy and imaging data presented in GALEX, in the NASA-Sloan Atlas (http://www.nsatlas.org/). Using the same methods for selecting isolated galaxies as Liu et al. 2011, Strigari et al. ensure an isolated sample of MW and M31 analogues, selecting nearby ($z < 0.055$, or those less distant than 230 Mpc) galaxies that have no neighbours brighter than the Milky Way or Andromeda within 400 kpc. These authors also exclude any primary candidate galaxies with $m_r < 11$, an angular size less than 5 times the 50% light radius from the Sersic profile fit, or with a negative g-r colour in order to exclude the most nearby galaxies which may have incorrect photometry. Around these primaries, Strigari et al. search for satellite galaxies using the DR8 photometry and spectroscopic catalogue, excluding those primaries for which the photometry is incomplete within a projected 250 kpc. Of the other methods reviewed, Strigari et al. most closely resembles the aim of our research, with very similar isolation criteria and the same focus of extending the search for satellite galaxies to the faint end of the luminosity function with the nearest primaries, though our sample of primaries is closer, extending to only 42 Mpc, allowing us to put better constraints on the faint end of the luminosity function.

3.4.5 Nierenberg et al. 2011/2012

Nierenberg et al. (2011,2012) [73, 74] study faint satellite abundances around a sample early-type hosts in the GOODS fields from the catalogue of Bundy et al. [16]. The primary sample of Nierenberg et al. lies at an intermediate redshift range $0.1 < z < 0.8$ and is cut by magnitude such that all objects are brighter than the detection threshold, $m_{\rm host} + \Delta m < m_{\rm max} = 26.5$. The final host sample totals 202, 127, and 71 primaries complete to $\Delta m = 6.0$, 5.5, and 5.0 respectively. Nierenberg et al. find that the signal-to-noise is maximized at $\Delta m = 5.5$ and use this in their primary analysis. Background subtraction is performed using SEXTRACTOR on high resolution Hubble Space Telescope image cutouts centred on the host galaxy, where the light from the primary is modelled as a B-spline before being subtracted to obtain a residual image from which associated object detections are made. Compared to the methods of the other authors reviewed and our own, the primary sample of Nierenberg et al. extends the furthest in redshift and the background subtraction method is unique and well suited to the study of faint satellite abundances around more a more distant primary sample. The number of primaries in the final sample of Nierenberg et al. is similar to our own, and we therefore expect similar error bars on our cumulative Δm abundances. While the limiting magnitude of the primary sample of Nierenberg et al. extends to several magnitudes fainter than SDSS, we expect to detect fainter satellites down to a magnitude difference of $\Delta m = 10$ due to the proximity of our sample.

Chapter 4

Results

Whether the "missing dwarf problem" is endemic to all galaxy groups or if the Local Group is an exception, is currently unknown. In order to determine whether the Local Group is statistically representative of other galaxy groups, and whether the apparent lack of dark matter subhalos, as indicated by the presence of dwarf galaxies, is endemic to all galaxy groups we obtain a sample of bright primaries and photometry around each of these primaries to build a statistical sample of associated satellites. After cuts are applied to the data and the background around each isolated primary is subtracted, masked regions are detected and corrected for, and the sample is stacked. We look for an excess of signal in the inner 500 kpc region of each primary. In comparison with recent authors (Guo et al. (2011,2012) [33, 34]; Liu et al. (2011) [59]; Lares et al. (2011) [57]; Strigari et al. (2012) [88]; Nierenberg et al. (2011,2012) [73, 74]), our search strategy focuses on a complete sample of nearby ($D \leq 42$ Mpc) primaries in order to sample as far down the luminosity function as Sloan Digital Sky Survey DR8 imaging limits allow.

In the following sections, we present a consistent, statistically significant excess of signal that is dependent on central galaxy morphology and magnitude in the inner region around each primary. In the following subsections, we show the excess of signal in galaxy count, number density, apparent magnitude, and spectroscopic redshift, and then show the dependence in number density on central galaxy magnitude and morphology. At the end of this chapter, we contrast our results with studies performed by other authors (Guo et al. (2011,2012) [33, 34]; Liu et al. (2011) [59]; Lares et al. (2011) [57]; Strigari et al. (2012) [88]; Nierenberg et al. (2011,2012) [73, 74]), whose methods were described in the previous chapter.

4.1 Density Profile

After the background data is reduced by the application of our exclusion criteria, projected separations from the central primaries are calculated. Galaxies are binned by separation from the primary in 50 kpc bin widths and the area on the sky in each circular annulus corresponding to each separation bin is calculated. From bin areas and counts, a number density in each bin ρ_b is then computed and the overdensity P_b in each bin is calculated as

$$P_b = \frac{\rho_b}{\bar{\rho}} - 1,$$

where $\bar{\rho}$ is the average bin density in the outer (> 500 kpc) region. We expect that the inner-most projected radial separation (0-50 kpc) bin may be contaminated by bright globular clusters or HII regions associated with the primary, although it is not excluded here. The resulting projected radial density profile for the cut sample is shown in Figure 4.1. An excess, corresponding to an over-density of objects at separations < 500 kpc projected, is detected at S/N ~ 8. The r.m.s. scatter in the background surface density is shaded in grey. For comparison, we calculate the projected density profile for the Local Group if it were observed at a distance of 25 Mpc and had the same cuts and magnitude limits applied, indicated as a red dashed line in Figure 4.1. Our detection corresponds to about 4.8 ± 0.6 satellites per central galaxy, in keeping with expectations from the Local Group. We notice that while the density profile in the outer region (> 500 kpc) is defined to be flat on average, there is very small statistically significant scatter above the background, which indicates that the data reduction is successful in producing a uniform background of unassociated galaxies around each central primary. Obtaining a uniform background of unassociated galaxies has allowed us to more accurately determine the signal produced by bound structure as an overdensity in the inner region.

In galaxies, if one assumes the galactic dark matter halo is spherical, the observed flatness of galactic rotation curves indicates that halo masses must increase linearly with radius, with a corresponding halo density that therefore drops as $\rho(r) \propto r^{-2}$ [8]. These so-called isothermal profiles produce constant velocity dispersions and flat rotation curves and have been used to model virialized dark matter halos. We plot the logarithmic, stacked density profile for our sample in Figure 4.2. Consistent with an isothermal density profile, we find a slope of -0.98 ± 0.1. This result is discussed further in the final chapter.

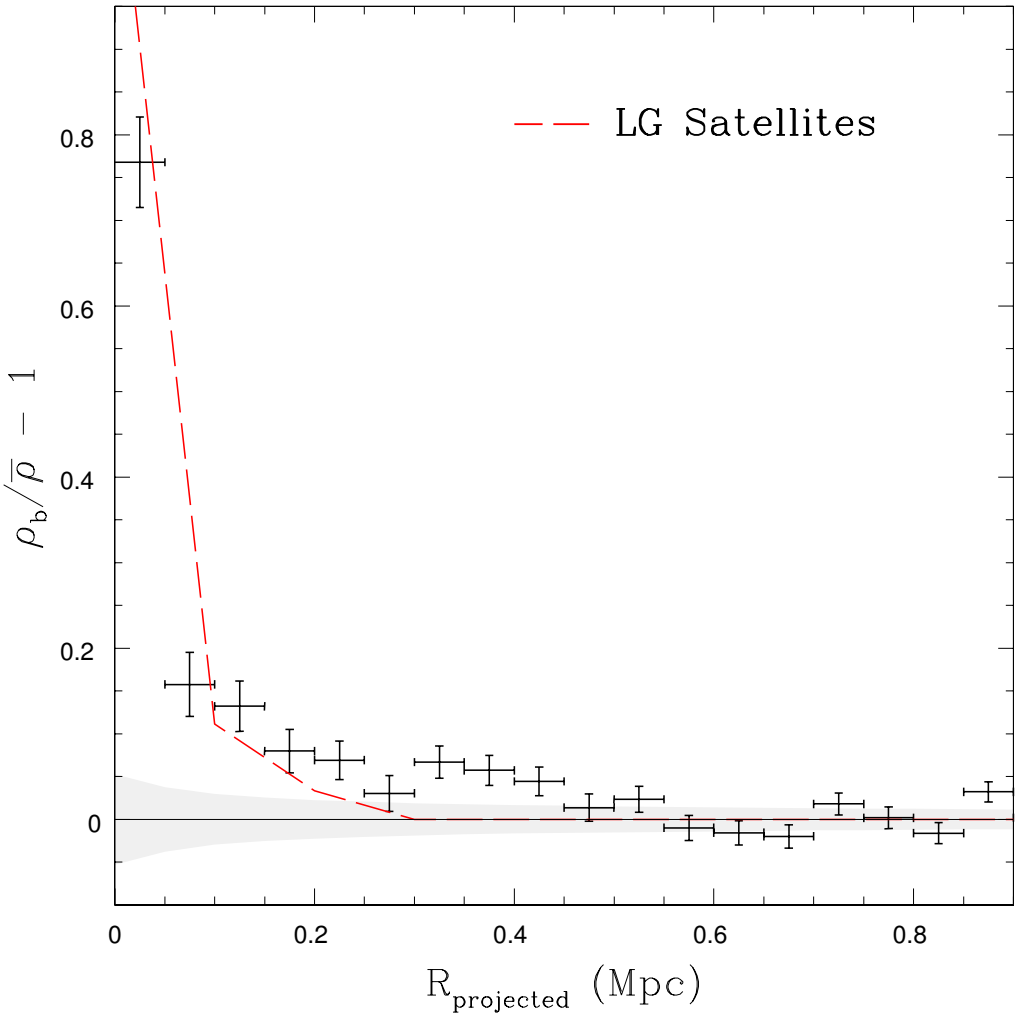

Figure 4.1: Projected radial density profile for the final sample, with r.m.s. scatter in the background surface density indicated in grey and radial density profile of Local Group satellites (observed at 25 Mpc away with the same cuts and magnitude limits) using the average of 3 different projections, indicated by a dashed line. The horizontal error bars indicate bin widths, while the r.m.s scatter is indicated by the vertical error bars.

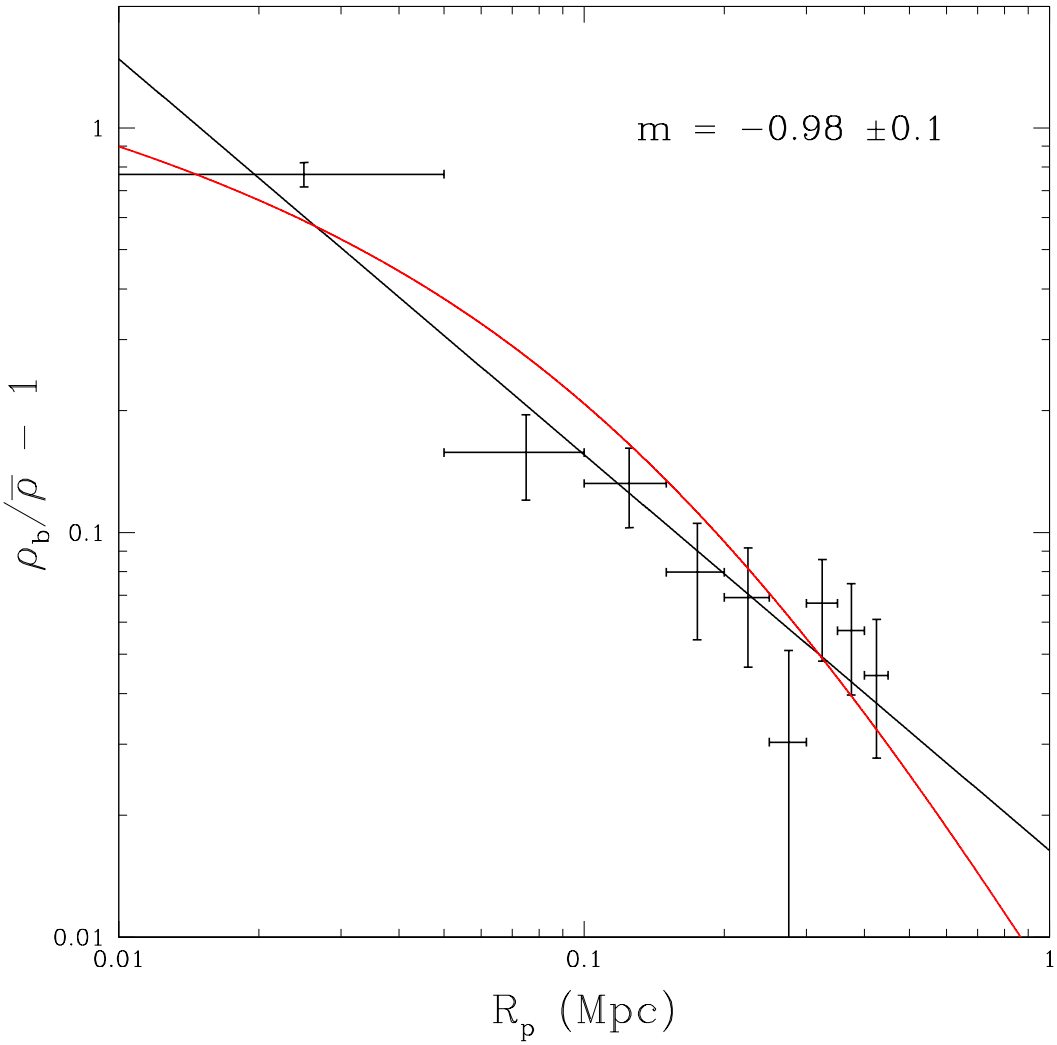

Figure 4.2: The logarithmic projected radial over-density profile for the inner bins, showing an approximately isothermal density profile with slope -0.98 ± 0.1. The projected NFW profile [1] with concentration parameter $c = 6$ is shown in red for comparison. Horizontal error bars indicate bin width, while vertical error bars show the r.m.s scatter in the background.

4.2 Number Profile

Stacked galaxy counts are binned by projected separation in 50 kpc bin widths, as in the case of the density profile, and corrected annulus areas are also stacked. The average satellite count $N_{\rm sat}$ in radial bin b per primary is determined as:

$$N^b_{\rm sat} = \frac{1}{N_{\rm gal}} \left(N^b_{\rm inner} - \frac{A^b_{\rm inner}}{A_{\rm outer}} N_{\rm outer} \right)$$

Where $N_{\rm gal}$ is the total number of primaries, $N^b_{\rm inner}$ is the number of galaxies in inner bin b, $A^b_{\rm inner}$ is the annulus area in bin b in the inner region, $A_{\rm outer}$ is the total area of the outer region, and $N_{\rm outer}$ is the number of galaxies in the outer region. To find the total number of satellites detected over the background, the cumulative count is also determined. Using the Poisson standard deviation of the bin count as the noise, the signal-to-noise is also calculated as the ratio of the cumulative count and the Poisson standard deviation added in quadrature, and error bars are placed on bins indicating the bin width and Poisson standard deviation of the bin. This number overdensity profile per galaxy in radial bins and the cumulative (shaded region) and corresponding errors and signal-to-noise is shown in Figure 4.3. Here, we do exclude the inner (0-50 kpc) bin in order to prevent any inclusion in our satellite overdensity count objects such as bright globular clusters or HII regions associated with the primary. Corresponding to the isothermal distribution shown in the logarithmic overdensity profile (Figure 4.2), there is an approximately constant number of satellites per bin found over the background in the first 8 radial bins ($r_p < 450$ kpc). The signal-to-noise, indicated by a dashed line, reaches a maximum of 7.9 at the 450 kpc (projected) radial bin where a cumulative excess of 4.2 ± 0.53 satellites per host are detected. The signal reaches a maximum of 4.8 ± 0.65 satellites detected over the background in the 550 kpc radial bin with a slightly lower signal-to-noise of 7.5. This is in good agreement with our preliminary prediction of 5 detectable satellites at a signal to noise of ~ 7 in the previous section.

Next, the sample is split by central galaxy absolute k-band magnitude (M_k) and morphology and cumulative number over-density profiles are calculated for each. As before, our error bars on the cumulative counts represent the Poisson standard deviation of individual bins added in quadrature. The projected number over-density per galaxy in radial bins split by absolute k-band magnitude is shown in Figure 4.4. Primaries with k-band magnitudes $M_k \leq -23.5$, shown in blue, represent the brightest $\sim 15\%$ of the sample and have the greatest signal of 9.5 ± 1.3 galaxies in excess of the background at a signal-to-noise

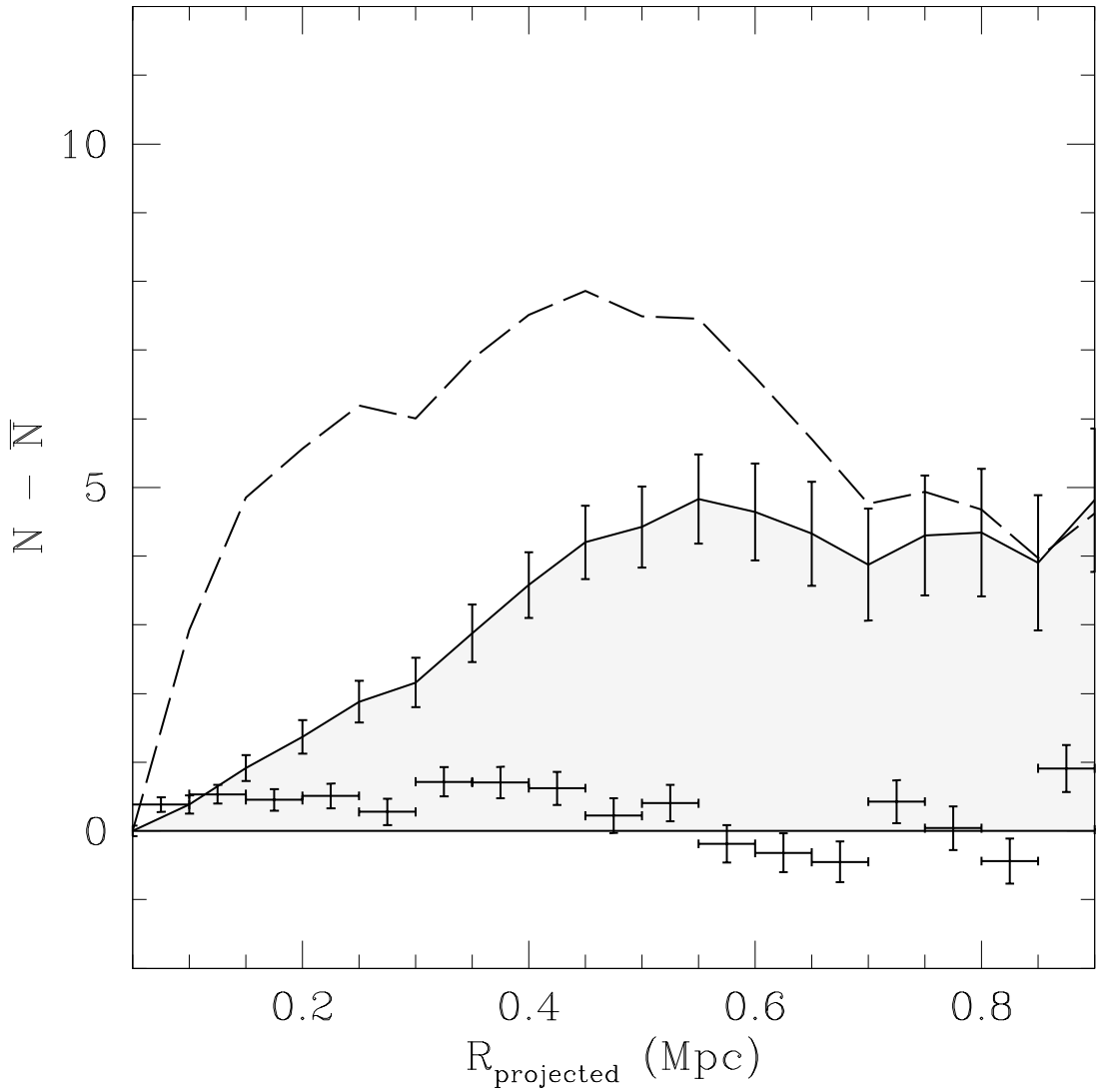

Figure 4.3: The binned and cumulate number over-density profile per galaxy in radial bins. Error bars on each bin indicate bin width and Poisson standard deviation. The shaded region indicates the cumulative over-density, shown with the error added in quadrature. The dashed line indicates signal-to-noise.

of 7.1 in the 600 kpc projected radial separation bin. The signal-to-noise for primaries with $M_k \leq -23.5$ reaches a maximum of 8.3, corresponding to 7.62 ± 0.9 galaxies in excess of the background, in the 400 kpc projected radial separation bin. Primaries with absolute k-band magnitudes $M_k > -23.5$, shown in red, represent the remaining, fainter subset of the sample and signal from this subset of primaries reaches a maximum of 3.2 ± 0.8 galaxies in excess of the background at a signal-to-noise of 4.1 in the 550 kpc radial bin, which is also the maximum signal-to-noise. Clearly, we find a strong dependence in the number of associated satellites on primary magnitude, with the brightest 15% of the sample having a cumulative count of associated satellites between 3-4 times higher than the remaining sample. The shape of the cumulative number profile also changes with primary magnitude, with the total number of satellites of the fainter ($M_K > -23.5$) primaries being suppressed at closer projected separations, showing evidence of stronger clustering amongst brighter primaries. The combined sample (Figure 4.3) is plotted against the sample subsets in grey for comparison.

The projected number over-density per galaxy in radial bins split by morphology is shown in Figure 4.5. We split our 249 primary galaxy sample by morphology into Elliptical and Spiral morphologies. Elliptical primaries show the greatest signal of 10.85 ± 2.3 galaxies in excess of the background at a signal-to-noise of 4.7 in the 550 kpc projected radial separation bin. The signal-to-noise for ellipticals reaches a maximum of 5.1 in the 500 kpc radial separation bin, corresponding to a signal of 10.78 ± 2.1 galaxies in excess of the background. Amongst primaries with a spiral morphology, the signal reaches a maximum of 4.28 ± 0.7 galaxies in excess of the background in the 500 kpc bin, having a signal-to-noise of 6.3. The signal-to-noise for spirals reaches a maximum of 6.7 in the 450 kpc projected radial separation bin, corresponding to a signal of 3.73 ± 0.5 galaxies in excess of the background at this signal-to-noise. Here again, the combined sample (Figure 4.3) is plotted against the sample subsets in grey for comparison.

Our results show quite clearly that group properties are strongly dependent on the properties of the central host galaxy, having split the sample by primary magnitude and morphology. Taken together, these plots indicate that the majority of the signal is contributed by bright elliptical primaries. This is in keeping with expectations based on our census of the local and neighbouring galaxy groups presented in the Karachentsev catalogue, considering that the Centaurus A galaxy is the only bright elliptical central galaxy in the sample and hosts the largest number of known satellite galaxies in the same magnitude range.

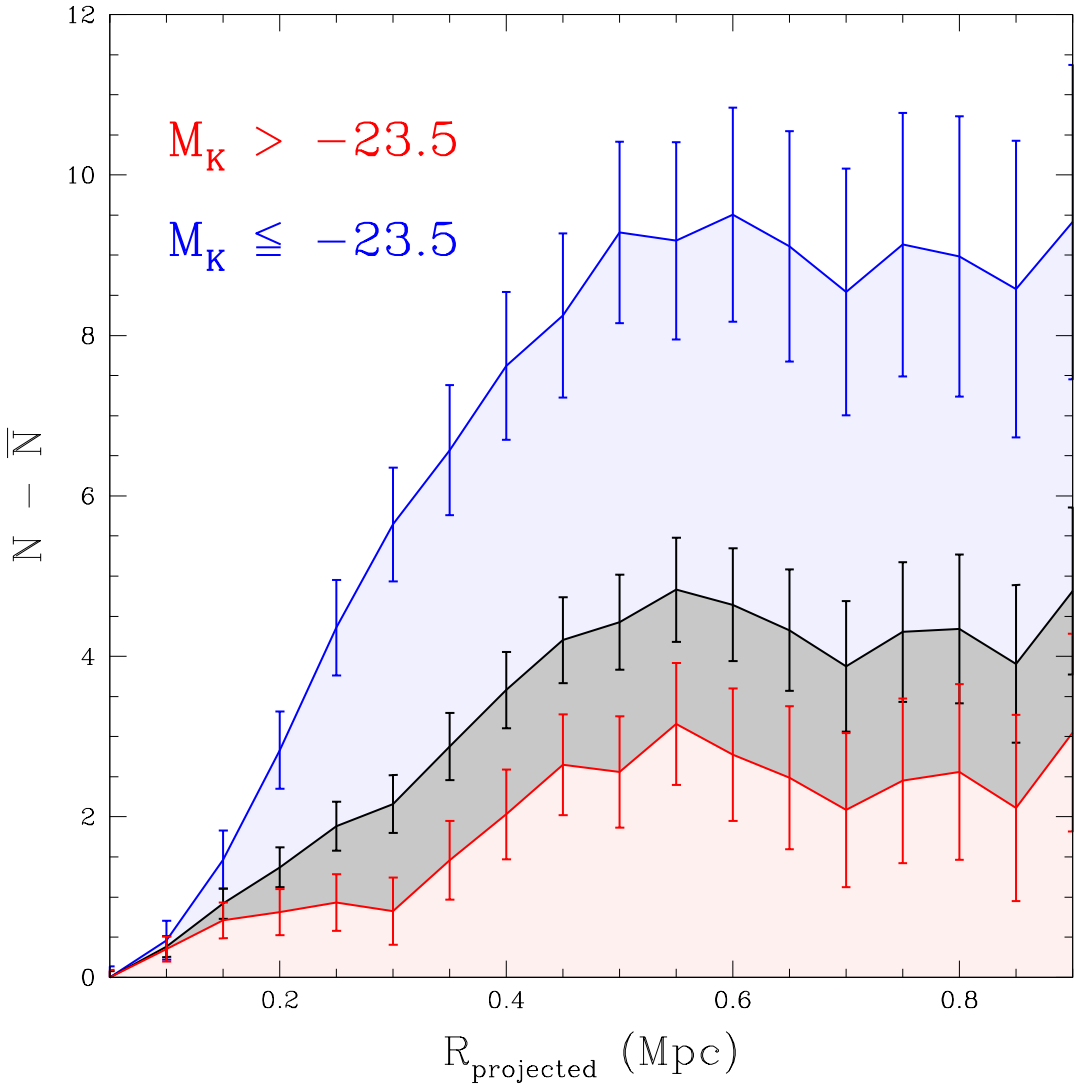

Figure 4.4: The cumulative number over-density profile per galaxy, split by magnitude, in radial bins. The signal from primaries with $M_k \leq -23.5$ is shown in blue, and from primaries with $M_k > -23.5$ in red. Signal from the combined sample is in grey. Shaded regions indicate the cumulative over-density.

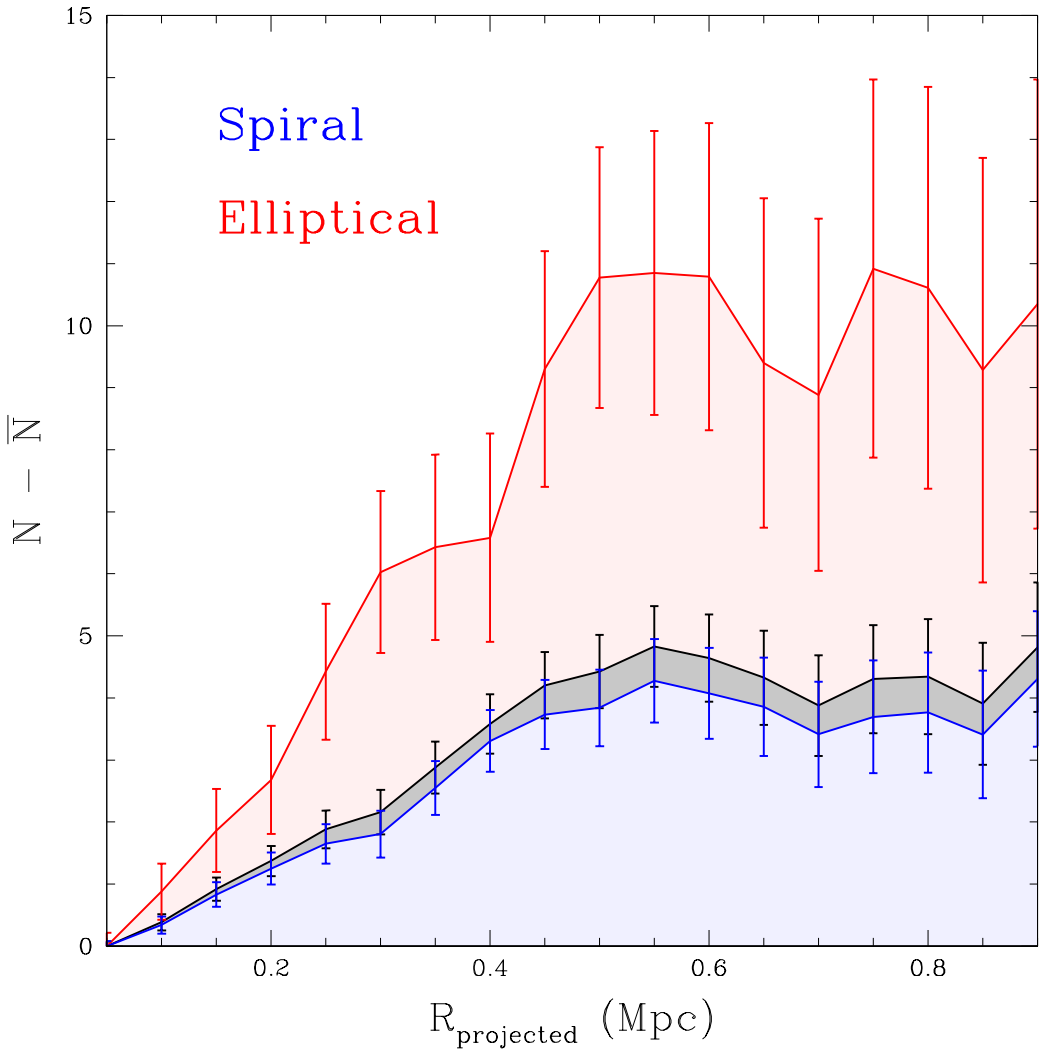

Figure 4.5: The cumulative number over-density profile per galaxy, split by morphology, in radial bins. The signal from primaries with elliptical morphology is shown in blue, and from primaries with spiral morphology in red. Signal from the combined sample is in grey. Shaded regions indicate the cumulative over-density.

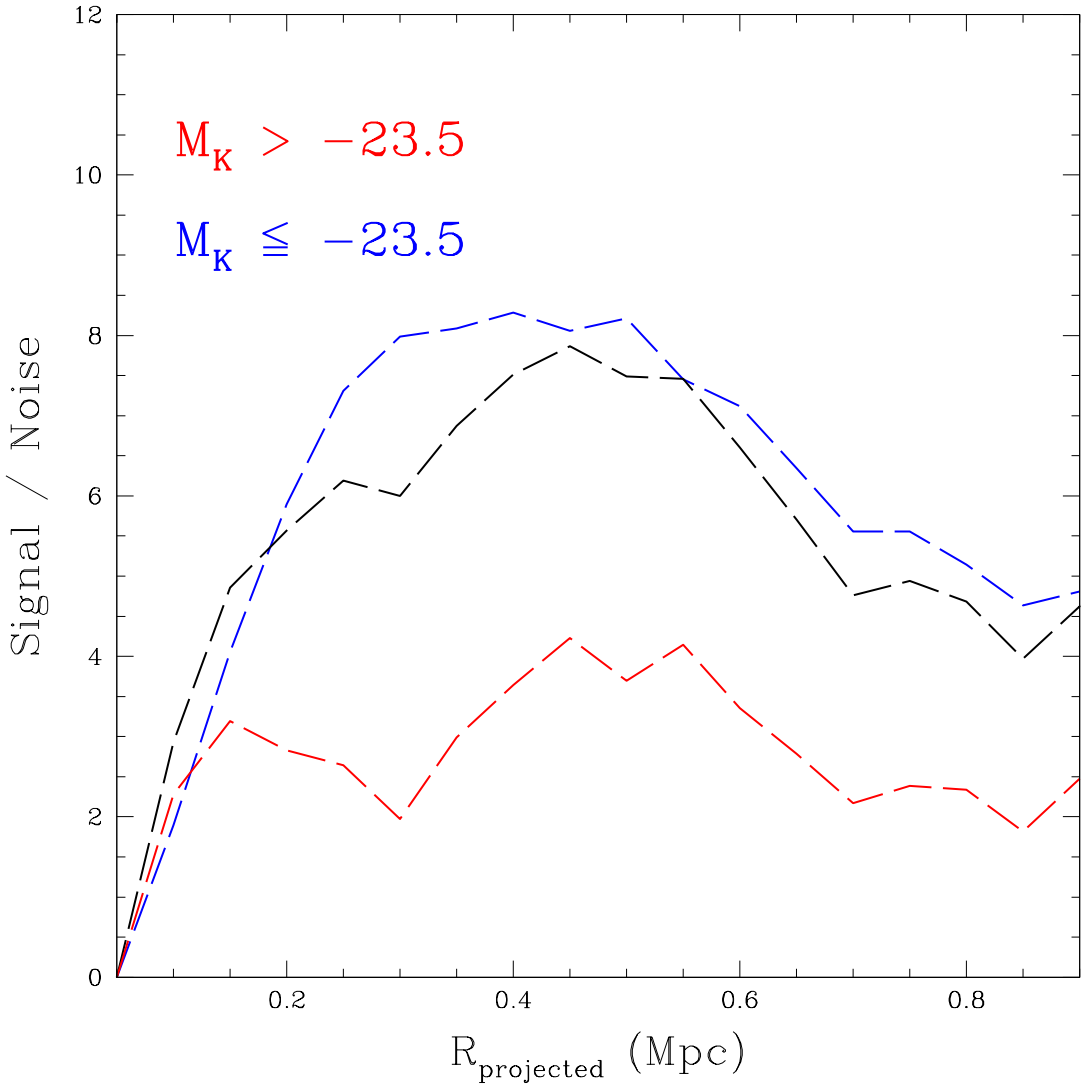

Figure 4.6: The signal to noise on the cumulative number over-density profile per galaxy, split by magnitude, in radial bins. Here, the signal is calculated as the cumulative number of galaxies in excess of the background, and the noise is the Poisson standard deviation of the background summed in quadrature.

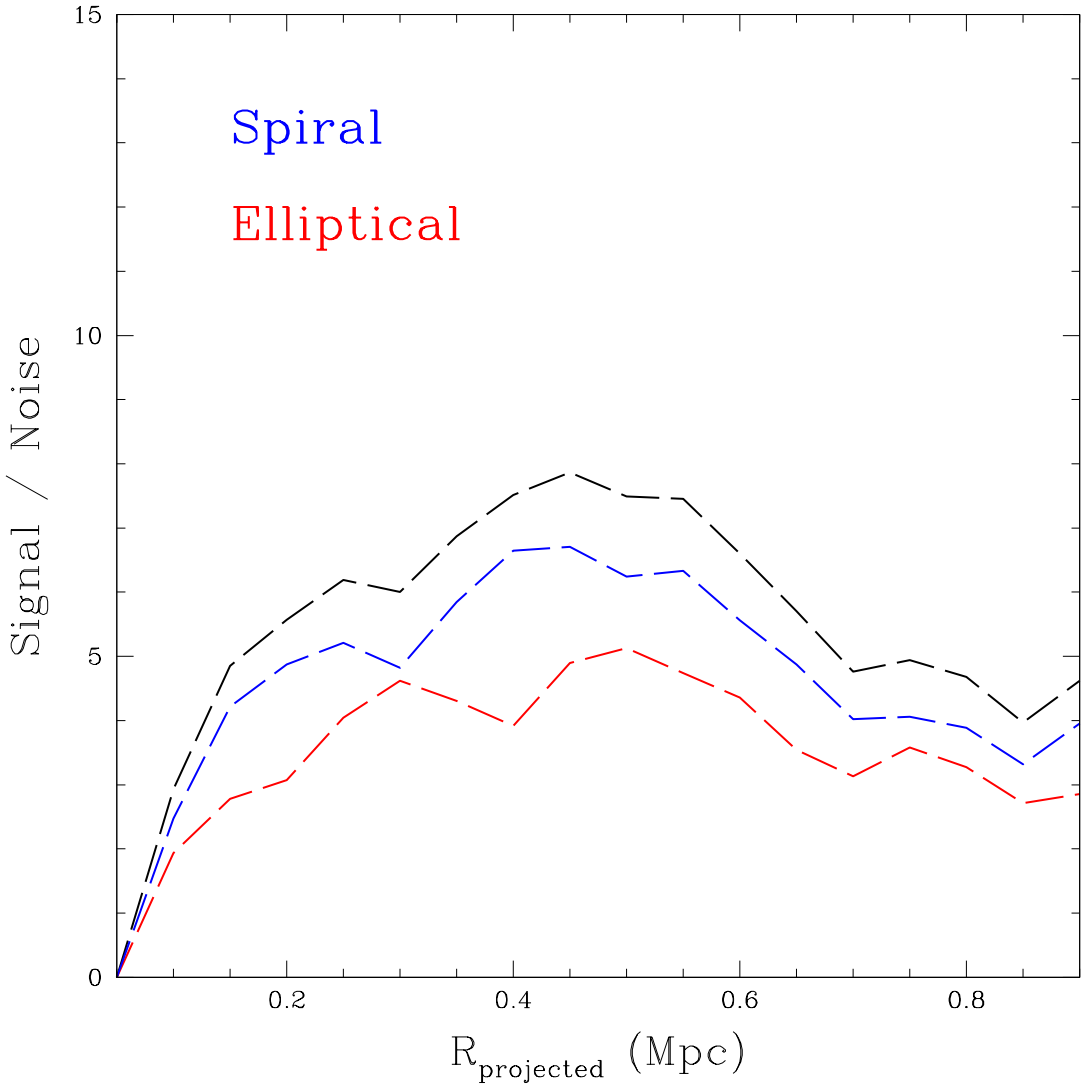

Figure 4.7: The signal to noise on the cumulative number over-density profile per galaxy, split by morphology, in radial bins. Here, the signal is calculated as the cumulative number of galaxies in excess of the background, and the noise is the Poisson standard deviation of the background summed in quadrature.

4.3 Number vs. ΔM

Next, we show the satellite luminosity function per galaxy as a function of separation in apparent (SDSS r-band) magnitude from the central primary for primaries in the magnitude range $M_r = -21.6 \pm 0.5$ (Figure 4.9) in order to compare with the distribution of the Milky Way and recent results from authors such as Guo et al. (2011,2012) [33, 34]; Liu et al. (2011) [59]; Lares et al. (2011) [57]; Strigari et al. (2012) [88]; and Nierenberg et al. (2011,2012) [73, 74]. Due to the sample size, splitting the satellite sample into Δm magnitude bins is an expensive operation in terms of signal-to-noise. The Poisson standard deviation of a bin with total number N is $\sigma_1 = \sqrt{N}$. Assuming we split this bin into n equal bins, the new Poisson standard deviation would be $\sigma_2 = \sqrt{\frac{N}{n}}$, and the noise therefore increases as $\sigma_1/\sigma_2 = \sqrt{n}$. By splitting the satellite sample into n Δm magnitude bins, we therefore roughly expect the noise to be increased by a factor $\sqrt{n}$. Due to the drastic reduction, we also re-introduce the problem of non-uniform backgrounds since we are computing number profiles for individual Δm bins with roughly a factor n less galaxies. In order to overcome this we use a simulated background, where we simulate the background of the i'th primary in the Δm magnitude bin as the fraction of the total Δm magnitude bin (summed over all galaxies) normalized to the total background count of the i'th primary:

$$N^i_{\Delta m} = \left(\frac{n^i_{\Delta m}}{\sum_i n^i_{\Delta m}} \right) \sum_{\Delta m} n^i_{\Delta m}$$

Here, N is the simulated background galaxy count and n is the measured count, and we use superscript i to denote the i'th primary and subscript Δm to denote the Δm magnitude separation bin. Although the total number in the background is kept the same in our simulated count, this method decreases the bin-to-bin variance by producing a finer-grained (real-numbered) measure of the background number of galaxies in magnitude bin Δm of the i'th primary. The next problem we face due to the Δm reduction in total galaxy count is in accurately estimating the variance on the bin content for small n. We therefore weight the Δm magnitude bins by the (Poisson) bin variance, where the weighted quantity $\bar{x}$ has the general formula:

$$\bar{x} = \frac{\sum_{i=1}^{n} (x_i/\sigma_i^2)}{\sum_{i=1}^{n} (1/\sigma_i^2)}$$

Here, x is the unweighted quantity and σ is the standard deviation. Since our primary galaxies are at different distances, the magnitude limit of the survey will exclude different

Δm bins for different primaries from contributing. The weighting produces the desired effect of favouring primary magnitude bins that are well sampled and within detection limits. The unweighted Δm luminosity function without using a simulated background is shown in Figure 4.8 for comparison. While the shape of the luminosity function is fairly robust, the largest effect of the weighting and background simulation is the reduction in standard deviation. The background-simulated and variance-weighted satellite luminosity function in Δm magnitude bins is used in our comparison to the Milky Way in Figure 4.9, with the Milky Way observed at a distance of 25 Mpc and having the same cuts and magnitude limits applied.

The weighted Δm satellite luminosity function increases to reach a maximum per-primary average cumulative excess of 5.7 ± 1.5 for galaxies within 10 magnitudes of the host, after which the error, calculated as total cumulative error by summing the Poisson standard deviation of the background count in quadrature, increases greatly due to the limiting magnitude of the survey leaving very few foreground galaxies in the 11'th and 12'th Δm magnitude bins. This extends recent measures of satellite abundance around more distant galaxies (e.g. Guo et al. (2011,2012) [33, 34]; Liu et al. (2011) [59]; Lares et al. (2011) [57]; Strigari et al. (2012) [88]; and Nierenberg et al. (2011,2012) [73, 74]) by about 5 magnitudes fainter on the luminosity function. For comparison, we also show the cumulative Δm luminosity function of the Milky Way calculated at a distance of 25 Mpc, considering the survey magnitude limits and our cuts on: magnitude, size, and colour. This finding is consistent with the previously detected total number overdensity of 4.8 ± 0.65 associated satellites per primary (Figure 4.3,4.4,4.5). In the last section of this chapter, we will make a detailed comparison between this result and the results of Guo et al. (2011,2012) [33, 34]; Lares et al. (2011) [57]; Liu et al. (2011) [59]; Strigari et al. (2012) [88]; and Nierenberg et al. (2011,2012) [73, 74].

4.4 Velocity Offset

The spectroscopic r-band limiting magnitude in SDSS is 4.5 magnitudes brighter than that of the photometric r-band and contains only the brightest satellites for the primaries in our sample. With the spectroscopic catalogue, we construct the stacked satellite number over-density profile as a function of velocity offset offset from the central primary within a projected separation of 1 Mpc as a consistency check with our previous number over-density results. We first apply the same cuts to the spectroscopic catalogue as we do the photomet-

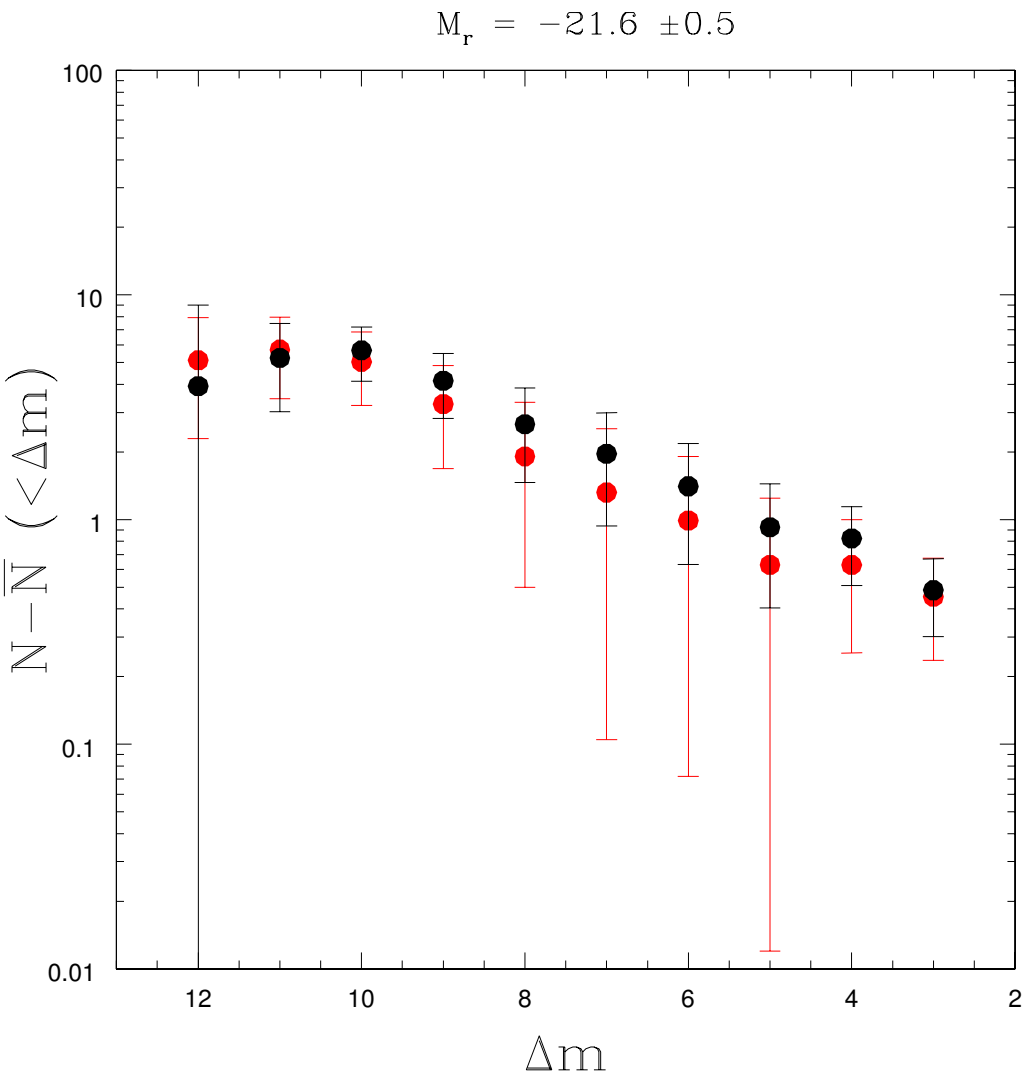

Figure 4.8: Here we plot the cumulative excess clustering (per-galaxy) signal binned by difference in apparent magnitude from central galaxy. We show the background-simulated, variance-weighted version in red for comparison against the unweighted version where the background has not been simulated, in black. The error shown is the total cumulative error calculated by summing the Poisson standard deviation of the background count in individual bins in quadrature.

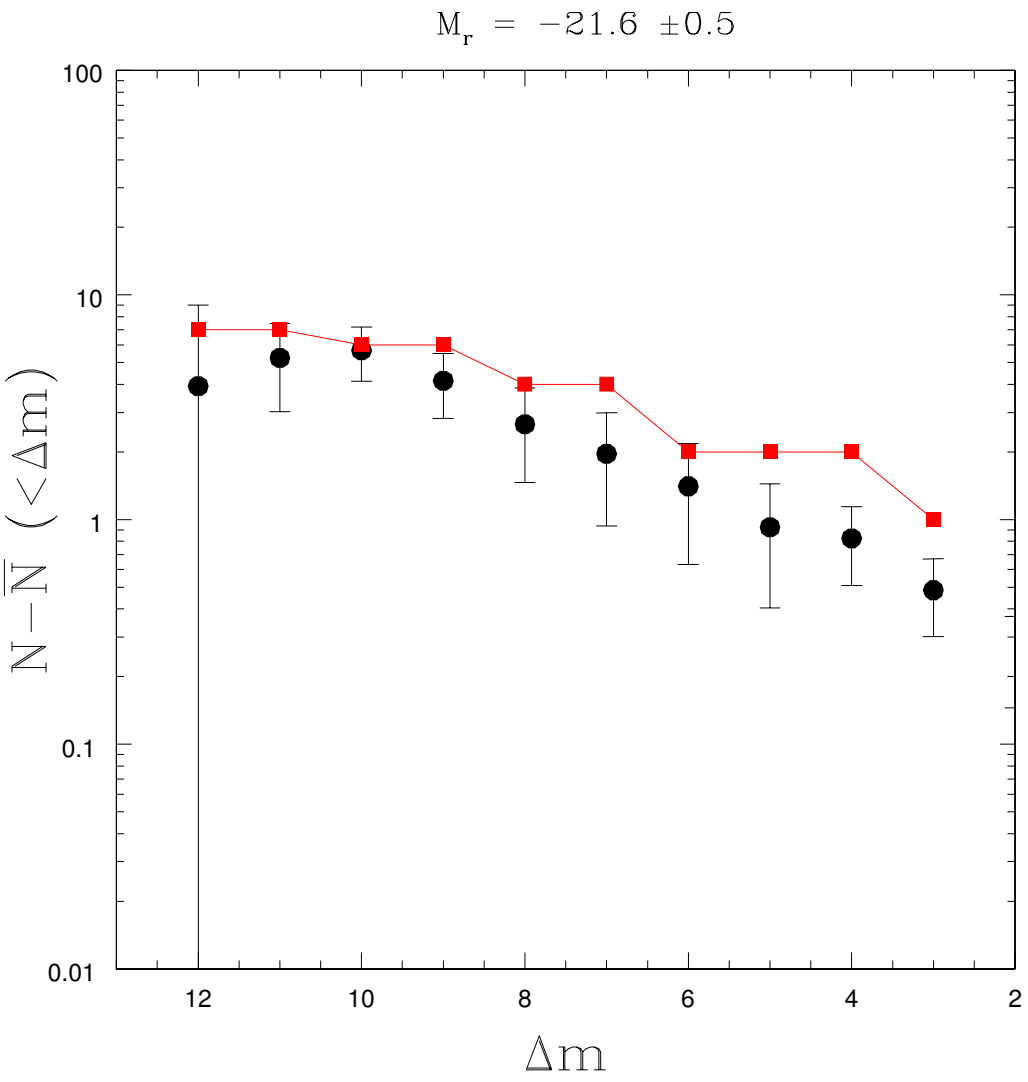

Figure 4.9: The cumulative excess clustering (per-galaxy) signal binned by difference in apparent magnitude from central galaxy. The error shown is the total cumulative error calculated by summing the Poisson standard deviation of the background count in individual bins in quadrature. The Δm luminosity function of the Milky Way, placed at a distance of 25 Mpc and with the same cuts and magnitude limits applied, is shown in red for comparison.

ric catalogue, bin by velocity offset from the central galaxy (using primary redshifts from the NASA/IPAC Extragalactic Database (NED) (http://ned.ipac.caltech.edu/) and spectroscopic redshifts from the SDSS DR8 spectroscopic catalogue, and then calculate the number over-density in the inner bins in the same method as before, this time taking velocity offsets of > 300 km/s as the background (Figure 4.11).

Error bars corresponding to the Poisson standard deviation in each bin are indicated. The cumulative over-density with corresponding errors added in quadrature are shown. We see from Figure 4.11, the number over-density first reaches a maximum of 2.8 ± 0.14 in the 500 kpc projected radial separation bin. From Figure 4.9 we see that the difference between spectroscopic and photometric limiting magnitudes in the r-band is 4.5, and by looking at the number over-density as a function of apparent magnitude separation (and taking a Δm of ~ 12 as being detections at the limiting photometric magnitude), we notice that the number over-density from the velocity offset plot in the 7'th and 8'th Δm magnitude bins is consistent with what is shown in this plot, to within the estimated Poisson error. From Figure 4.9, we can therefore confirm that our results are self-consistent. Further, the consistent over-density found in velocity offset confirms the association of our statistical sample of satellites.

4.5 Comparison With Previous Results

Satellite abundances around more distant galaxies have been investigated recently by several authors, including: Guo et al. (2011,2012) [33, 34]; Lares et al. (2011) [57]; Liu et al. (2011) [59]; Strigari et al. (2012) [88]; and Nierenberg et al. (2011,2012) [73, 74]. While these groups use a similar strategy for detecting associated satellites around bright primaries, their larger samples of more distant primaries extends to much further redshifts than our sample. While the larger upper limit on primary galaxy redshift allows these authors to incorporate more galaxies, it limits their investigations to the bright end of the luminosity function. While these groups find a statistically significant abundance of galaxies within ~ 5 magnitudes of the host, our search is more sensitive to the faint end. We find a consistent over-density within the overlapping magnitude range and extend these results further down the luminosity function due to the intermediate distance of our sample, which extends to 42 Mpc. We find a luminosity function that is slightly shallower at the bright end, but which continues to rise steadily to $\Delta m = 10$ before the noise overwhelms the signal, with a cumulative over-density reaching 5.7 ± 1.5 galaxies and showing no sign of flattening until that point.

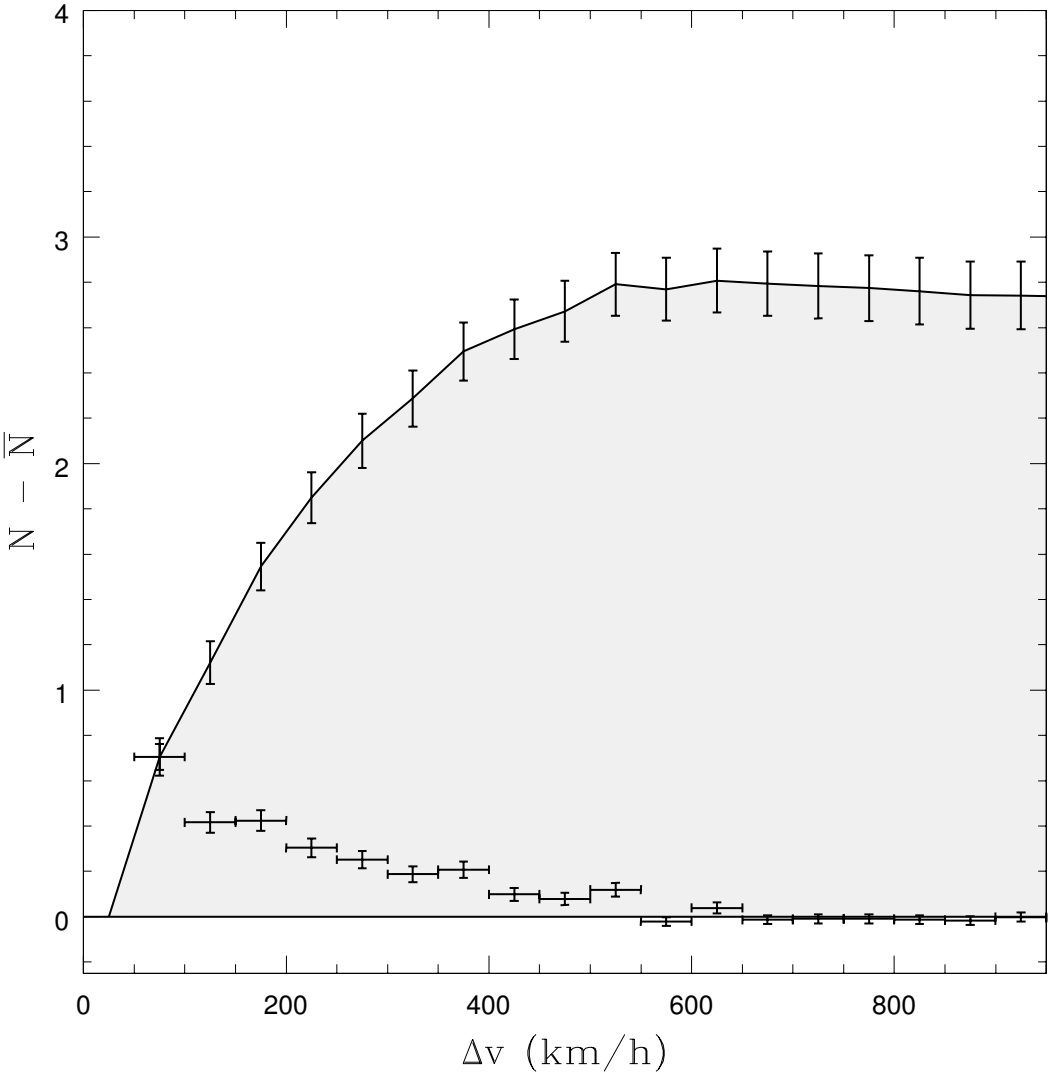

Figure 4.10: The binned and cumulative number over-density profile per galaxy in radial bins for the spectroscopic sample. Error bars on each bin indicate bin width and Poisson error. The shaded region indicates the cumulative over-density, shown with the cumulative Poisson error added in quadrature.

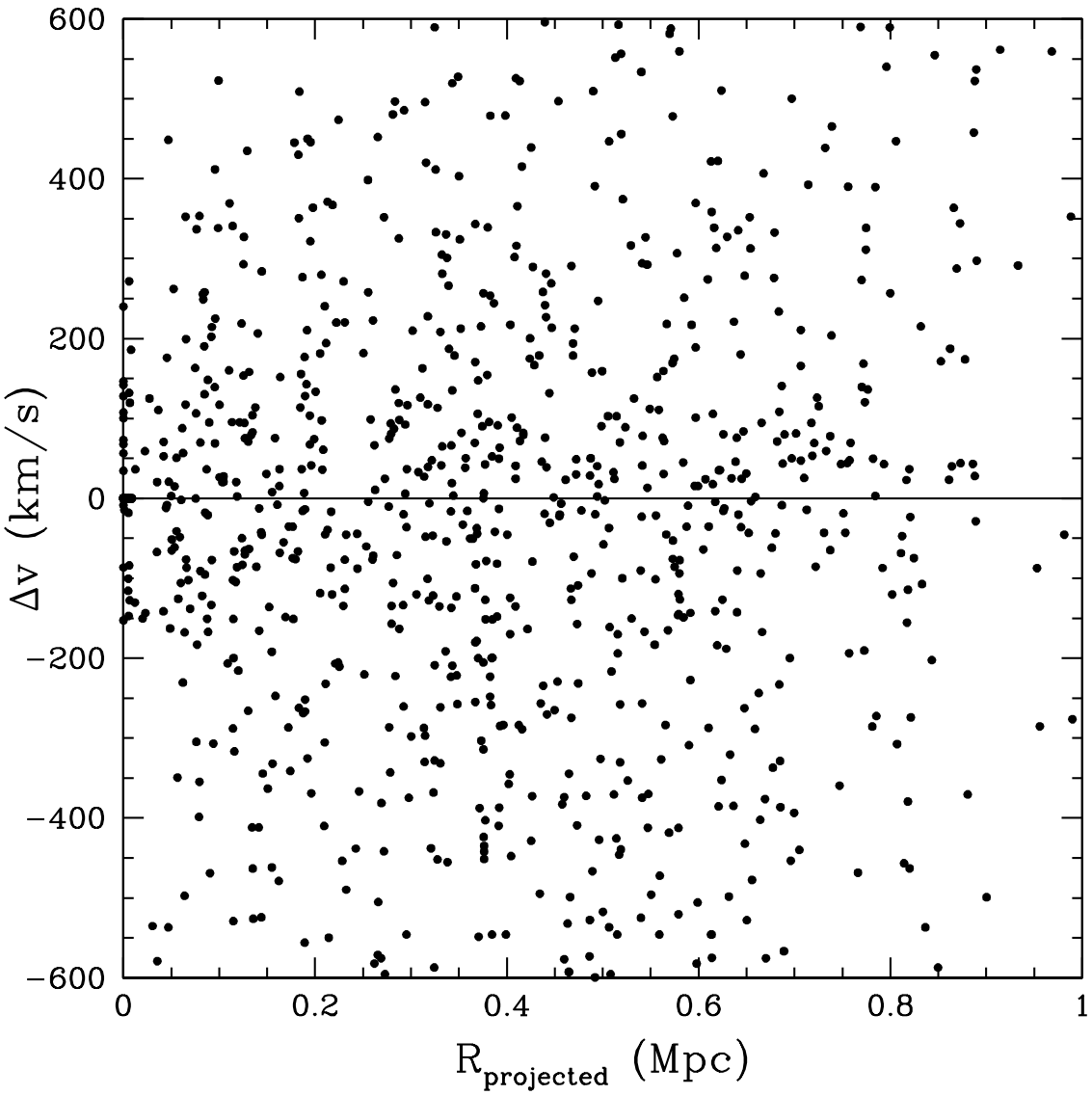

Figure 4.11: The velocity offset from central host vs projected separation shown for spectroscopic detections of the brightest satellites having spectroscopic redshifts within a projected 1 Mpc.

4.5.1 Guo et al. 2011

Similar to our results, Guo et al. (2011) [33] find a satellite luminosity function that depends on primary morphology and magnitude, with bright early-types having larger amplitudes for brighter primaries at the rate of approximately 2 per M_V magnitude. While our smaller sample of primaries does not allow us to bin by single magnitude separations and retain robust statistics, we see that bright primaries with $M_K \leq -23$, representing the brightest 15% of the sample, host a factor of 3-4 times the cumulative number of those of the fainter 85%. Guo et al. find that for $-14 < M_V < -19$, the satellite luminosity function has a very similar slope to the average of the Milky Way and M31, but with a factor of two fewer satellites in all luminosity bins. This is in good agreement with our results, as can be seen in Figure 4.9, as we find a lack of bright, Magellanic Cloud-like satellites compared to the Milky Way, having detected on average only 0.93 ± 0.5 satellites within 5 magnitudes of the primary, but with a $10 < \Delta m < 6$ that is in keeping with expectations from the Milky Way. The signal found by Guo et al. becomes very noisy for $M_V > -14$, while the proximity of our sample allows us to probe the satellite luminosity function 4 magnitudes fainter to reach down to $\Delta m = 12$, where the Δm luminosity function reaches a maximum of 5.7 ± 1.5 and shows no sign of turning off beyond the effect of survey limiting magnitude.

4.5.2 Lares et al. 2011

Lares et al. (2011) find that bright primaries ($M_r < -21.5$) host on average 7 satellites while lower luminosity primaries ($-21.5 < M_r < -20.5$) host a mean of only 1 satellite galaxy per primary. Instead of SDSS r-band magnitudes, we use 2MASS k-band magnitudes to split our primary sample by absolute magnitude, and find a similar dependence the primary magnitude dependence on satellite abundance, as we find the k-magnitude 15% brightest galaxies in our sample host 9.5 ± 1.3 satellites within 600 kpc, while our low-luminosity primaries $M_K > -23.5$ host only 2.8 ± 0.8 within the same projected separation.

4.5.3 Liu et al. 2011

Employing search strategy similar to ours, Liu et al. (2011) [59] look for Magellanic Cloud-like satellites around bright Milky Way analogues using the SDSS DR7 spectroscopic catalogue. Liu et al. searched for bright satellites analogous to the Large and Small Magellanic Clouds by searching for satellite galaxies within 150 kpc of the host that are 2-4 magnitudes fainter than their host galaxies, which lie in the magnitude range $M_r = -21.2 \pm 0.2$. They find that 11.6% host one such satellite and only 3.5% host two and find a mean of 0.29 satellites per primary. We find a similar lack of bright Magellanic Cloud-like satellites and that Milky Way analogues with $M_r = -21.6 \pm 0.5$ host on average only 0.83 ± 0.315 with $\Delta m < 4$.

4.5.4 Strigari et al. 2012

For primaries within r-band magnitudes of -20.4 ± 0.25, Strigari et al. [88] also find a cumulative mean satellite number profile that under-predicts the number of bright satellites within 4 magnitudes, finding on average only 0.25 galaxies within 4 magnitudes of the primary, while we find on average 0.83 ± 0.32 within the same range for primaries in the magnitude range $M_r = -21.6 \pm 0.5$. For magnitudes $8 \leq \Delta m \leq 10$, Strigari et al. place upper limits on the mean satellite number $< \Delta m$ of 12, 60, and 300 in cumulative Δm magnitude bins of 8, 9, and 10, respectively. These results do not significantly constrain our results or the results obtained by other authors so far.

4.5.5 Nierenberg et al. 2011/2012

To within 5 magnitudes of the host galaxy, Nierenberg et al. 2011 [73] find satellite abundances around early-type galaxies at $0.1 < z < 0.8$ of $0.5^{+0.8}_{-0.4}$, which is consistent with our result of 0.9 ± 0.5 satellites within 5 magnitudes of hosts as luminous as the Milky Way. Furthermore, Nierenberg et al 2012 [74] find that the average projected radial density profile of satellite distributions is on average isothermal, with a logarithmic density profile slope of -1 ± 0.3. This is consistent with our finding, where the slope of the logarithmic density profile is -0.98 ± 0.1. Our result of bright, early-type galaxies accounting for the majority of the signal is also consistent with Nierenberg et al. 2012, who find that more massive early-type hosts host significantly more galaxies than late-type hosts of the same stellar mass.

Chapter 5

Discussion and Conclusion

The abundance of satellite galaxies predicted by models of structure formation in ΛCDM is a critical test of ΛCDM on small scales. From comparing the predictions of Cold Dark Matter stucture formation with observations of local dwarfs there is a 1-2 order of magnitude difference in satellites with circular velocities larger than the Draco and Ursa Minor systems [70], leading to the so-called "missing satellites" problem. Comparisons between simulation and observations have, however, been limited to only the most local galaxy groups (the Milky Way and Andromeda groups). Whether the abundance of dwarf satellites observed in the Local Group is typical of other groups in the greater universe is unknown. Using the Atlas3D parent catalogue, we have constructed a volume-limited sample of galaxies down to a well-defined stellar mass limit extending to a distance of 42 Mpc. We have applied cuts on the background based on the properties of known dwarf satellites of the Local Group in order to statistically identify associated satellites around galaxies in our primary catalogue using both the SDSS DR8 spectroscopic and photometric galaxy catalogues. Stacking these systems and subtracting the background, we have estimated the average density and number profile and the dependence on the morphology and magnitude of the primary. We have also constructed a Δm luminosity function for galaxies as bright as the Milky Way in order to facilitate a comparison in the number of satellites per magnitude bin. Our work has extended the work of previous authors such as Guo et al. (2011,2012) [33, 34]; Liu et al. (2011) [59]; Lares et al. (2011) [57]; Strigari et al. (2012) [88]; and Nierenberg et al. (2011,2012) [73, 74] by several magnitudes further down the faint end of the luminosity function. In the this chapter we summarize our main results and discuss the implications of ours and several other authors's work.

Our main results are as follows:

- We detect an over-density of faint objects at projected separations of < 500 kpc at S/N ~ 8, corresponding to an average of 4.8 ± 0.65 satellite detections per primary.
- We find that the overdense regions within the typical clustering scale length have a projected radial distribution consistent with an isothermal profile, having a logarithmic projected radial density profle slope of -0.98 ± 0.1.
- We find a strong dependence in satellite abundance on primary brightness and morphological type. Bright ($M_K \leq -23.5$) primaries are found to host on average 7.62 ± 0.9 satellites within 400 kpc and show stronger signs of clustering, with ellipticals hosting on average 10.85 ± 2.3 within a projected 550 kpc. Our finding that bright, early-type primaries host a larger number of satellites (Figures 4.5, 4.4) is consistent with what we observe amongst neighbouring galaxy groups. Centaurus A, which is the only example of a bright early-type galaxy, has more known dwarfs than any neighbouring galaxy group. This finding is in agreement with recent results from Guo et al. (2011,2012) [33, 34]; Liu et al. (2011) [59]; Lares et al. (2011) [57]; Strigari et al. (2012) [88]; and Nierenberg et al. (2011,2012) [73, 74].
- We find a distinct lack of Magellanic Cloud analogues, with Milky Way-like galaxies having on average only 0.93 ± 0.5 satellite galaxies within 5 magnitudes of the host. This is in contrast to the Milky Way satellite luminosity function at the bright end, where the Large and Small Magellanic Clouds are found at ~ 3 and ~ 5 r-band magnitudes fainter than the Milky Way, respectively (Figure 4.9). This finding is also consistent with recent results from Guo et al. (2011,2012) [33, 34]; Liu et al. (2011) [59]; Lares et al. (2011) [57]; Strigari et al. (2012) [88]; and Nierenberg et al. (2011,2012) [73, 74]. Despite the mismatch in satellite abundances at the bright end of the luminosity function, our cumulative satellite abundances at the faint end are consistent with expectations from the Milky Way.

Our results extend recent measures of satellite abundance around more distant galaxies 4 magnitudes further down the luminosity function. Due to the drastic effect of the cut, it is virtually guaranteed that there exist more dwarf satellites around the primaries analyzed in our sample that have been excluded. Of the other works reviewed, there is broad agreement that more luminous primaries host more satellites, which is confirmed by our results. The other main conclusion from the other works reviewed is that the Milky Way is atypical in its number of bright satellites. This is also in agreement with our results (Figure 3.5,4.9). Our finding that the bright primaries in our sample host, on average, 6 satellite galaxies within 10 magnitudes of the host and that the luminosity function shows

no sign of flattening inside survey magnitude limits is encouraging for resolving the apparent lack of substructure that we observe relative to the predictions of structure formation in a ΛCDM universe. Our methodology has allowed us to probe the luminosity function of hosts as luminous as the Milky Way to fainter magnitudes. Our finding that cumulative satellite abundances are consistent at the faint end ($\Delta m \sim 10 - 12$) is novel amongst the works considered here and one of our main results.

Among individual field galaxies, where mass-to-light ratios are $M/L \lesssim 10$, mass distributions inferred from galaxy-scale gravitational lensing are found to be well-fit by isothermal density profiles [28, 54, 90]. The effect of baryons, which play a more dominant role than in clusters, is to steepen the inner mass density profile from dark matter only simulations. In galaxy clusters, where typical mass-to-light ratios are on the order of $M/L \propto 100$, the stellar content plays less of a role in determining the density profile. Mass density profiles for galaxy clusters have been obtained through gravitational lensing, stellar kinematics, and x-ray observations, and are found to be well-fit by the Navarro-Frenk-White profile [61, 14, 19]. It is not yet known if galaxy groups are better fit by the NFW or isothermal density profiles, which lie intermediate in scale between field galaxies and galaxy clusters. The over-density profile we obtain is consistent with an isothermal density profile, as we find a logarithmic density profile slope of -0.98 ± 0.1 (Figure 4.2). Recently, McKean et al. (2010)[69] performed a lensing and kinematics analysis of a galaxy group gravitational lens system at redshift $z = 0.365$, CLASS B2108+213. The investigation of the lensing structure by McKean et al. revealed a mass density profile for the group that was found to be isothermal inside the Einstein radius, on average.

The results of this work and work by authors such as Guo et al. [33, 34] place constraints on current structure formation models. A mismatch between the number of bright, Magellanic Cloud-like satellites we observe locally and the number predicted by theory has suggested that the Milky Way is unusual in this respect. ΛCDM models of structure formation predict that satellite galaxies as bright as the Large and Small Magellanic Clouds should be rare when we see two such galaxies within the Local Group. Authors such as Boylan-Kolchin et al. [13], who has found that less than 10% of Milky Way-mass halos host two galaxies as bright as the Magellanic Clouds in simulation, have concluded that the Local Group is uncommon. Our results are in agreement with this conclusion as we detect, over average, fewer than 1 satellite galaxy within 5 magnitudes of hosts as bright as the Milky Way (Figure 4.9). Authors such as Liu et al. [59], who have used the same technique on a larger sample of more distant primaries, find that 11.6% host one such satellite and only 3.5% host two. Here, it seems that both theory and observation are in agreement

that the Milky Way is unusual in its abundance of bright satellites. The faint-end satellite abundance we find, however, is in keeping in agreement with the Local Group (Figure 4.9), as it can also be seen from Figure 4.9 that while the bright end satellite abundances mismatch, the faint end cumulative satellite excess is consistent with the projected Milky Way satellites to within Poisson error. Also suggestive of this consistency is the average number over-density of ~ 5 satellites per primary, as it agrees well with the number of Local Group satellites placed at a distance of 25 Mpc that would not be excluded by our cut (Figure 3.5).

The investigation of dwarf satellite abundances in galaxy groups is a useful observational probe of hierarchical structure formation in ΛCDM, and we expect that our results and the recent results of other authors reviewed here will, in the future, help to refine theories of hierarchical assembly of dark matter halos and in so doing, help to illuminate the nature of dark matter.

References

[1] M. Bartelmann. Arcs from a universal dark-matter halo profile. A&A, 313:697–702, September 1996.

[2] V. Belokurov, M. G. Walker, N. W. Evans, G. Gilmore, M. J. Irwin, D. Just, S. Koposov, M. Mateo, E. Olszewski, L. Watkins, and L. Wyrzykowski. Big Fish, Little Fish: Two New Ultra-faint Satellites of the Milky Way. ApJ, 712:L103–L106, March 2010.

[3] V. Belokurov, M. G. Walker, N. W. Evans, G. Gilmore, M. J. Irwin, M. Mateo, L. Mayer, E. Olszewski, J. Bechtold, and T. Pickering. The discovery of Segue 2: a prototype of the population of satellites of satellites. MNRAS, 397:1748–1755, August 2009.

[4] V. Belokurov, D. B. Zucker, N. W. Evans, J. T. Kleyna, S. Koposov, S. T. Hodgkin, M. J. Irwin, G. Gilmore, M. I. Wilkinson, M. Fellhauer, D. M. Bramich, P. C. Hewett, S. Vidrih, J. T. A. De Jong, J. A. Smith, H.-W. Rix, E. F. Bell, R. F. G. Wyse, H. J. Newberg, P. A. Mayeur, B. Yanny, C. M. Rockosi, O. Y. Gnedin, D. P. Schneider, T. C. Beers, J. C. Barentine, H. Brewington, J. Brinkmann, M. Harvanek, S. J. Kleinman, J. Krzesinski, D. Long, A. Nitta, and S. A. Snedden. Cats and Dogs, Hair and a Hero: A Quintet of New Milky Way Companions. ApJ, 654:897–906, January 2007.

[5] V. Belokurov, D. B. Zucker, N. W. Evans, M. I. Wilkinson, M. J. Irwin, S. Hodgkin, D. M. Bramich, J. M. Irwin, G. Gilmore, B. Willman, S. Vidrih, H. J. Newberg, R. F. G. Wyse, M. Fellhauer, P. C. Hewett, N. Cole, E. F. Bell, T. C. Beers, C. M. Rockosi, B. Yanny, E. K. Grebel, D. P. Schneider, R. Lupton, J. C. Barentine, H. Brewington, J. Brinkmann, M. Harvanek, S. J. Kleinman, J. Krzesinski, D. Long, A. Nitta, J. A. Smith, and S. A. Snedden. A Faint New Milky Way Satellite in Bootes. ApJ, 647:L111–L114, August 2006.

[6] B. Binggeli and L. M. Cameron. Dwarf galaxies in the Virgo cluster. I - The systematic photometric properties of early-type dwarfs. A&A, 252:27–52, December 1991.

[7] B. Binggeli, G. A. Tammann, and A. Sandage. Studies of the Virgo cluster. VI - Morphological and kinematical structure of the Virgo cluster. AJ, 94:251–277, August 1987.

[8] J. Binney and S. Tremaine. *Galactic Dynamics: Second Edition*. Princeton University Press, 2008.

[9] M. R. Blanton, D. J. Schlegel, M. A. Strauss, J. Brinkmann, D. Finkbeiner, M. Fukugita, J. E. Gunn, D. W. Hogg, Ž. Ivezić, G. R. Knapp, R. H. Lupton, J. A. Munn, D. P. Schneider, M. Tegmark, and I. Zehavi. New York University Value-Added Galaxy Catalog: A Galaxy Catalog Based on New Public Surveys. AJ, 129:2562–2578, June 2005.

[10] A. Bouchard, G. S. Da Costa, and H. Jerjen. The Environmental Influence on the Evolution of Local Galaxies. AJ, 137:3038–3052, February 2009.

[11] A. Bouchard, H. Jerjen, G. S. Da Costa, and J. Ott. Interstellar Medium Disruption in the Centaurus A Group. AJ, 133:261–269, January 2007.

[12] M. S. Bovill and M. Ricotti. Pre-Reionization Fossils, Ultra-Faint Dwarfs, and the Missing Galactic Satellite Problem. ApJ, 693:1859–1870, March 2009.

[13] M. Boylan-Kolchin, J. S. Bullock, and M. Kaplinghat. The Milky Way's bright satellites as an apparent failure of ΛCDM. MNRAS, 422:1203–1218, May 2012.

[14] T. Broadhurst, K. Umetsu, E. Medezinski, M. Oguri, and Y. Rephaeli. Comparison of Cluster Lensing Profiles with ΛCDM Predictions. ApJ, 685:L9–L12, September 2008.

[15] J. S. Bullock, A. V. Kravtsov, and D. H. Weinberg. Reionization and the Abundance of Galactic Satellites. ApJ, 539:517–521, August 2000.

[16] K. Bundy, R. S. Ellis, and C. J. Conselice. GOODS Morphological Catalog (Bundy+, 2005). *VizieR Online Data Catalog*, 7246:0, November 2005.

[17] M. T. Busha, R. H. Wechsler, P. S. Behroozi, B. F. Gerke, A. A. Klypin, and J. R. Primack. Statistics of Satellite Galaxies around Milky-Way-like Hosts. ApJ, 743:117, December 2011.

[18] M. Cappellari, E. Emsellem, D. Krajnović, R. M. McDermid, N. Scott, G. A. Verdoes Kleijn, L. M. Young, K. Alatalo, R. Bacon, L. Blitz, M. Bois, F. Bournaud, M. Bureau, R. L. Davies, T. A. Davis, P. T. de Zeeuw, P.-A. Duc, S. Khochfar, H. Kuntschner, P.-Y. Lablanche, R. Morganti, T. Naab, T. Oosterloo, M. Sarzi, P. Serra, and A.-M. Weijmans. The ATLAS^{3D} project - I. A volume-limited sample of 260 nearby early-type galaxies: science goals and selection criteria. MNRAS, 413:813–836, May 2011.

[19] J. M. Comerford and P. Natarajan. The observed concentration-mass relation for galaxy clusters. MNRAS, 379:190–200, July 2007.

[20] G. de Vaucouleurs. Classification and Morphology of External Galaxies. *Handbuch der Physik*, 53:275, 1959.

[21] J. Diemand and B. Moore. The Structure and Evolution of Cold Dark Matter Halos. *Advanced Science Letters*, 4:297–310, February 2011.

[22] A. Dressler. Galaxy morphology in rich clusters - Implications for the formation and evolution of galaxies. ApJ, 236:351–365, March 1980.

[23] P. R. Durrell, A. Sarajedini, and R. Chandar. Deep HST/ACS Photometry of the M81 Halo. ApJ, 718:1118–1127, August 2010.

[24] R. S. Ellis. Faint Blue Galaxies. ARA&A, 35:389–443, 1997.

[25] Aihara et al. The Eighth Data Release of the Sloan Digital Sky Survey: First Data from SDSS-III. ApJS, 193:29, April 2011.

[26] J. A. Frieman, M. S. Turner, and D. Huterer. Dark Energy and the Accelerating Universe. ARA&A, 46:385–432, September 2008.

[27] M. Fukugita, K. Shimasaku, and T. Ichikawa. Galaxy Colors in Various Photometric Band Systems. PASP, 107:945, October 1995.

[28] R. Gavazzi, T. Treu, L. V. E. Koopmans, A. S. Bolton, L. A. Moustakas, S. Burles, and P. J. Marshall. The Sloan Lens ACS Survey. VI. Discovery and Analysis of a Double Einstein Ring. ApJ, 677:1046–1059, April 2008.

[29] M. Girardi, E. Rigoni, F. Mardirossian, and M. Mezzetti. Morphology and luminosity segregation of galaxies in nearby loose groups. A&A, 406:403–414, August 2003.

[30] C. J. Grillmair. Four New Stellar Debris Streams in the Galactic Halo. ApJ, 693:1118–1127, March 2009.

[31] J. E. Gunn, M. Carr, C. Rockosi, M. Sekiguchi, K. Berry, B. Elms, E. de Haas, Ž. Ivezić, G. Knapp, R. Lupton, G. Pauls, R. Simcoe, R. Hirsch, D. Sanford, S. Wang, D. York, F. Harris, J. Annis, L. Bartozek, W. Boroski, J. Bakken, M. Haldeman, S. Kent, S. Holm, D. Holmgren, D. Petravick, A. Prosapio, R. Rechenmacher, M. Doi, M. Fukugita, K. Shimasaku, N. Okada, C. Hull, W. Siegmund, E. Mannery, M. Blouke, D. Heidtman, D. Schneider, R. Lucinio, and J. Brinkman. The Sloan Digital Sky Survey Photometric Camera. AJ, 116:3040–3081, December 1998.

[32] J. E. Gunn and J. R. Gott, III. On the Infall of Matter Into Clusters of Galaxies and Some Effects on Their Evolution. ApJ, 176:1, August 1972.

[33] Q. Guo, S. Cole, V. Eke, and C. Frenk. The satellite luminosity functions of galaxies in Sloan Digital Sky Survey. MNRAS, 417:370–381, October 2011.

[34] Q. Guo, S. Cole, V. Eke, and C. Frenk. Satellite Galaxy Number Density Profiles in the Sloan Digital Sky Survey. *ArXiv e-prints*, January 2012.

[35] G. L. H. Harris. NGC 5128: The Giant Beneath. PASA, 27:475–481, October 2010.

[36] G. L. H. Harris, M. Rejkuba, and W. E. Harris. The Distance to NGC 5128 (Centaurus A). PASA, 27:457–462, October 2010.

[37] P. A. Henning. HI searches in the Zone of Avoidance: Past and present (and future). PASA, 14:21–24, April 1997.

[38] P. W. Hodge. *Galaxies*. 1986.

[39] H. Hoekstra, M. Franx, K. Kuijken, R. G. Carlberg, H. K. C. Yee, H. Lin, S. L. Morris, P. B. Hall, D. R. Patton, M. Sawicki, and G. D. Wirth. Weak-Lensing Study of Low-Mass Galaxy Groups: Implications for Ω_m. ApJ, 548:L5–L8, February 2001.

[40] E. P. Hubble. *Realm of the Nebulae*. 1936.

[41] R. A. Ibata, G. Gilmore, and M. J. Irwin. Sagittarius: the nearest dwarf galaxy. MNRAS, 277:781–800, December 1995.

[42] M. J. Irwin, V. Belokurov, N. W. Evans, E. V. Ryan-Weber, J. T. A. de Jong, S. Koposov, D. B. Zucker, S. T. Hodgkin, G. Gilmore, P. Prema, L. Hebb, A. Begum, M. Fellhauer, P. C. Hewett, R. C. Kennicutt, Jr., M. I. Wilkinson, D. M. Bramich,

S. Vidrih, H.-W. Rix, T. C. Beers, J. C. Barentine, H. Brewington, M. Harvanek, J. Krzesinski, D. Long, A. Nitta, and S. A. Snedden. Discovery of an Unusual Dwarf Galaxy in the Outskirts of the Milky Way. ApJ, 656:L13–L16, February 2007.

[43] M. J. Irwin, P. S. Bunclark, M. T. Bridgeland, and R. G. McMahon. A new satellite galaxy of the Milky Way in the constellation of Sextans. MNRAS, 244:16P–19P, May 1990.

[44] M. J. Irwin, A. M. N. Ferguson, A. P. Huxor, N. R. Tanvir, R. A. Ibata, and G. F. Lewis. Andromeda XVII: A New Low-Luminosity Satellite of M31. ApJ, 676:L17–L20, March 2008.

[45] F. P. Israel. Centaurus A - NGC 5128. A&A Rev., 8:237–278, 1998.

[46] N. Jarosik, C. L. Bennett, J. Dunkley, B. Gold, M. R. Greason, M. Halpern, R. S. Hill, G. Hinshaw, A. Kogut, E. Komatsu, D. Larson, M. Limon, S. S. Meyer, M. R. Nolta, N. Odegard, L. Page, K. M. Smith, D. N. Spergel, G. S. Tucker, J. L. Weiland, E. Wollack, and E. L. Wright. Seven-year Wilkinson Microwave Anisotropy Probe (WMAP) Observations: Sky Maps, Systematic Errors, and Basic Results. ApJS, 192:14, February 2011.

[47] H. Jerjen, K. C. Freeman, and B. Binggeli. Surface Brightness Fluctuation Distances to Dwarf Elliptical Galaxies in the Sculptor Group. AJ, 116:2873–2885, December 1998.

[48] I. D. Karachentsev. The Local Group and Other Neighboring Galaxy Groups. AJ, 129:178–188, January 2005.

[49] I. D. Karachentsev, E. K. Grebel, M. E. Sharina, A. E. Dolphin, D. Geisler, P. Guhathakurta, P. W. Hodge, V. E. Karachentseva, A. Sarajedini, and P. Seitzer. Distances to nearby galaxies in Sculptor. A&A, 404:93–111, June 2003.

[50] I. D. Karachentsev, V. E. Karachentseva, W. K. Huchtmeier, and D. I. Makarov. A Catalog of Neighboring Galaxies. AJ, 127:2031–2068, April 2004.

[51] I. D. Karachentsev, M. E. Sharina, A. E. Dolphin, E. K. Grebel, D. Geisler, P. Guhathakurta, P. W. Hodge, V. E. Karachentseva, A. Sarajedini, and P. Seitzer. Galaxy flow in the Canes Venatici I cloud. A&A, 398:467–477, February 2003.

[52] I. D. Karachentsev, R. B. Tully, A. Dolphin, M. Sharina, L. Makarova, D. Makarov, S. Sakai, E. J. Shaya, O. G. Kashibadze, V. Karachentseva, and L. Rizzi. The Hubble

Flow around the Centaurus A/M83 Galaxy Complex. AJ, 133:504–517, February 2007.

[53] A. Klypin, A. V. Kravtsov, O. Valenzuela, and F. Prada. Where Are the Missing Galactic Satellites? ApJ, 522:82–92, September 1999.

[54] L. V. E. Koopmans, T. Treu, A. S. Bolton, S. Burles, and L. A. Moustakas. The Sloan Lens ACS Survey. III. The Structure and Formation of Early-Type Galaxies and Their Evolution since z ˜ 1. ApJ, 649:599–615, October 2006.

[55] S. Koposov, V. Belokurov, N. W. Evans, P. C. Hewett, M. J. Irwin, G. Gilmore, D. B. Zucker, H.-W. Rix, M. Fellhauer, E. F. Bell, and E. V. Glushkova. The Luminosity Function of the Milky Way Satellites. ApJ, 686:279–291, October 2008.

[56] J. M. Kubo, S. S. Allam, J. Annis, E. J. Buckley-Geer, H. T. Diehl, D. Kubik, H. Lin, and D. Tucker. The Sloan Bright Arcs Survey: Six Strongly Lensed Galaxies at z = 0.4-1.4. ApJ, 696:L61–L65, May 2009.

[57] M. Lares, D. G. Lambas, and M. J. Domínguez. Properties of Satellite Galaxies in the SDSS Photometric Survey: Luminosities, Colors, and Projected Number Density Profiles. AJ, 142:13, July 2011.

[58] M. Limousin, R. Cabanac, R. Gavazzi, J.-P. Kneib, V. Motta, J. Richard, K. Thanjavur, G. Foex, R. Pello, D. Crampton, C. Faure, B. Fort, E. Jullo, P. Marshall, Y. Mellier, A. More, G. Soucail, S. Suyu, M. Swinbank, J.-F. Sygnet, H. Tu, D. Valls-Gabaud, T. Verdugo, and J. Willis. A new window of exploration in the mass spectrum: strong lensing by galaxy groups in the SL2S. A&A, 502:445–456, August 2009.

[59] L. Liu, B. F. Gerke, R. H. Wechsler, P. S. Behroozi, and M. T. Busha. How Common are the Magellanic Clouds? ApJ, 733:62, May 2011.

[60] E. L. Łokas, S. Kazantzidis, and L. Mayer. Evolutionary Tracks of Tidally Stirred Disky Dwarf Galaxies. ApJ, 739:46, September 2011.

[61] P. A. A. Lopes, R. R. de Carvalho, J. L. Kohl-Moreira, and C. Jones. NoSOCS in SDSS - I. Sample definition and comparison of mass estimates. MNRAS, 392:135–152, January 2009.

[62] S. R. Majewski, R. L. Beaton, R. J. Patterson, J. S. Kalirai, M. C. Geha, R. R. Muñoz, M. S. Seigar, P. Guhathakurta, K. M. Gilbert, R. M. Rich, J. S. Bullock,

and D. B. Reitzel. Discovery of Andromeda XIV: A Dwarf Spheroidal Dynamical Rogue in the Local Group? ApJ, 670:L9–L12, November 2007.

[63] N. F. Martin, A. W. McConnachie, M. Irwin, L. M. Widrow, A. M. N. Ferguson, R. A. Ibata, J. Dubinski, A. Babul, S. Chapman, M. Fardal, G. F. Lewis, J. Navarro, and R. M. Rich. PAndAS' CUBS: Discovery of Two New Dwarf Galaxies in the Surroundings of the Andromeda and Triangulum Galaxies. ApJ, 705:758–765, November 2009.

[64] R. O. Marzke and L. N. da Costa. The Galaxy Luminosity Function at $z \leq 0.05$: Dependence on Color. AJ, 113:185, January 1997.

[65] M. L. Mateo. Dwarf Galaxies of the Local Group. ARA&A, 36:435–506, 1998.

[66] A. W. McConnachie and P. Côté. Revisiting the Influence of Unidentified Binaries on Velocity Dispersion Measurements in Ultra-faint Stellar Systems. ApJ, 722:L209–L214, October 2010.

[67] A. W. McConnachie, A. Huxor, N. F. Martin, M. J. Irwin, S. C. Chapman, G. Fahlman, A. M. N. Ferguson, R. A. Ibata, G. F. Lewis, H. Richer, and N. R. Tanvir. A Trio of New Local Group Galaxies with Extreme Properties. ApJ, 688:1009–1020, December 2008.

[68] A. W. McConnachie and M. J. Irwin. Structural properties of the M31 dwarf spheroidal galaxies. MNRAS, 365:1263–1276, February 2006.

[69] J. P. McKean, M. W. Auger, L. V. E. Koopmans, S. Vegetti, O. Czoske, C. D. Fassnacht, T. Treu, A. More, and D. D. Kocevski. The mass distribution of a moderate redshift galaxy group and brightest group galaxy from gravitational lensing and kinematics. MNRAS, 404:749–766, May 2010.

[70] B. Moore, S. Ghigna, F. Governato, G. Lake, T. Quinn, J. Stadel, and P. Tozzi. Dark Matter Substructure within Galactic Halos. ApJ, 524:L19–L22, October 1999.

[71] B. Moore, N. Katz, and G. Lake. On the Destruction and Overmerging of Dark Halos in Dissipationless N-Body Simulations. ApJ, 457:455, February 1996.

[72] J. F. Navarro, C. S. Frenk, and S. D. M. White. A Universal Density Profile from Hierarchical Clustering. ApJ, 490:493, December 1997.

[73] A. M. Nierenberg, M. W. Auger, T. Treu, P. J. Marshall, and C. D. Fassnacht. Luminous Satellites of Early-type Galaxies. I. Spatial Distribution. ApJ, 731:44, April 2011.

[74] A. M. Nierenberg, M. W. Auger, T. Treu, P. J. Marshall, C. D. Fassnacht, and M. T. Busha. Luminous Satellites. II. Spatial Distribution, Luminosity Function, and Cosmic Evolution. ApJ, 752:99, June 2012.

[75] N. D. Padilla, C. M. Baugh, V. R. Eke, P. Norberg, S. Cole, C. S. Frenk, D. J. Croton, I. K. Baldry, J. Bland-Hawthorn, T. Bridges, R. Cannon, M. Colless, C. Collins, W. Couch, G. Dalton, R. De Propris, S. P. Driver, G. Efstathiou, R. S. Ellis, K. Glazebrook, C. Jackson, O. Lahav, I. Lewis, S. Lumsden, S. Maddox, D. Madgwick, J. A. Peacock, B. A. Peterson, W. Sutherland, and K. Taylor. The 2dF Galaxy Redshift Survey: the clustering of galaxy groups. MNRAS, 352:211–225, July 2004.

[76] T. Padmanabhan. *Structure Formation in the Universe*. June 1993.

[77] P. J. E. Peebles. *The large-scale structure of the universe*. 1980.

[78] S. Perlmutter, G. Aldering, G. Goldhaber, R. A. Knop, P. Nugent, P. G. Castro, S. Deustua, S. Fabbro, A. Goobar, D. E. Groom, I. M. Hook, A. G. Kim, M. Y. Kim, J. C. Lee, N. J. Nunes, R. Pain, C. R. Pennypacker, R. Quimby, C. Lidman, R. S. Ellis, M. Irwin, R. G. McMahon, P. Ruiz-Lapuente, N. Walton, B. Schaefer, B. J. Boyle, A. V. Filippenko, T. Matheson, A. S. Fruchter, N. Panagia, H. J. M. Newberg, W. J. Couch, and Supernova Cosmology Project. Measurements of Omega and Lambda from 42 High-Redshift Supernovae. ApJ, 517:565–586, June 1999.

[79] W. H. Press and P. Schechter. Formation of Galaxies and Clusters of Galaxies by Self-Similar Gravitational Condensation. ApJ, 187:425–438, February 1974.

[80] W. H. Press, S. A. Teukolsky, W. T. Vetterling, and B. P. Flannery. *Numerical recipes in C. The art of scientific computing*. 1992.

[81] J. C. Richardson, M. J. Irwin, A. W. McConnachie, N. F. Martin, A. L. Dotter, A. M. N. Ferguson, R. A. Ibata, S. C. Chapman, G. F. Lewis, N. R. Tanvir, and R. M. Rich. PAndAS' Progeny: Extending the M31 Dwarf Galaxy Cabal. ApJ, 732:76, May 2011.

[82] A. G. Riess, A. V. Filippenko, P. Challis, A. Clocchiatti, A. Diercks, P. M. Garnavich, R. L. Gilliland, C. J. Hogan, S. Jha, R. P. Kirshner, B. Leibundgut, M. M. Phillips, D. Reiss, B. P. Schmidt, R. A. Schommer, R. C. Smith, J. Spyromilio, C. Stubbs,

N. B. Suntzeff, and J. Tonry. Observational Evidence from Supernovae for an Accelerating Universe and a Cosmological Constant. AJ, 116:1009–1038, September 1998.

[83] B. Ryden. *Introduction to cosmology*. 2003.

[84] D. J. Schlegel, D. P. Finkbeiner, and M. Davis. Maps of Dust Infrared Emission for Use in Estimation of Reddening and Cosmic Microwave Background Radiation Foregrounds. ApJ, 500:525, June 1998.

[85] J. L. Sérsic. Influence of the atmospheric and instrumental dispersion on the brightness distribution in a galaxy. *Boletin de la Asociacion Argentina de Astronomia La Plata Argentina*, 6:41, 1963.

[86] M. F. Skrutskie, R. M. Cutri, R. Stiening, M. D. Weinberg, S. Schneider, J. M. Carpenter, C. Beichman, R. Capps, T. Chester, J. Elias, J. Huchra, J. Liebert, C. Lonsdale, D. G. Monet, S. Price, P. Seitzer, T. Jarrett, J. D. Kirkpatrick, J. E. Gizis, E. Howard, T. Evans, J. Fowler, L. Fullmer, R. Hurt, R. Light, E. L. Kopan, K. A. Marsh, H. L. McCallon, R. Tam, S. Van Dyk, and S. Wheelock. The Two Micron All Sky Survey (2MASS). AJ, 131:1163–1183, February 2006.

[87] M. A. Strauss, D. H. Weinberg, R. H. Lupton, V. K. Narayanan, J. Annis, M. Bernardi, M. Blanton, S. Burles, A. J. Connolly, J. Dalcanton, M. Doi, D. Eisenstein, J. A. Frieman, M. Fukugita, J. E. Gunn, Ž. Ivezić, S. Kent, R. S. J. Kim, G. R. Knapp, R. G. Kron, J. A. Munn, H. J. Newberg, R. C. Nichol, S. Okamura, T. R. Quinn, M. W. Richmond, D. J. Schlegel, K. Shimasaku, M. SubbaRao, A. S. Szalay, D. Vanden Berk, M. S. Vogeley, B. Yanny, N. Yasuda, D. G. York, and I. Zehavi. Spectroscopic Target Selection in the Sloan Digital Sky Survey: The Main Galaxy Sample. AJ, 124:1810–1824, September 2002.

[88] L. E. Strigari and R. H. Wechsler. The Cosmic Abundance of Classical Milky Way Satellites. ApJ, 749:75, April 2012.

[89] J. E. Taylor. Dark Matter Halos from the Inside Out. *Advances in Astronomy*, 2011, 2011.

[90] T. Treu and L. V. E. Koopmans. Massive Dark Matter Halos and Evolution of Early-Type Galaxies to z $\sim$ 1. ApJ, 611:739–760, August 2004.

[91] S. van den Bergh. Updated Information on the Local Group. PASP, 112:529–536, April 2000.

[92] R. P. van der Marel, G. Besla, T. J. Cox, S. T. Sohn, and J. Anderson. The M31 Velocity Vector. III. Future Milky Way M31-M33 Orbital Evolution, Merging, and Fate of the Sun. ApJ, 753:9, July 2012.

[93] S. M. Walsh, H. Jerjen, and B. Willman. A Pair of Boötes: A New Milky Way Satellite. ApJ, 662:L83–L86, June 2007.

[94] D. R. Weisz, A. E. Dolphin, J. J. Dalcanton, E. D. Skillman, J. Holtzman, B. F. Williams, K. M. Gilbert, A. C. Seth, A. Cole, S. M. Gogarten, K. Rosema, I. D. Karachentsev, K. B. W. McQuinn, and D. Zaritsky. How Typical Are the Local Group Dwarf Galaxies? ApJ, 743:8, December 2011.

[95] A. B. Whiting, M. J. Irwin, and G. K. T. Hau. A new galaxy in the local group: The Antlia dwarf galaxy. AJ, 114:996–1001, September 1997.

[96] W. Wild and A. Eckart. Dense gas in the dust lane of Centaurus A. A&A, 359:483–488, July 2000.

[97] B. Willman, M. R. Blanton, A. A. West, J. J. Dalcanton, D. W. Hogg, D. P. Schneider, N. Wherry, B. Yanny, and J. Brinkmann. A New Milky Way Companion: Unusual Globular Cluster or Extreme Dwarf Satellite? AJ, 129:2692–2700, June 2005.

[98] B. Willman, J. Dalcanton, Ž. Ivezić, T. Jackson, R. Lupton, J. Brinkmann, G. Hennessy, and R. Hindsley. An SDSS Survey For Resolved Milky Way Satellite Galaxies. I. Detection Limits. AJ, 123:848–854, February 2002.

[99] B. Willman, J. J. Dalcanton, D. Martinez-Delgado, A. A. West, M. R. Blanton, D. W. Hogg, J. C. Barentine, H. J. Brewington, M. Harvanek, S. J. Kleinman, J. Krzesinski, D. Long, E. H. Neilsen, Jr., A. Nitta, and S. A. Snedden. A New Milky Way Dwarf Galaxy in Ursa Major. ApJ, 626:L85–L88, June 2005.

[100] J. S. B. Wyithe and A. Loeb. Suppression of dwarf galaxy formation by cosmic reionization. Nature, 441:322–324, May 2006.

[101] M. S. Yun, P. T. P. Ho, and K. Y. Lo. A high-resolution image of atomic hydrogen in the M81 group of galaxies. Nature, 372:530–532, December 1994.

[102] A. R. Zentner and J. S. Bullock. Halo Substructure and the Power Spectrum. ApJ, 598:49–72, November 2003.

[103] S. E. Zepf and K. M. Ashman. Globular Cluster Systems Formed in Galaxy Mergers. MNRAS, 264:611, October 1993.

[104] D. B. Zucker, V. Belokurov, N. W. Evans, J. T. Kleyna, M. J. Irwin, M. I. Wilkinson, M. Fellhauer, D. M. Bramich, G. Gilmore, H. J. Newberg, B. Yanny, J. A. Smith, P. C. Hewett, E. F. Bell, H.-W. Rix, O. Y. Gnedin, S. Vidrih, R. F. G. Wyse, B. Willman, E. K. Grebel, D. P. Schneider, T. C. Beers, A. Y. Kniazev, J. C. Barentine, H. Brewington, J. Brinkmann, M. Harvanek, S. J. Kleinman, J. Krzesinski, D. Long, A. Nitta, and S. A. Snedden. A Curious Milky Way Satellite in Ursa Major. ApJ, 650:L41–L44, October 2006.

[105] D. B. Zucker, V. Belokurov, N. W. Evans, M. I. Wilkinson, M. J. Irwin, T. Sivarani, S. Hodgkin, D. M. Bramich, J. M. Irwin, G. Gilmore, B. Willman, S. Vidrih, M. Fellhauer, P. C. Hewett, T. C. Beers, E. F. Bell, E. K. Grebel, D. P. Schneider, H. J. Newberg, R. F. G. Wyse, C. M. Rockosi, B. Yanny, R. Lupton, J. A. Smith, J. C. Barentine, H. Brewington, J. Brinkmann, M. Harvanek, S. J. Kleinman, J. Krzesinski, D. Long, A. Nitta, and S. A. Snedden. A New Milky Way Dwarf Satellite in Canes Venatici. ApJ, 643:L103–L106, June 2006.

[106] D. B. Zucker, A. Y. Kniazev, D. Martínez-Delgado, E. F. Bell, H.-W. Rix, E. K. Grebel, J. A. Holtzman, R. A. M. Walterbos, C. M. Rockosi, D. G. York, J. C. Barentine, H. Brewington, J. Brinkmann, M. Harvanek, S. J. Kleinman, J. Krzesinski, D. Long, E. H. Neilsen, Jr., A. Nitta, and S. A. Snedden. Andromeda X, a New Dwarf Spheroidal Satellite of M31: Photometry. ApJ, 659:L21–L24, April 2007.